NUREG/CR-2320
UCRL-15380

Seismic Structural Fragility Investigation for the Zion Nuclear Power Plant

Seismic Safety Margins Research Program (Phase I)

D. A. Wesley, P. S. Hashimoto - Structural Mechanics Associates

Prepared for
U.S. Nuclear Regulatory Commission

Lawrence Livermore National Laboratory

Available from

GPO Sales Program
Division of Technical Information and Document Control
U. S. Nuclear Regulatory Commission
Washington, D. C. 20555

Printed copy price: $6.00

and

National Technical Information Service
Springfield, Virginia 22161

NUREG/CR-2320
UCRL-15380
RD, RM

Seismic Structural Fragility Investigation for the Zion Nuclear Power Plant

Seismic Safety Margins Research Program (Phase I)

Manuscript Completed: March 1981
Date Published: October 1981

Prepared by
D. A. Wesley, P. S. Hashimoto - Structural Mechanics Associates

Lawrence Livermore National Laboratory
7000 East Avenue
Livermore, CA 94550

Prepared for
Office of Nuclear Regulatory Research
U.S. Nuclear Regulatory Commission
Washington, D.C. 20555
NRC FIN No. **A0126**

Availability of Reference Materials Cited in NRC Publications

Most documents cited in NRC publications will be available from one of the following sources:

1. The NRC Public Document Room, 1717 H Street., N.W.
   Washington, DC 20555

2. The NRC/GPO Sales Program, U.S. Nuclear Regulatory Commission,
   Washington, DC 20555

3. The National Technical Information Service, Springfield, VA 22161

Although the listing that follows represents the majority of documents cited in NRC publications, it is not intended to be exhaustive.

Referenced documents available for inspection and copying for a fee from the NRC Public Document Room include NRC correspondence and internal NRC memoranda; NRC Office of Inspection and Enforcement bulletins, circulars, information notices, inspection and investigation notices; Licensee Event Reports; vendor reports and correspondence; Commission papers; and applicant and licensee documents and correspondence.

The following documents in the NUREG series are available for purchase from the NRC/GPO Sales Program: formal NRC staff and contractor reports, NRC-sponsored conference proceedings, and NRC booklets and brochures. Also available are Regulatory Guides, NRC regulations in the *Code of Federal Regulations*, and *Nuclear Regulatory Commission Issuances*.

Documents available from the National Technical Information Service include NUREG series reports and technical reports prepared by other federal agencies and reports prepared by the Atomic Energy Commission, forerunner agency to the Nuclear Regulatory Commission.

Documents available from public and special technical libraries include all open literature items, such as books, journal and periodical articles, transactions, and codes and standards. *Federal Register* notices, federal and state legislation, and congressional reports can usually be obtained from these libraries.

Documents such as theses, dissertations, foreign reports and translations, and non-NRC conference proceedings are available for purchase from the organization sponsoring the publication cited.

Single copies of NRC draft reports are available free upon written request to the Division of Technical Information and Document Control, U.S. Nuclear Regulatory Commission, Washington, DC 20555.

ABSTRACT

An evaluation of the seismic capacity of the essential structures for the Zion Nuclear Power Plant in Zion, Illinois, was conducted as part of the Seismic Safety Margins Research Program (SSMRP). The structures included the reactor containment building, the turbine/auxiliary building, and the crib house (intake structure). The evaluation was devoted to seismically induced failures rather than those resulting from combined Loss of Coolant Accident (LOCA) or other extreme load combinations.

The seismic loads used in the investigation were based on elastic analyses. The loads for the reactor containment and turbine/auxiliary buildings were developed by Lawrence Livermore Laboratory using time history analyses. The loads used for the crib house were the original seismic design loads developed by Sargent & Lundy. No nonlinear seismic analyses were conducted.

The seismic capacity of the structures accounted for the actual concrete and steel material properties including the aging of the concrete. Median centered properties were used throughout the evaluation including levels of damping considered appropriate for structures close to collapse as compared to the more conservative values used for design. The inelastic effects were accounted for using ductility modified response spectrum techniques based on system ductility ratios expected for structures near collapse.

Sources of both inherent randomness and uncertainties resulting from lack of knowledge or approximations in analytical modelling were considered in developing the dispersion of the structural dynamic characteristics. Coefficients of variation were developed assuming lognormal distributions for all variables. The earthquake levels for many of the seismically induced failure modes are so high as to be considered physically incredible.

TABLE OF CONTENTS

TABLE OF CONTENTS (Continued)

LIST OF FIGURES

LIST OF FIGURES (Continued)

LIST OF FIGURES (Continued)

LIST OF FIGURES (Continued)

LIST OF TABLES

EXECUTIVE SUMMARY

The evaluation of the seismic capacity of the essential structures of a typical PWR nuclear power plant is presented in this report. This evaluation was completed as part of the Seismic Safety Margins Research Program (SSMRP) being conducted by the Lawrence Livermore National Laboratory (LLNL) for the U.S. Nuclear Regulatory Commission (NRC). The plant selected for the evaluation was the Zion Nuclear Plant located in Zion, Illinois. The structures included in the evaluation were the reactor containment building, the turbine/auxiliary building, and the crib house (intake structure). The investigation was devoted to seismically induced failures rather than those resulting from combined Loss of Coolant Accident (LOCA) or other extreme load combinations. The seismic failure capacities of the structures were determined to occur when the inelastic deformations of the structure were large enough to potentially cause failure or loss of function of the critical equipment, and do not necessarily imply collapse of the structure.

The seismic loads for the reactor containment and turbine/auxiliary buildings were developed by LLNL using time history analysis including soil-structure interaction techniques. The seismic loads used for the evaluation of the crib house seismic capacity were the original design loads developed by Sargent & Lundy. All seismic loads used in this evaluation were based on elastic analysis and no nonlinear seismic analyses were conducted in this phase of the SSMRP although inelastic effects may be expected to be significant at very high seismic response levels.

Although no nonlinear analyses were conducted, a much more accurate assessment of the structure seismic capacities can be expected if the inelastic effects are considered. In the current evaluation, these effects were accounted for using ductility modified response spectrum techniques based on system ductility ratios expected for structures near collapse. Also, the seismic capacities of the structures were based on the actual concrete and steel material properties including

the aging of the concrete. Median centered properties were used throughout the evaluation including levels of damping considered appropriate for structures close to collapse as compared to the more conservative values used for design.

Seismic fragility curves for potential modes of failure for the structures are presented in terms of frequency (or fractile) of failure as a function of either response or ground acceleration level. Sources of both inherent randomness and uncertainties resulting from lack of knowledge or approximations in analytical modelling were considered in developing the dispersion of the dynamic characteristics. For many variables required in the evaluation, inadequate data exists to provide an accurate statistical distribution. For most variables for which data does exist, the lognormal distribution provides a good approximation and coefficients of variation were developed assuming lognormal distributions for all variables.

Some potential modes of seismic failure involve only a localized failure of the structure while others include the entire building. Based on the elastic load distributions used, less confidence exists for capacities of modes of failure which involve sequential failure of a structure. For almost all the lowest capacity failure modes, a median factor of safety of 4 to 5 exists when compared to the SSE design level. Many other potential failure modes have significantly higher factors of safety.

1. INTRODUCTION

The evaluation of the potential seismic failure modes of a system of structures as complex as a nuclear power plant involves consideration of a great many items such as strengths and building response characteristics. In most cases, values of many of the parameters affecting structure seismic capacity levels are not known exactly and substantial dispersion in both material and structure response characteristics exists. Variations can occur in virtually every aspect of the seismic fragility evaluation including structure frequencies and dynamic response, strength and inelastic energy absorption capacity, and structure response effects resulting from different earthquake dynamic characteristics. The dispersion can result from both sources of inherent randomness and from uncertainty concerning the values of the sources. In this context, inherent randomness is considered to represent those sources of dispersion which cannot be reduced by additional analysis or more data. Modelling uncertainty, on the other hand, is considered to be the result of lack of knowledge of material properties and other parameters, and approximations in analytical modelling.

The Seismic Safety Margins Research Program (SSMRP) was developed to investigate the effects of variability in the seismic methodology and obtain quantitative estimates of the conservatism introduced throughout the seismic design and analysis of a nuclear power facility. An overall probabilistic methodology (Reference 1) is being developed by Lawrence Livermore Laboratory (LLL) which will be able to identify and quantify these sources of seismic variability on reactor risk. The facility selected for initial evaluation is the Zion Nuclear Power Plant in Zion, Illinois.

The Zion facility consists of Units 1 and 2 which are comprised of several structures. The most important of these from the viewpoint of seismic safety are the containment building, the turbine/auxiliary building, and the crib house (intake structure). The auxiliary building and the turbine buildings for Units 1 and 2 are structurally coupled and include the diesel generator buildings and the fuel storage building. Also included in this report is an evaluation of the seismic capacity of the condensate storage tanks and a typical underground pipe.

This investigation is directed principally towards seismically induced failure of structures. Equipment anchorage failure involving shear or pullout of concrete anchor bolts or local equipment failures are not discussed in this report. Although such details may be within the civil/structural scope of supply, this type of failure results from equipment response which is not considered here. Also, the emphasis is on seismically induced failure modes rather than on those resulting from combined Loss of Coolant Accident (LOCA) or other extreme load combinations. This assumption was based on the low probability of the maximum earthquake and LOCA loads occurring at the same time. Even if a LOCA occurs as a result of an earthquake, sufficient time may be expected to elapse such that the maximum seismic and LOCA loads are not expected to occur together. Should such an event occur, however, as for instance in the possible case of aftershocks, a significant amount of the capacity within the containment vessel would not be available to withstand the seismic loads. For the most part, failure of equipment is not expected to significantly effect the seismic fragility levels of the structures within which the equipment is housed. This is due to the relatively small mass of most equipment items. However, some exceptions exist such as failure of the reactor building polar crane which can result in loss of liner integrity and possibly in loss of some prestress tendons, pressurizer enclosure structure failure, etc. More significant would be damage to the pressurizer or steam generators with subsequent LOCA, which would affect the seismic capacity of the containment vessel significantly.

To some extent, modes involving soil foundation failures are discussed insofar as they result in structural failure. However, failure modes involving soil liquefaction, surface faulting, tsunamis, etc., are considered outside the scope of this evaluation. The effects of inelastic energy dissipation are included in the determination of the structural fragility levels by means of simplified approaches based on reductions from linear response levels. No nonlinear analysis of any of the Zion structures was conducted during Phase I of the SSMRP. In actuality, very few structures respond completely elastically, even at very low response levels. Variations in dynamic response characteristics of structures would normally be expected during and after virtually any level of earthquake. Often, however, the structure will shake down for low to moderate level earthquakes so that variations due to subsequent excitations may not be as large as from the initial excitation.

The earthquake levels for seismically induced failure for many of the failure modes discussed in this report are so high as to be physically incredible. The ability of the soil to transmit forces of this magnitude does not exist. Also, other effects such as the structures being thrown in the air would be expected before the levels required for many of these failures are reached. Fragility curves for some of these failure modes are included for completeness, however, and to indicate the extreme remoteness of failure expected.

2. METHOD OF FRAGILITY EVALUATION

The approach used in the evaluation of the Zion structures fragility levels is to compute median factors of safety compared to the original design values for the important parameters and determine the variability associated with each parameter. Variability in the dynamic response and failure levels of structures can originate from a great many potential sources. Many of these sources are associated with the random variability resulting from material properties and geometry. Other sources are introduced by modelling uncertainties caused by lack of precise knowledge by the analyst. Often, these modelling uncertainties are recognized, and conservative assumptions are introduced to account for them at various stages throughout the analysis process. These tend to introduce a systematic bias in many aspects of the analysis, which may or may not be recognized. In many cases, this bias is legislated by code or licensing requirements.

It is often difficult to completely separate random variability and uncertainty. An attempt to do so has been maintained throughout this investigation, however. Much of the uncertainty associated with analytical assumptions and techniques will be quantified during Phase I for the reactor buildings and the turbine/auxiliary building. Similar analyses will not initially be conducted for the crib house. In order to provide a more direct comparison of failure levels for the three structures as well as provide an evaluation of the uncertainty, variations due to both random effects and modelling uncertainties are provided.

In order to develop quantitative estimates of the variability, it is necessary to define a mean or median value of the parameter and a measure of dispersion in terms of standard deviation depending on whether a normal, lognormal, or other distribution is used. For most sources of random variability, inadequate information exists to exactly define which statistical distribution most accurately represents the data. For most sources of structural variability, the lognormal distribution provides a good representation (Ref. 2 and 3), so long as the extreme tails are not of primary concern. Furthermore, the central limit theorem states that a distribution consisting of products and quotients of distributions of several variables tends to be lognormal even if the individual variable distributions are not lognormal. Also, the lognormal distribution is mathematically tractable. For all variables discussed in this evaluation of the dynamic characteristics of structures, a lognormal distribution is assumed. For values of the logarithmic standard deviation less than about one-half, the logarithmic standard deviation and the coefficient of variation (COV) are approximately equal and are often used interchangeably.

2.1 ZION DESIGN BASIS

The Zion Nuclear Power Generating Station was designed in the late 1960's in accordance with criteria and codes in effect at that time (Ref. 4). Some additional reanalysis has subsequently been performed. The plant was designed to withstand both an Operating Basis Earthquake (OBE) and a Design Basis Earthquake (DBE). For the OBE loading condition, the Nuclear Steam Supply System (NSSS) was designed to be capable of continued safe operation. For the DBE loading condition, the Reactor Coolant System (RCS) and its components were designed to assure no loss of function. The peak ground acceleration levels used in the design of structures and equipment are:

	Horizontal (g)	Vertical (g)
OBE	0.08	0.05
DBE	0.17	0.11

The original design ground response spectra for the OBE and DBE are shown in Figures 2-1 and 2-2, respectively.

Structure and equipment were originally divided into three seismic classes. The seismic definitions are:

SEISMIC CLASS I

Those structures, mechanical components, the reactor protection system, and engineered safety feature actuation system whose failure might cause or increase the severity of a loss-of-coolant accident (LOCA). Also, those structures and components vital to safe shutdown and isolation.

SEISMIC CLASS II

Those structures and mechanical components not Class I which function in direct support of reactor operation.

SEISMIC CLASS III

Those structures and components which are neither Class I or Class II.

With the exception of the condensate storage tank and some buried piping, all the systems identified as important to safety are located in Class I structures. The containment building and the auxiliary building are both Class I structures. The diesel generator buildings are located at both ends of the auxiliary building and form an integral structure with the auxiliary building. The control room is located in the auxiliary building. That portion of the intake structure (crib house) enclosing the service water pumps and related essential piping is also a Class I structure.

The basic design criteria of the containment structure was to ensure that the integrity of the liner was guaranteed under all loading conditions and to ensure the structure has a low-strain elastic response so that this response was predictable under the required load conditions (Ref. 4). The design was in accordance with ACI Code 318-63 (Ref. 5) except for several more conservative restrictions. The Zion design did not make use of the ultimate strength assumptions of the ACI Code for concrete beams in flexure which permit strains beyond yield. The maximum strain in the concrete was limited to that corresponding to the 28-day design compressive strength (f_c').

The reinforcing steel forming part of the load carrying system was allowed to reach yield strength, but no yielding was allowed. A further definition of "yielding" was that deformation of the structure did not cause strains in the steel liner to exceed 0.005 in/in. The yielding of non-prestress reinforcing steel was allowed, either in tension or compression, provided the liner strain was not exceeded. The allowable stresses for both the working stress design and the yield limit design are shown in Table 2-1.

Based on a soil investigation conducted by Dames and Moore, the ultimate soil bearing capacity was determined to be 40,000 psf. The design allowable soil bearing pressures were 13,000 psf for permanent loads, and 16,000 psf for short-term loads.

2.2 DIFFERENCES BETWEEN DESIGN CRITERIA AND FRAGILITY EVALUATION

A number of differences exist between criteria used for design of structures and those used for evaluation of failure levels. For design, conservative assumptions are made where uncertainties exist. In determining fragility levels, an attempt is made to determine median centered properties for all parameters. Since the design of Zion, a number of changes in design and qualification criteria for structures have been implemented. The general trend has been to increase allowable stresses but also to increase the number of loading conditions to be considered simultaneously.

The degree of sophistication used in analysis has also increased since the design of Zion. However, many uncertainties, such as specification of appropriate ground response spectra, directional combinations, modal combinations, and soil-structure interaction effects, still currently exist. The seismic safety margins and variabilities for many of these parameter will be determined for the Zion reactor building and turbine/auxiliary building as part of the SSMRP. Consequently, for these structures, a fragility parameter such as response at a location within the structure is a logical choice assuming median centered strength and ductility values are used in the fragility evaluation. For the crib house, however, no new analysis is being conducted as part of Phase I of the SSMRP. For this structure, differences in expected modal combination methods, directional components, damping, ground resp se spectra, and soil-structure effects used in design compared to current methodology must be considered in addition to strength and ductility capacities. The remainder of this section discusses some of the more important of these differences. Strength and ductility capacities are discussed in the following chapter.

2.2.1 Damping

Damping values used for design analysis of current plants are typically those specified in R.G. 1.61 (Ref. 6). These values are considered to be quite conservative, particularly at response levels of structures and equipment near or at failure levels. Very little actual test data exists at failure levels, particularly for structures. However, the damping values recommended in Refs. 7 and 8 are considered representative. These damping values for structures and equipment at or near yield are shown in Table 2-2 together with those used for design analysis for the DBE. In accordance with Ref. 7, the lower levels of the pairs of values shown in Table 2-2 are considered to be nearly lower bounds while the upper levels are considered t essentially average values. The values of damping used for thi uation for all structures were taken from Table 2-2 assuming the upper level to be a median value.

2.2.2 Load Combinations

The Zion design criteria combined the DBE seismic loading of 0.17g with normal loading functions such as pressure, weight and other mechanical loads. In the containment design, the LOCA static pressure was also combined with the DBE and normal loading. Current load combination criteria specified in Ref. 9 define a large number of load combinations that must be considered in design. These combinations include a combination of the SSE and transient LOCA loads. Such combinations of events have an extremely low probability of occurrence, and even given the condition of the SSE event, the probability of peak responses to transient LOCA events coinciding with peak response to a short duration earthquake is considered small. It is assumed in this study that there is a much greater probability of the event that some of the safety equipment that is most seismic sensitive would fail in a relatively larger seismic event than the event that equipment affected by both a LOCA transient load and a seismic load would fail in a situation (i.e., relatively smaller seismic event) where a combination of peak responses to both loads would be necessary to induce failure. Consequently, no attempt was made in this study to include transient LOCA or other extreme load events with seismic events to determine safety factors and variability for the combined dynamic events.

2.2.3 Combination of Responses for Earthquake Directional Components

In the Zion plant design analyses, the greatest horizontal response to seismic excitation was added absolutely to the vertical response to obtain resulting design level stresses.

Current criteria specified in Regulatory Guide 1.92, Ref. 10, require that the two horizontal direction responses and the vertical direction response for the end item of interest be combined as the square-root-of-the-sum-of-the-squares of the three components. This approach can lead to inconsistencies between loads, displacements and stresses depending on what is considered the end item of interest and depending on the geometry of the structure. An alternate method (Ref. 7) consists of combining 100% of the response due to one earthquake component with 40% of the response due to the other components. This approach is simpler to use than the SRSS method and has the advantage of retaining a consistent load and stress relationship. This method is assumed to be median centered and is used in the current study for all structures. For most structures, both methods yield similar results which are more realistic than used in the original Zion analysis.

2.2.4 Free Field Structural Response Spectrum Anchored to Peak Ground Acceleration

The Zion plant was designed for the response shown in Figures 2-1 and 2-2. Typical current practice is to specify either site dependent spectra, or, more often, broadband ground spectra such as those in R.G 1.60 (Ref. 11). These spectra are based on the mean plus one standard deviation of spectra generated from a series of strong-motion earthquake records that include horizontal and vertical components for both rock and soil sites. Considerations of response spectra do not directly affect the fragility evaluations of either the reactor building or the auxiliary building since building responses for these structures will be determined from a series of time history analyses. Only if a significant shift in load distribution (as opposed to load magnitude) were observed from the results of time history analyses compared to the response spectrum results would the shape of the response spectrum be of importance for the reactor and auxiliary buildings. Since no new time history results are being generated for the crib house, the assumption is made that the loads obtained from the original response spectrum design analysis may be used once they have been modified to reflect the effects of what is currently expected to be a median centered ground spectrum for soil sites. For this reason, 50 percentile spectra for alluvium sites (Ref. 12) were used as the median centered values for the crib house evaluation.

Rather than compare response spectra directly for equal damping values, it is more informative to include representative damping expected at high levels of response rather than the low levels used for design. Figure 2-3 shows a comparison of the DBE ground response spectra used for design with corresponding median centered spectra from Ref. 12. For concrete structures, for instance, the 2 or 5% damped design spectrum may be compared with the more representative 10% damped spectrum used for this evaluation.

In general, the damping values used in the design of Zion are lower than the median expected damping values at failure response levels both for structures and equipment. Thus, while the original design spectra for given damping values are generally less than current median centered spectra, this is offset by larger expected damping levels.

2.2.5 Location at Which Free Field Ground Response Spectra Are Specified

In the Zion plant designs, the ground response spectra were specified to occur at the foundation level for all structures regardless of the depth of the foundation. Consequently, for partially embedded structures on soil sites, the Zion plant design criteria were more conservatively applied than current criteria would require.

In current plant analysis, the design response spectra are specified at the free ground surface of the site in the absence of any structures. The designer is allowed to account for a moderate amount of deamplification of ground motion with depth below the ground surface. This effect will be determined for the reactor buildings and auxiliary building as part of the soil-structure interaction analysis of the SSMRP. For the soil site at Zion, the ground motion applicable to the foundation of a partially buried structure such as the crib house is also expected to be reduced from the motion at the ground surface when the design response spectra are specified at the free ground surface. In order to provide a more realistic comparison of fragility levels between the reactor and auxiliary buildings and the crib house, this effect must be estimated for the crib house.

2.3 FORMULATION USED FOR FRAGILITY CURVES

Seismic induced fragility data are generally unavailable for nuclear power plant structures. Thus, fragility curves must be developed primarily from analysis combined heavily with engineering judgment supported by very limited test data. Such fragility curves will contain a great deal of uncertainty, and it is imperative that this uncertainty be recognized in all subsequent analyses. Because of this uncertainty, great precision in attempting to define the shape of these curves is unwarranted. Thus, a procedure which requires a minimum amount of information, incorporates uncertainty into the fragility curves, and easily enables the use of engineering judgment, was used in this investigation.

The entire fragility curve for a structure and its uncertainty can be expressed in terms of the best estimate of the median ground acceleration or in-structure response capacity, $\check{A}$, times the product of random variables. Thus, the parameter, A, corresponding to failure us given by:

$$A = \check{A}\,\epsilon_R \epsilon_U \qquad (2\text{-}1)$$

in which ϵ_R and ϵ_U are random variables with unity median representing the inherent randomness (frequency) about the median and the uncertainty (probability) in the median value. Equation 2-1 enables the fragility curve and its uncertainty to be represented as shown in Figure 2-4.

Next, it is assumed that both ϵ_R and ϵ_U are lognormally distributed with logarithmic standard deviation of β_R and β_U, respectively. The advantages of this formulation are:

1. The entire fragility curve and its uncertainty can be expressed by three parameters - $\check{A}$, β_R, and β_U. With the very limited available data on fragility, it is much easier to only have to consider three parameters rather than the entire shape of the fragility curve and its uncertainty.

2. The formulation in Equation 2-1 and the lognormal distribution are very tractable mathematically.

Another advantage of the lognormal distribution is that it is easy to convert Equation 2-1 to a deterministic composite "best estimate" fragility curve (i.e., one which does not separate out uncertainty from underlying randomness) defined by:

$$A = \check{A}\,\epsilon_C \qquad (2\text{-}2)$$

where ϵ_C is a lognormal random variable with unity median and logarithmic standard deviation β_C given by:

$$\beta_C = \sqrt{\beta_R^2 + \beta_U^2} \qquad (2\text{-}3)$$

This composite fragility curve (shown in Figure 2-4) can be used in preliminary deterministic safety analyses if one only needs a "best estimate" on release frequency and does not desire an estimate of the uncertainty.

The lognormal distribution can be justified as a reasonable distribution since the statistical variation of many material properties (References 2 and 3) and seismic response variables may reasonably be represented by this distribution so long as one is not primarily concerned with the extreme tails of the distribution. In addition, the central limit theorem states that a distribution consisting of products and quotients of distributions of several variables tends to be lognormal even if the individual variable distributions are not lognormal. Use of this distribution for estimating frequencies of failure on the order of one percent or greater is considered to be quite reasonable. Lower frequency estimates which are associated with the extreme tails of distribution must be considered more suspect. However, use of the lognormal distribution for estimating very low failure frequencies of components or structures associated with the tails of the distribution is considered to be conservative since the low probability tails of the lognormal distribution generally extend further from the median than actual structural resistance or response data might extend since such data generally shows cut-off limits beyond which there is essentially zero probability of occurrence.

Characteristics of the lognormal distribution which are useful to keep in mind when generating estimates of $\check{A}$, β_R, and β_U are summarized (References 13 and 14). A random variable x is said to be lognormally distributed if its natural logarithm $\tilde{x}$ given by

$$\tilde{x} = \ln(x) \tag{2-4}$$

is normally distributed with the mean of $\tilde{x}$ equal to $\ln \check{x}$ where $\check{x}$ is the median of x, and with the standard deviation of $\tilde{x}$ equal to β which will be defined herein as the logarithmic standard deviation of x. Then, the coefficient of variation, COV, is given by the relationship:

$$COV = \sqrt{\exp(\beta^2) - 1} \tag{2-5}$$

For β values less than about 0.5, this equation becomes approximately:

$$COV \approx \beta \tag{2-6}$$

and COV and β are often used interchangeably.

For a lognormal distribution, the median value is used as the characteristic parameter of central tendency (50% of the values are above the median value and 50% are below the median value). The logarithmic standard deviation, β, or the coefficient of variation, COV, are used as a measure of the dispersion of the distribution.

The relationship between the median value, $\check{x}$, logarithmic standard deviation, β, and any value x of the random variable can be expressed as:

$$x = \check{x} \cdot \exp(f \cdot \beta) \tag{2-7}$$

where f is the standarized Gaussian random variable (mean zero, standard deviation one). Therefore, the probability that x is less than any value x' equals the probability that f is less than f' where:

$$f' = \frac{\ln (x'/\check{x})}{\beta} \qquad (2\text{-}8)$$

Because f is a standarized Gaussian random variable, one can simply enter standardized Gaussian tables to find the probability that f is less than f' which equals the probability that x is less than x'. Using cumulative distribution tables for the standarized Gaussian random variable, it can be shown that $\check{x} \cdot \exp(+\beta)$ of a lognormal distribution corresponds to the 84 percentile value, (i.e., 84 percent of the data fall below the $+\beta$ value). The $\check{x} \cdot \exp(-\beta)$ value corresponds to the value for which 16 percent of the data fall below.

One implication of the usage of the lognormal distribution is that if a, b, and c are independent lognormally distributed random variables, and if

$$d = \frac{a^r \cdot b^s}{c^t} q \qquad (2\text{-}9)$$

where q, r, s and t are given constants, then d is also a lognormally distributed random variable. Further, the median value of d, denoted by $\check{d}$, and the logarithmic variance β_d^2, which is the square of the logarithmic standard deviation, β_d, of d, are given by:

$$\check{d} = \frac{\check{a}^r \cdot \check{b}^s}{\check{c}^t} q$$

and

$$\beta_d^2 = r^2\beta_a^2 + s^2\beta_b^2 + t^2\beta_c^2$$

where a, b, and c are the median values, and β_a, β_b, and β_c are the logarithmic standard deviations of a, b, and c, respectively.

The formulation for fragility curves given by Equation 2-1 and shown in Figure 2-4 and the use of the lognormal distribution enables easy development and expression of these curves and their uncertainty. However, expression of uncertainty as shown in Figure 2-4 in which a range of peak accelerations are presented for a given frequency of failure is not necessarily very usable in the systems analyses for frequency of release. For the systems analyses, it may be preferable to express uncertainty in terms of a range of failure fractiles (frequencies of failure) for a given ground or response acceleration. Conversion from the one description of uncertainty to the other is easily accomplished as illustrated in Figure 2-5 and summarized below.

With perfect knowledge, (i.e., only accounting for the random variability, β_R), the frequency of failure, $p_{f(A)}$, for a given acceleration A can be obtained from:

$$p_{f(A)} = \Phi\left(\frac{\ln(A/\check{A})}{\beta_R}\right) \qquad (2\text{-}12)$$

in which $\Phi(\cdot)$ is the standard Gaussian cumulative function, $\check{A}$ is the "best estimate" of the median ground acceleration capacity, and β_R is the logarithmic standard deviation associated with the underlying randomness of the capacity. The following simplification in notation will be used:

$$p_f = p_{f(A)}$$
$$p_f' = p_{f(A')}$$
$$p_f'' = p_{f(A'')}$$

i.e., p_f is the frequency of failure based on the underlying randomness associated with ground acceleration A, p_f' is the failure frequency associated with acceleration A', etc. Then, with perfect knowledge (no uncertainty in the frequencies) the ground acceleration A' corresponding to a given frequency of failure p_f' is given by:

$$A' = \check{A} \exp \left[\beta_R \Phi^{-1} \ (p_f') \right] \qquad (2\text{-}13)$$

The uncertainty in ground acceleration capacity corresponding to a given probability of failure as a result of uncertainty of the median capacity can then be expressed by the following probability statement:

$$p \left[A > A'' \mid p_f' \right] = 1 - \Phi \left(\frac{\ln(A''/A)}{\beta_U} \right) \qquad (2\text{-}14)$$

in which $P \left[A > A'' \mid p_f' \right]$ represents the probability that the ground acceleration A exceeds A" for a given failure frequency p_f'. This probability is shown shaded in Figure 2-5. However, one wishes to transform this probability statement into a statement on the probability that the frequency of failure p_f is less than p_f' for a given ground acceleration A", or in symbols $p \left[p_f \leq p_f' \mid A'' \right]$. This probability is also shown shaded in Figure 2-5. It follows that:

$$P \left[p_f \leq p_f' \mid A'' \right] = p \left[A > A'' \mid p_f' \right] \qquad (2\text{-}15)$$

Thus, from Equations 2-13 and 2-14:

$$P \left[p_f \leq p_f' \mid A'' \right] = P \left[A > A'' \mid p_f' \right] \qquad (2\text{-}16)$$

from which:

$$P \left[p_f > p_f \mid A'' \right] = \Phi \left(\frac{\ln(A''/\check{A} \exp \left[\beta_R \Phi^{-1} \ (p_f') \right]}{\beta_U} \right) \qquad (2\text{-}17)$$

which is the basic statement expressing the probability that the failure frequency exceeds p_f' for a ground acceleration A" given the "best estimate" of the median ground acceleration capacity A, and the logarithmic standard deviation β_R and β_U associated with randomness and uncertainty respectively.

As an example, if:

$$\check{A} = 0.77, \qquad \beta_R = 0.36, \qquad \beta_U = 0.39$$

then from Equation 2-17 for typical values of p_f and A",

$$P\left[p_f > 0.5 \mid A'' = 0.40\right] = 0.05$$

which says that there is a 5 percent probability that the failure frequency exceeds 0.5 for a ground acceleration of 0.40g.

TABLE 2-1

ALLOWABLE STRESSES (Ref. 4)

WORKING STRESS DESIGN

CONCRETE				
	Containment	Fiber	f_{cf}	= 3300 psi
		Axial	f_{ca}	= 1650 psi
		Shear	v_c	= 81 psi
	Base Slab	Fiber	f_{cf}	= 2250 psi
		Axial	f_{ca}	Not Applicable
		Shear	v_c	= 78 psi
REINFORCING				
	#18 and #14	Flexure	f_s	= 20,000 psi
	#11 and smaller	Flexure	f_s	= 24,000 psi
		Shear	f_s	= 20,000 psi
			v_s	varies with the area of reinforcing steel

YIELD LIMIT DESIGN

CONCRETE			
	Containment	Fiber	$f_{cf} = \phi f_c' = (0.9)\ (5500) = 4950$
		Axial	$f_{ca} = \phi f_c' = (0.85)\ (5500) = 4670$
		Shear	$v_c = (0.85)\ (148) = 126$
	Base Slab	Fiber	$f_{cf} = \phi f_c' = (0.9)\ (5000) = 4500$
		Axial	$f_{ca} = \phi f_c' = (0.85)\ (5000) = 4250$
		Shear	$v_c = (0.85)\ (141) = 120$
	Reinforcing Steel		
		Flexure	$f_s = \phi f_y = (0.90)\ (60,000) = 54,000$ (psi)
		Shear	$f_s = \phi f_y = (0.85)\ (60,000) = 51,000$ (psi)
			v_s varies with the area of reinforcing steel

TABLE 2-1 (Continued)

NOTATIONS

D	Dead Load
F	Prestressing Force
P	Internal Pressure
E	Design Basis Earthquake
E'	Maximum Credible Earthquake
T_A	Accident Temperature
f_c'	Ultimate Concrete Strength
f_y	Yield Strength of Reinforcing Steel
ϕ	Capacity Reduction Factor
t	Thickness of Concrete Section
p	Reinforcing Percentage
m	Subscript for Meridional Direction
h	Subscript for Hoop Direction
o	Subscript for Outside Face
i	Subscript for Inside Face
f	Subscript for Fiber Stress
a	Subscript for Axial Stress
r	Subscript for Radial Direction
f_c	Allowable Concrete Stress
f_s	Allowable Reinforcing Steel Stress
v_c	Allowable Nominal Concrete Shear Stress (for Reinforced Concrete)
v_s	Shear Stress Carried by the Reinforcing Steel
v	Allowable Concrete Shear Stress Including Shear Reinforcing (if any)
τ	Computed Nominal Concrete Shear Stress
σ_c	Computed Concrete Stress
σ_s	Computed Reinforcing Steel Stress
+	Tensile Stress
-	Compressive Stress
f_s'	Tensile Strength of Prestressing Steel
f'_{ci}	Initial Ultimate Concrete Strength

TABLE 2-2

COMPARISON OF DAMPING VALUES

Type and Condition of Structure	Zion DBE Analysis (Ref. 4) (% of Critical)	Zion Fragility Eval. (at or near yield - Ref. 7) (% of Critical)
a. Vital piping	1	2 to 3
b. Welded steel	2	5 to 7
c. Prestressed Concrete w/o loss of prestress	5*	5 to 7
d. Prestressed Concrete (w/no prestress left)	—	7 to 10
e. Reinforced Concrete	5*	7 to 10
f. Bolted Steel	2	10 to 15

* In the FSAR (Ref. 4), the DBE damping for concrete structures is listed as 5%. However, for the reactor building, the original structure DBE loads were developed on the basis of 2% of critical for both the OBE and SSE.

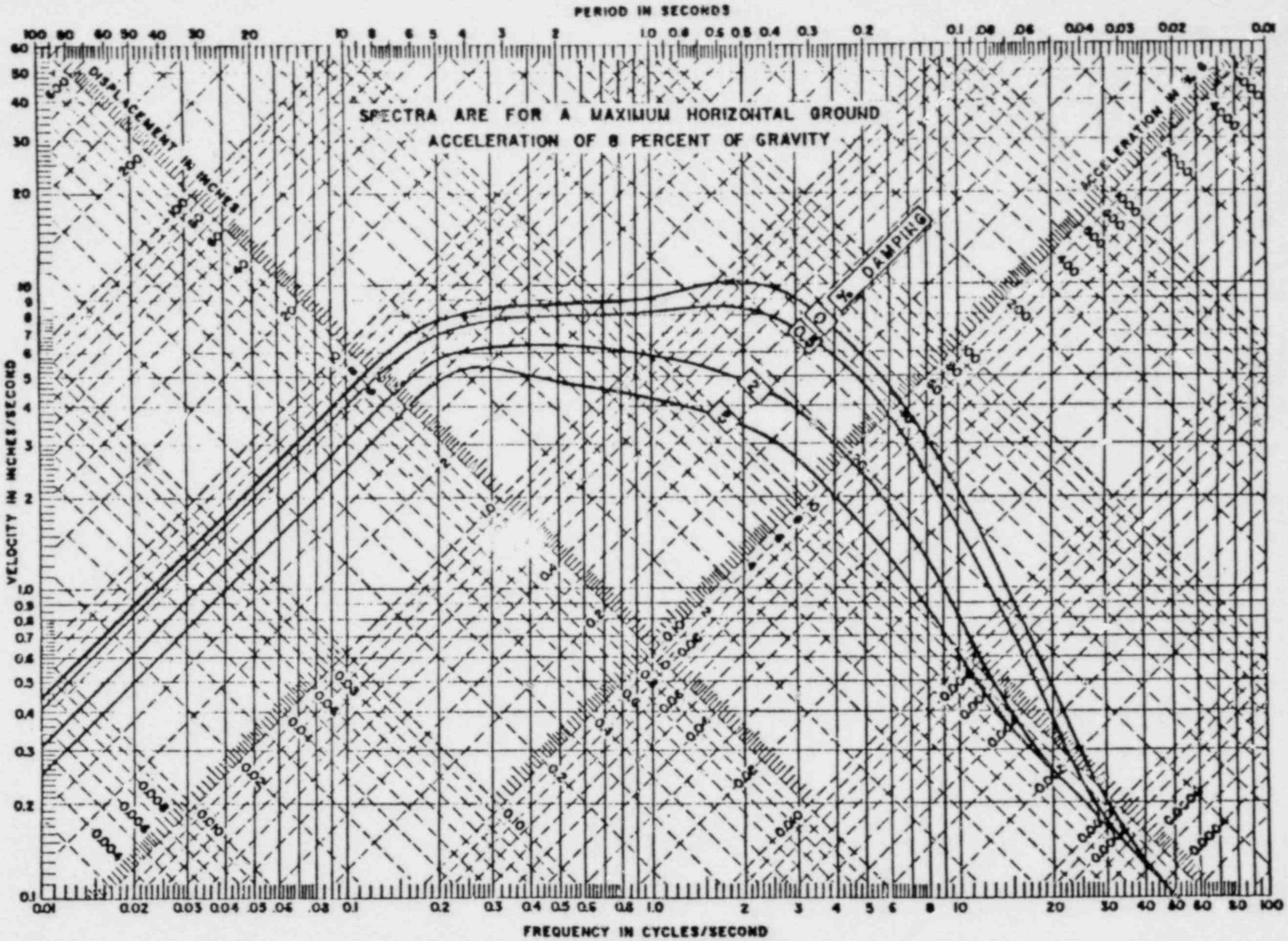

FIGURE 2-1. ORIGINAL OBE GROUND RESPONSE SPECTRA

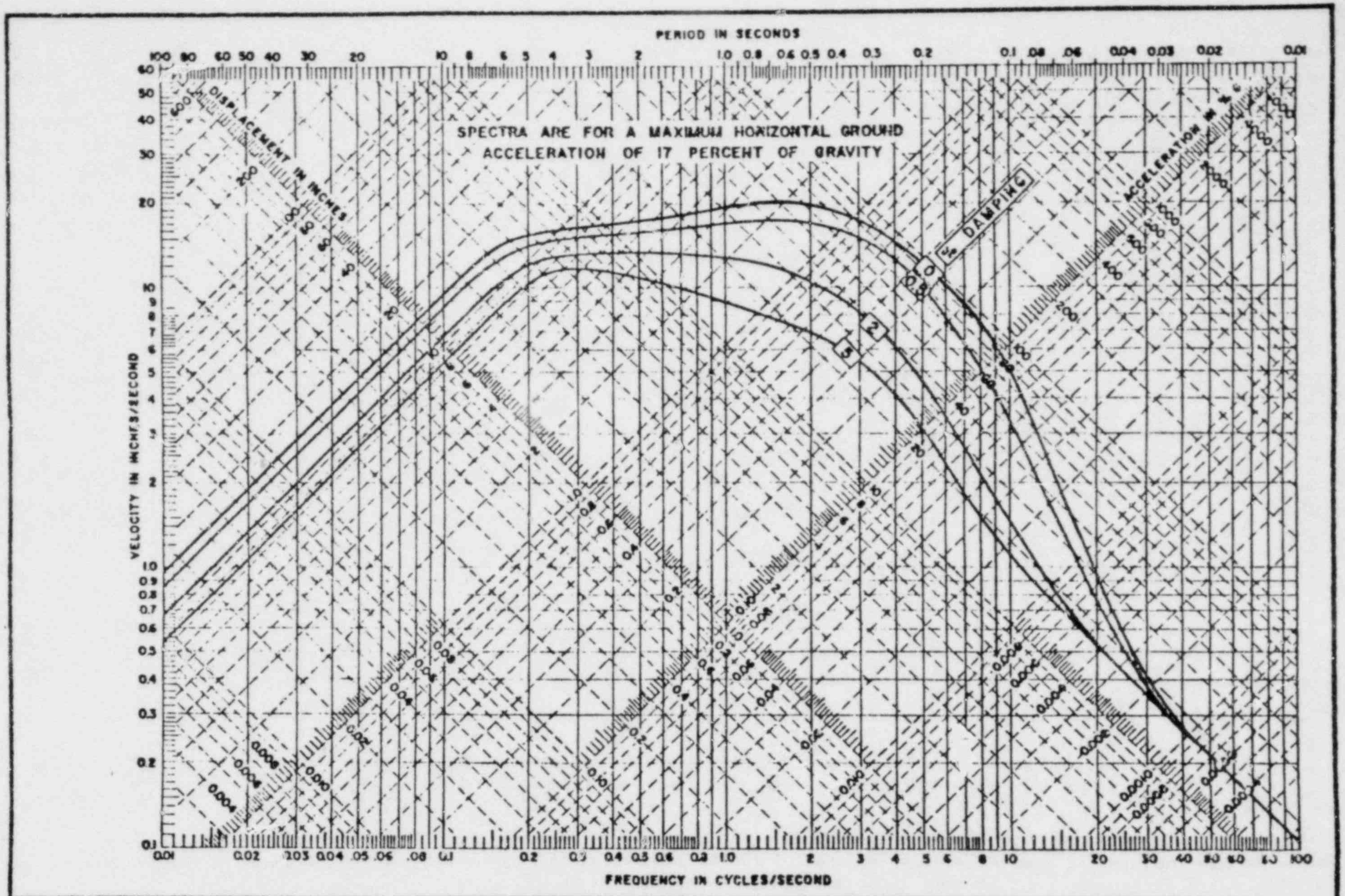

FIGURE 2-2. ORIGINAL DBE GROUND RESPONSE SPECTRA

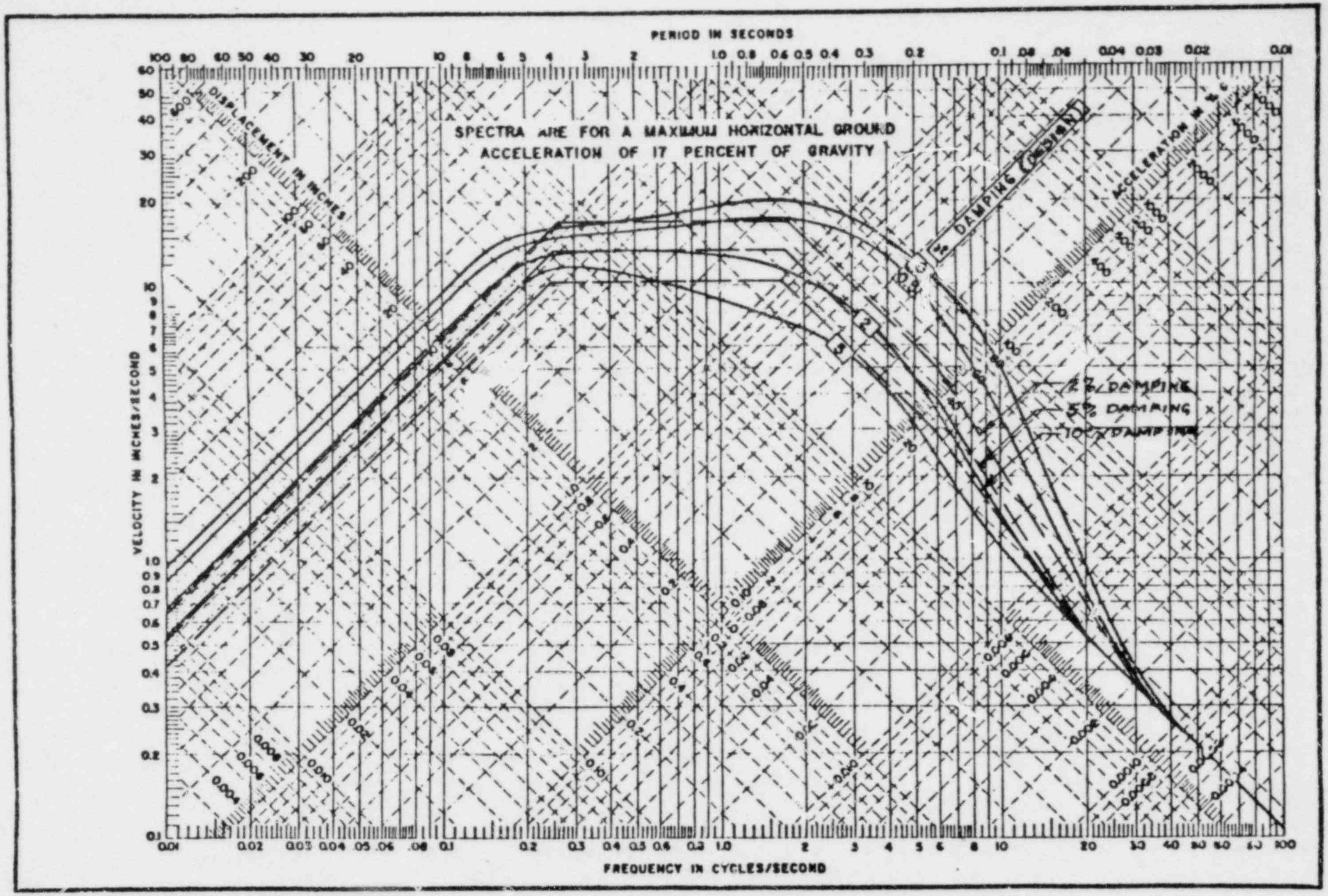

FIGURE 2-3. COMPARISON OF ORIGINAL DBE AND MEDIAN ALLUVIUM SPECTRA

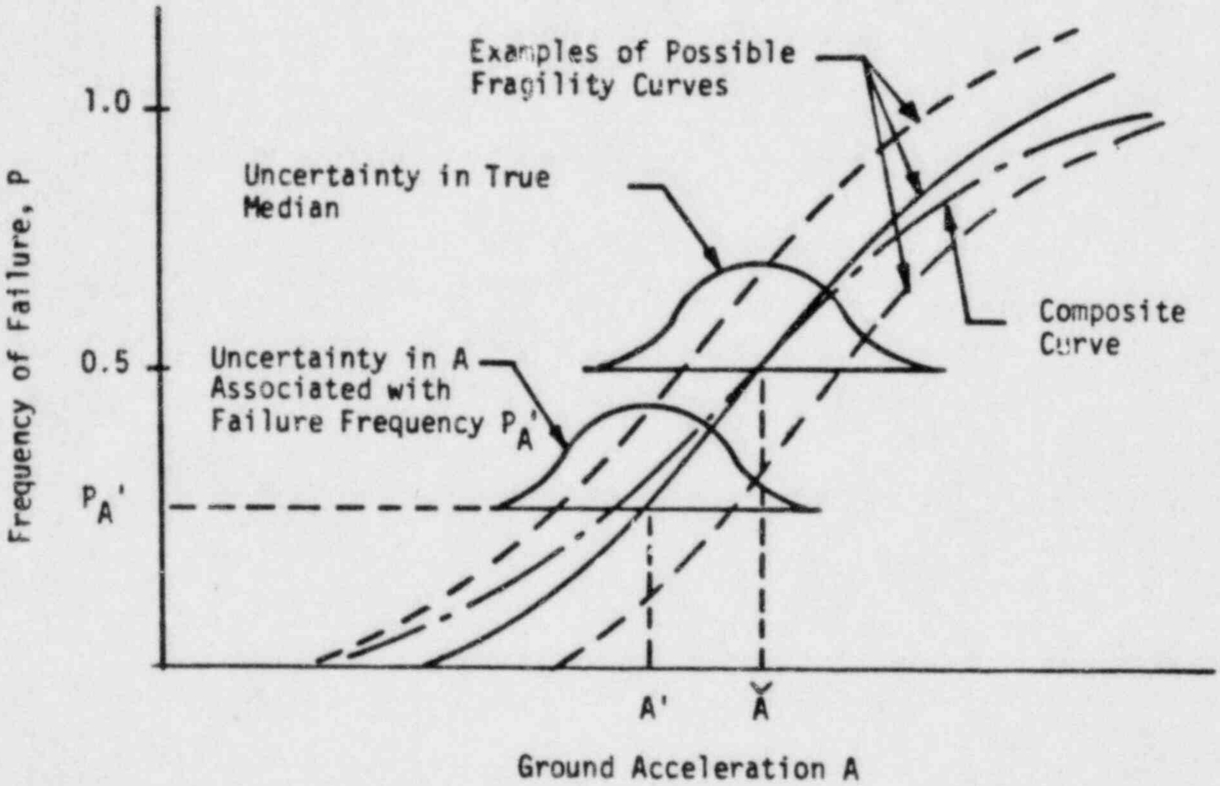

FIGURE 2-4. SIMPLIFIED REPRESENTATION OF FRAGILITY CURVE

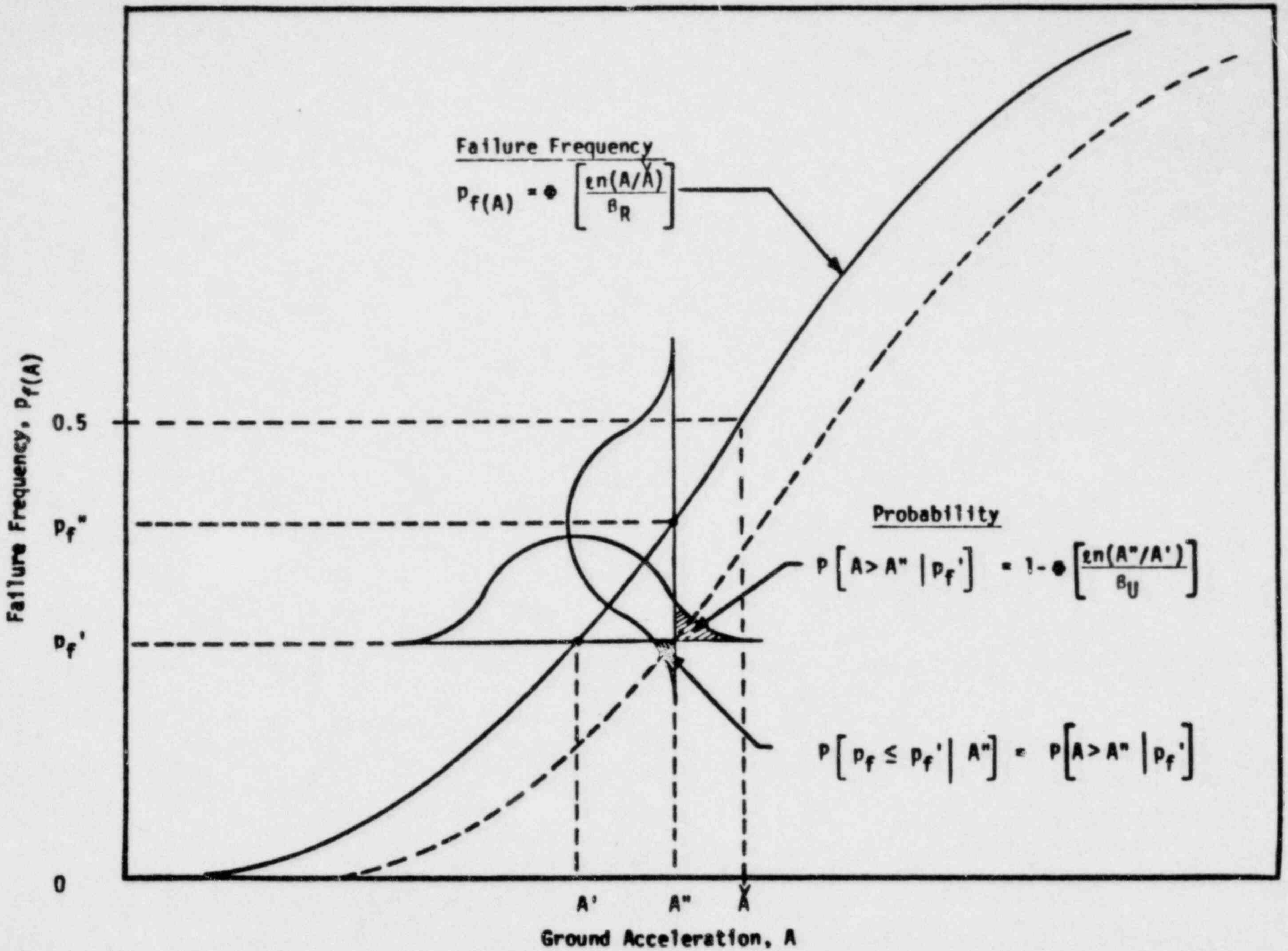

FIGURE 2-5. RELATIONSHIP BETWEEN UNCERTAINTY IN GROUND ACCELERATION FOR A GIVEN FAILURE FREQUENCY AND UNCERTAINTY IN FAILURE FREQUENCY FOR A GIVEN GROUND ACCELERATION

3. CAPACITY EVALUATION

In this chapter, the methods used in the development of the median factors of safety and logarithmic standard deviations for the Zion structures are discussed. Based on these methods, median failure levels together with upper and lower bounds are developed for the individual structures in subsequent chapters.

In order to estimate the median factor of safety against structure or component failure for the DBE ground acceleration (0.17g), it is necessary to define what constitutes failure. For purposes of this study, structures are considered to fail functionally when inelastic deformations of the structure under seismic load are estimated to be sufficient to potentially interfere with the operability of safety related equipment attached to the structure. These limits on inelastic energy absorption capability (ductility limits) chosen for the structures are estimated to correspond to the onset of significant structural damage. This is believed to represent a conservative bound on the level of inelastic structural deformation which might interfere with the operability of components housed within the structure. It is important to note that considerably greater margins of safety against structural collapse are believed to exist for these structures than most cases reported within this study. Thus, the conditional probabilities of failure for a given free field ground acceleration reported herein for structures are considered appropriate for operability limits and should not necessarily be inferred as corresponding to structure collapse. Piping and the condensate storage tanks are considered to have failed once the pressure boundary integrity can no longer be guaranteed.

From the results of the analyses of the structures together with a knowledge of the deterministic design criteria utilized, median factors of safety associated with the DBE ground acceleration of 0.17g can be determined. These are most conveniently separated into those items associated with the seismic strength capacity of the structure and those items associated with the expected structure response. Only the seismic strength capacities are determined for the reactor and auxiliary buildings since the building responses and their uncertainties will be evaluated during the SSMRP structures analysis project.

The factor of safety for the structure seismic capacity consists of two parts:

1. the strength factor, F_s, based on the ratio of actual member strength to the design forces and

2. the inelastic energy absorption factor, F_μ, related to the ductility of the structure

Associated with the median strength factor $\check{F}_s$ and the median ductility factor $\check{F}_\mu$ are the corresponding logarithmic standard deviations β_s and β_μ. The structure strength factors of safety and logarithmic standard deviations vary from structure to structure and according to the different failure modes within a given structure. Factors of safety for the most important modes of failure are summarized in subsequent sections.

The factor of safety, F_R, related to structure response is determined from a number of variables which include:

1. The response spectra used for design compared to the median centered spectra for soil sites from multiple seismic events.

2. Damping used in the analysis compared with damping expected at failure.

3. Modal combination methods

4. Combination of earthquake components

5. Soil-structure interaction effects

6. Soil deamplification with foundation depth

7. Modelling accuracy

These effects are not considered for the reactor buildings or turbine/auxiliary building.

Based on the characteristics of the lognormal distribution, factors of safety and logarithmic standard deviations for the various contributing effects can be combined to yield the overall effects. For instance, the capacity factor of safety of a structure F_c is obtained from the product of the strength and ductility factors of safety which in turn, may include effects of more than one variable.

$$F_c = F_s \cdot F_\mu \tag{3-1}$$

The methods of determining the strength and ductility safety factors are discussed in the following sections. The logarithmic standard deviation on capacity, β_c, is found by:

$$\beta_c = \sqrt{\beta_s^2 + \beta_\mu^2} \tag{3-2}$$

As discussed in Section 2.3, the logarithmic standard deviations are composed of both an inherent randomness and uncertainty in the median value.

The variables which are related to the structure response can be grouped into several main categories for which factors of safety and the logarithmic standard deviations may be combined in a similar manner.

3.1 STRUCTURE CAPACITY

The primary lateral load carrying systems of the major Zion structures are constructed from concrete. The reactor building containment vessels are prestressed while the concrete internal structures and base slabs are reinforced. The upper stories of the auxiliary building includes a braced steel frame structure embedded within the reinforced concrete walls and floor slabs. The braced steel frame structure of the turbine building is not Class I so that the determination of the factors of safety of the major structures is centered primarily on concrete construction and design criteria.

3.1.1 Concrete Compressive Strength

The evaluation of the strength of most concrete elements whether loaded in compression or shear, is based on the concrete compressive strength, f'_c. Concrete compressive strength used for design is normally specified as some value at a specific time from mixing (for example, 90 days). This value is verified by laboratory testing of mix samples. The strength must meet specified values allowing a finite number of failures per number of trials. There are two major factors which justify the selection of a median value of concrete strength somewhat above the design strength.

1. To meet the design specifications, the contractor attempts to create a mix that has an "average" strength somewhat above the design strength.

2. As concrete ages, it increases in strength.

For the Zion Class I structures, results of concrete compression tests are available (Ref. 15). These tests are 90 day strength tests and are divided into tests for the containment buildings and base mats for Units 1 and 2, the auxiliary building foundations, slabs and walls, and the crib house. Table 3-1 shows the average values, standard deviations, and numbers of samples tested.

As concrete ages, its strength increases and this must also be accounted for in determining the median strength compared to the design strength. Figure 3-1 from Reference 16 shows the increase of the concrete compressive strength with time for several different curing methods. It is assumed that the concrete poured in the field is represented by the curve designated as "air cured, dry at test". At 28 days, the concrete has a relative strength of 50% which approaches 60% asymptotically. The factor relating the strength of aged concrete to the 28 day design strength is therefore 1.2. At 90 days, the concrete has a relative strength of 55% so that the factor relating the strength of aged concrete to 90 day design strength is 1.09. No information is available on the standard deviation expected for aging. The estimated logarithmic standard deviation for aging is 0.1. For a small standard deviation, the median may be taken as approximately equal to the mean. Thus, the factor relating median compressive strength including aging effects to design compressive strength is from 1.3 to 1.4 in the reactor buildings base mats and 1.31 to 1.35 in the containment shells. Corresponding logarithmic standard deviations are approximately 0.10 to 0.11. For the auxiliary building, the factor of median to design compressive strength is approximately 1.65 with logarithmic standard deviation of 0.13 for the walls and slabs. The crib house was designed for 3500 psi concrete so that the factor of median to design compressive strength for this building is approximately 1.74, again with a logarithmic standard deviation of 0.12.

Other effects which could conceivably be included in the concrete strength evaluation include some decrease in strength in the in-place condition as opposed to the test cylinder strength, and some increase in strength resulting from rate of loading at the seismic response frequencies of the structures. Although experimental data on these effects are extremely limited, what is available would tend to indicate these effects are relatively small and of the same order of magnitude and since the two effects are opposite, they were neglected.

3.1.2 Reinforcing Steel Yield Strength

Grade 60 reinforcing steel is used throughout the Zion Class I structures. Test results for the yield strength for large and small bar sizes are available (Ref. 15). These results are summarized in Table 3-2. The mean yield strength for No. 3 to 11 bar sizes was found to be 67.2 ksi with a standard deviation of 5.5 ksi and for No. 14 and 18 bars, the mean yield strength was 72.7 ksi with a standard deviation of 7.7 ksi.

Two other effects must be considered when evaluating the yield strength of reinforcing steel. These are the variations in the cross-sectional areas of the bars and the effects of the rate of loading. A survey of information (Ref. 17) determined that the ratio of actual to nominal bar area has a mean value of 0.99 and a coefficient of variation of 0.024. The same reference notes that the standard test rate of loading is 35 psi/sec. Accounting for the rate of loading anticipated in seismic response of structures results in a slight decrease in yield strength of reinforcing steel in tension. This effect is neglected in concrete compression. Below are listed the median yield strengths and logarithmic standard deviations:

	$\check{f}_y$	β_{fy}
No. 3 to 11 bars	66 ksi	0.09
No. 14 and 18 bars	71 ksi	0.11

3.1.3 Shear Strength of Concrete Walls

Recent studies have shown that the shear strength of low rise concrete shear walls with boundary elements is not accurately predicted by the ACI 318-77 (Ref. 18) Code provisions. This is particularly true for walls with height to length ratios in the order of 1 or less. Barda, et al (Ref. 19) determined that the ultimate shear strength of low rise walls they tested could be represented by the following relationship:

$$V_u = V_c + V_s$$
$$= 8.3 \sqrt{f'_c} - 3.4 \sqrt{f'_c}\,(h_w/\ell_w - 1/2) + \rho_n f_y \qquad \text{(psi)} \tag{3-3}$$

where

V_u = Ultimate shear strength
V_c = Contribution from concrete
V_s = Contribution from steel reinforcement
f'_c = Concrete compressive strength
h_w = Wall height
ℓ_w = Wall length
ρ_n = Vertical steel reinforcement ratio
f_y = Steel yield strength

The contribution of the concrete to the ultimate shear strength of the wall as a function of h_w/ℓ_w is shown in Figure 3-2. Also shown in Figure 3-2 are the applicable test values from References 19 through 22 and the corresponding ACI 318-77 formulation. The tests included load reversals and varying reinforcement ratios and h/ℓ ratios. Web crushing generally controlled the failure of the test specimens. Testing was performed with no axial loads, but an increase in shear capacity of $N/4\ell_w h_w$ was recommended, where N is the axial load.

The contribution of the steel to the ultimate shear strength according to ACI 318-77 is

$$V_s = \rho_h f_y \tag{3-4}$$

where ρ_h = horizontal steel reinforcement ratio.

Furthermore, one of the conclusions reached in Reference 21 is that for low rise shear walls (specifically $h_w/\ell_w = 1$), vertical steel has no effect, and the entire contribution to shear strength is due to the horizontal steel.

In order to estimate the effect that the horizontal and vertical steel have, the steel contribution to wall shear strength was determined from test values for the range $0.5 < h_w/\ell_w < 2$. Test data from Refs. 19 through 22 were used. The effective steel shear strength was assumed in the form

$$V_{se} = AV_{sn} + BV_{sh} \tag{3-5}$$

where A, B are constants

$V_{sn} = \rho_n f_y$ = vertical steel contribution

$V_{sh} = \rho_h f_y$ = horizontal steel contribution

The constants A and B were then calculated assuming the concrete contribution to the ultimate stength is given as shown in Equation (3-3). Based on the results of this evaluation, the constants A and B can be shown to be

$A = 1$	$B = 0$	$h_w/\ell_w \leq 0.5$
$= -2.0\,(h_w/\ell_w)+2.0$	$= 2.0\,(h_w/\ell_w)-1.0$	$0.5 < h_w/\ell_w \leq 1.0$
$= 0$	$= 1$	$1.0 < h_w/\ell_w$

and the median ultimate shear strength is given by

$$V_u = V_c + V_{se} \tag{3-6}$$

$$= 8.3\sqrt{f'_c} \;\; -3.4\sqrt{f'_c}\left[(h_w/\ell_w \;\; -1/2) + \frac{N}{4\ell_w/h_w}\right] + \rho_{se} f_y$$

where $\rho_{se} = A\rho_n + B\rho_h$ with A and B determined as shown above.

Based on an evaluation of the same experimental data from Refs. 20 through 23, the logarithmic standard deviation was calculated to be 0.15.

3.1.4 Strength of Shear Walls in Flexure under In-plane Forces

Data on reinforced concrete shear walls failing in flexure under in-plane forces can be found in Reference 22. Equations found in Reference 21 may be used to calculate the moment capacity for walls without chord steel. However, this can be accounted for by increasing the depth from the extreme compression fiber to the neutral axis to account for the yield strength of the tensile chord steel. The compression chord steel is neglected since it is near the neutral axis and its effect on the moment capacity is small. The total moment capacity of reinforced concrete shear walls in flexure under in-plane forces is then

$$M = \frac{A_s f_y \ell}{2}\left(1 + \frac{N}{A_s f_y}\right)\left(1 - \frac{\beta_1 c}{\ell}\right) + A_{ch} f_y \left(d - \frac{\beta_1 c}{2}\right) \quad (3\text{-}7)$$

where c = depth to neutral axis from extreme compression fiber

- A_s = total distributed steel
- A_{ch} = area of chord steel
- ℓ = wall length
- f_y = steel yield strength
- N = axial load
- d = distance from the extreme compressive fiber to the centroid of tensile chord steel
- β_1 = ratio of depth of equivalent rectangular concrete stress block to depth to neutral axis (c)

3.1.5 Strength of Shear Studs

Above El. 592' in the auxiliary building, braced steel framing is embedded in the concrete shear walls. In the common wall between the auxiliary building and the turbine building, steel shear studs are welded to the steel column webs to ensure a composite action between the concrete panels and the braced steel frame, and to provide continuity of the concrete wall across the columns.

Reference 27 reports that the following equation was used to specify design allowable shears for headed steel shear studs in the AISC Code (Reference 28):

$$q = \text{allowable shear}$$

$$= 372d^2\sqrt{f'_c} \quad \text{(lb)}$$

d = stud diameter (in)

f'_c = concrete compressive strength (psi)

Reference 28 notes that the factor of safety applied to the design allowables was 2.50. Thus, the ultimate strength of shear studs is:

$$q_u = 2.5q$$

$$= 930\, d^2\sqrt{f'_c} \quad \text{(lb)}$$

Shear studs typically exhibit brittle failure with a cone of concrete around the studs tearing out.

Since the stud strength varies as the square root of the concrete compressive strength, the random variability of the stud strength will be half that of the concrete strength. Uncertainty is introduced by the accuracy of the stud strength formula. The variability due to uncertainty is estimated to be 0.10. Estimated logarithmic standard deviations associated with randomness and uncertainty are:

$$\beta_R = 0.07$$

$$\beta_U = 0.10$$

3.2 STRUCTURE DUCTILITY

A much more accurate assessment of the seismic capacity of a structure can be obtained if the inelastic energy absorption of the structure is considered in addition to the strength capacity. No inelastic analyses are being performed during Phase I of the SSMRP, so that these effects must be estimated by other means. One tractable method involves the use of ductility modified response spectra to determine the deamplification effect resulting from the inelastic energy dissipation. Early studies indicated the deamplification factor was primarily a function of the ductility ratio, μ, defined as the ratio of maximum displacement to displacement at yield. Recent studies (Reference 23) have shown that for single-degree-of-freedom systems with resistance functions characterized by elastic-perfectly plastic, bilinear, or degrading models, the shape of the resistance function is, on the average, not particularly important. However, as opposed to the earlier studies, more recent analyses have shown the deamplification factor is also a function of the system damping. For systems in the acceleration region of the spectrum (i.e., approximately 2 hz and above), Figure 3-3 from Reference 23 shows the deamplification function for several damping values as a function of the ductility ratio.

The studies on inelastic structures conducted to date have been primarily concerned with single-degree-of-freedom systems. Consequently, considerable uncertainty exists in the application of these techniques to multi-degree-of-freedom systems. Questions of the appropriate system ductility to use once individual element or story ductilities have been determined exist, and the relationships between deamplification factors for acceleration and shear forces for MDOF systems is unknown. The assumption made in this investigation is that the average or system ductility expected will be close to the story ductility ratio for well-designed structures. For buildings with large localized ductilities, however, this assumption can be nonconservative.

Ductility ratios for reinforced concrete shear walls failing in shear from reversed loads were calculated from load deflection envelopes given in Reference 22. Only walls tested with axial loads were included in this evaluation. Assuming a lognormal distribution and using the applicable test data from Reference 22, a median shear wall ductility ratio of approximately 4 was calculated. The corresponding logarithmic standard deviation was calculated to be 0.18. The system ductility of a structure as complex as the Zion auxiliary building is typically less than the individual wall ductilities. A system ductility ratio of 2 was estimated for the auxiliary building.

3.3 STRUCTURE RESPONSE

The variables that effect the calculated response of structures other than the reactor and turbine/auxiliary building to a seismic event with a given free field ground acceleration can be conveniently grouped into four primary categories which are:

- Modal response to the specified seismic event
- Combination of modes
- Combination of earthquake components
- Soil structure interaction effects

Damping effects may be included in the modal response factor if different from the analysis from which structure loads were originally obtained as in the case of the crib house. Soil-structure interaction effects for structures other than the reactor buildings and the auxiliary building are limited to reduction in the ground motion between the free ground surface and the ground motion at the depth of the base mat for the crib house.

The median factor of safety on response $\check{F}_R$ calculated for a given peak effective ground acceleration is:

$$\check{F}_R = \check{F}_{MR} \cdot \check{F}_{MC} \cdot \check{F}_{EC} \cdot \check{F}_{SS} \quad (3\text{-}8)$$

where $\check{F}_{MR}$, $\check{F}_{MC}$, $\check{F}_{EC}$, and $\check{F}_{SS}$ are median factors of safety on modal response, mode combination, earthquake component combination, d soil-structure interaction effects, respectively. The logarithmic standard deviation on response β_R is then given by:

$$\beta_R = \sqrt{\beta_{MR}^2 + \beta_{MC}^2 + \beta_{EC}^2 + \beta_{SS}^2} \qquad (3\text{-}9)$$

where β_{MR}, β_{MC}, β_{EC}, and β_{SS} represent the estimated logarithmic standard deviations for each of these four primary response variables.

3.3.1 Modal Response

As discussed in Section 2.2.1,the Zion crib house was designed using the 5% damped ground response spectra shown in Figures 2-1 and 2-2. For the reinforced concrete comprising the lateral load carrying structures for Zion, 10% of critical damping is considered to be the median value expected at response levels near failure. The frequencies of interest for the crib house are well in excess of 1 hz. As is evident from Figure 2-3, the response of this structure using the 10% damped median centered response spectrum for alluvium sites exceeds the 5% damped design spectrum from the range of approximately 0.6 hz up to 20 hz where the two spectra become coincident. For the crib house, the normal modes and participation factors are known so that from the original design analysis the modal response factor of safety for the individual structures can be calculated using the modal contributions on a mode by mode basis. The modal response factor of safety is represented by:

$$\check{F}_{MR} = \frac{S_{D_{\zeta = 2,\ 5\%}}}{S_{m_{\zeta = \zeta = \zeta_m}}} \qquad (3\text{-}10)$$

where $S_{D_{\zeta = 5\%}}$ represents the 5% damped design spectral acceleration and $S_{M_{\zeta=10\%}}$ represents the median spectral acceleration associated with the median damping level of 10% of critical for failure.

In computing the modal factor of safety, it is convenient to combine the damping and ground response spectrum effects. In the development of logarithmic standard deviations on modal response, however, it is informative to consider the damping effects separately. This implies a factor of safety of unity on damping alone since it has already been included in the factor of safety on modal response. The logarithmic standard deviation on modal response can be estimated from:

$$\beta_{MR} \quad \sqrt{\beta_{SA}^{2} + \beta_{\zeta}^{2} + \beta_{M}^{2}} \tag{3-11}$$

where β_{SA} is the logarithmic standard deviation on spectral acceleration for a given ground acceleration, based on median estimates of damping and modal frequency, β_{ζ} is the deviation on spectral acceleration resulting from variability in damping, and β_M is the deviation on spectral acceleration from variability on estimated modal frequencies (modelling error).

β_{SA} may be obtained from the results presented in Reference 12 for alluvium soil sites in accordance with the relationship

$$\beta_{SA} \approx \ln\left(\frac{S_{+\beta_{\zeta} = 10\%}}{S_{M_{\zeta} = 10\%}}\right)$$

where $S_{+\beta_{\zeta=10\%}}$ is the 84% probability of non-exceedance 10% damped spectral acceleration and $S_{M_{\zeta=10\%}}$ is the median 10% damped spectral acceleration. Similarly, β_{ζ} can be estimated from

$$\beta_{\zeta} \approx \ln\left(\frac{S_{M_{\zeta} = 7\%}}{S_{M_{\zeta} = 10\%}}\right)$$

Variability in modelling predominantly influences the calculated mode shapes and modal frequencies. Since the concrete strength and, consequently, the stiffness of the crib house is above the design value, calculated frequencies would be expected to be somewhat less than actual values. Since the response of the crib house is not strongly dependent on the frequency for 10% damping, the assumption is made that the calculated frequencies and mode shapes are median centered for this structure. Consequently, these sources of variability do not influence the calculated median factor of safety on modal response. However, the modelling uncertainties from both the mode shapes and modal frequencies do enter into the uncertainty on calculated modal response as defined by β_M. Thus,

$$\beta_M = \sqrt{\beta_{MS}^2 + \beta_{MF}^2}$$

where β_{MS}, and β_{MF} are estimated logarithmic standard deviations on structural response of a given point in the structure due to uncertainties in mode shape and due to uncertainties in modal frequency, respectively. Based upon experience in performing similar analyses, β_{MS} associated with the crib house is estimated to be about 0.1. The modal frequency variability shifts the frequency at which spectral accelerations are to be determined, so that:

$$\beta_{MF} = \ln\left(\frac{S_{M_{f = f_{-\beta}}}}{S_{M_{f = f_M}}}\right)$$

where f_M is the median frequency estimate, and $f_{-\beta}$ is the 84 percent exceedance probability frequency estimate. The logarithmic standard deviation on frequency is estimated to be about 0.2 for the crib house.

For the crib house, the modal factors of safety vary from 0.77 to 1.0 with an overall value of 0.84 to 0.88 for the two principal directions. The overall modal response logarithmic standard deviation for the crib house is approximately 0.16.

3.3.2 Modal Combination

In the seismic design analysis conducted on the crib house, the individual modal responses were combined by the square-root-of-the-sum-of-the squares (SRSS). This is the current recommended practice of the USNRC given in Regulatory Guide 1.92, (Reference 10). Many studies have been conducted to determine the degree of conservatism or unconservatism obtained by use of SRSS combination of modes. Except for very low damping ratios, these studies have tended to show that SRSS combination of modal responses tend to be median centered. The coefficient of variation (approximate logarithmic standard deviation) tends to increase with increasing damping ratios. Figure 3-4 (taken from Reference 24) shows the actual time history calculated peak response versus SRSS combined modal responses for structural models with 4 predominant modes. Based upon these and other similar results, it is estimated for 10% structural damping that for typical structures, a logarithmic standard deviation for modal combination in the range of 0.17 is expected.

For the crib house, the absolute sum response as well as the SRSS response was available (Reference 25) and the logarithmic standard deviation was calculated to be 0.13 to 0.16 depending on the primary direction of excitation assuming the absolute sum was the upper bound.

3.3.3 Combination of Earthquake Components

The design of the Zion Class I structures was based on the absolute addition of one horizontal and one vertical load component. Current recommended practice is to combine the responses for the three principal simultaneous directions by the SRSS method. Alternatively, it is recommended (Reference 7) that directional effects be combined by taking 100% of the effects due to motion in one direction and 40% of the effects from the two remaining principal directions of motion.

Depending on the geometry of the particular structure under consideration together with the relative magnitude of the individual load or stress components, the expected variation in stresses due to either the SRSS or the 100%, 40%, 40% method of load combinations is from -30% to +40% when compared with the original design method. For shear wall structures where the shear walls in the two principal directions act essentially independently and are the controlling elements, the two horizontal loads do not combine to a significant degree except for the torsional coupling. Thus, only the vertical component affects the individual shear wall stress. A moderate amount of vertical load increases the ultimate shear load carrying capacity of reinforced concrete walls slightly. However, there is an equal probability the vertical seismic component will add to or subtract from the deadweight loads at the time of maximum horizontal load. Consequently, for shear wall structures such as the crib house, the factor of safety is not strongly influenced by the directional component assumptions.

For the Zion crib house, the amount of torsional coupling is available on a mode by mode basis. It is computationally more convenient to combine this effect in the factor of safety on strength, however, since the member loads from the design analysis include a cross-axis response contribution. Thus, a unit factor of safety is used for this effect for the crib house although the variability is retained separately.

3.3.4 Soil-Structure Interaction Effects

Two types of soil-structure interaction effects need to be considered in estimating the median response factor of safety and its variability. First, the potential deamplification of ground motion between the free ground surface and the free field ground motion at the depth of the base mat should be considered. Secondly, the relative response of the base slab of the structure and the free field soil at the base slab depth should be considered.

For the design of the Zion Class I structures, the free surface ground response spectrum (defined by the DBE peak ground acceleration of 0.17g) was also assumed to be appropriate at the base slab foundation level. Both wave propagation theory plus a limited amount of experimental data indicate reduction in ground motion with depth below the free ground surface. The amount of reduction which might result with depth is highly controversial. For the crib house foundation, approximately 50 feet below the ground surface in a firm soil site, it is estimated (probably conservatively) that the median ground motion is about 85 percent of that at the ground surface in the 10 to 20 hz frequency range with a coefficient of variaion on this estimate of about 0.15.

No soil-structure interaction effects were included in the original design analyses of the crib house. The analytical model for this structure assumed fixed base conditions, and ignored any radiation of energy from the structure into the soil. Only material soil damping corresponding to 5% equivalent viscous damping was included. Spacial variation of the ground motion over the planar extent of the foundation was also ignored. Both of these factors are considered to result in some slight overestimation of structural response. The combined effects for soil-structure interaction effects for the crib house are:

$$\check{F}_{SS} \approx 1.2; \qquad \beta_{SS} \approx 0.15$$

TABLE 3-1

ZION CONCRETE COMPRESSION TEST RESULTS

(Reference 15)

Reactor Bldg. Base Mat (Unit 1)	
Specified Strength	5,000 psi
Average Strength	5,948 psi
Standard Deviation	570 psi
No. Samples	76
Reactor Bldg. Base Mat (Unit 2)	
Specified Stength	5,000 psi
Average Strength	6,521 psi
Standard Deviation	661 psi
No. Samples	92
Reactor Containment Bldg. (Unit 1)	
Specified Strength	5,500 psi
Average Strength	6,812 psi
Standard Deviation	585 psi
No. Samples	415
Reactor Containment Bldg. (Unit 2)	
Specified Strength	5,500 psi
Average Strength	6,664 psi
Standard Deviation	617 psi
No. Samples	404
Auxiliary Bldg. Foundations	
Specified Strength	4,000 psi
Average Strength	6,072 psi
Standard Deviation	427 psi
No. Samples	22

TABLE 3-1 (Continued)

ZION CONCRETE COMPRESSION TEST RESULTS

(Reference 15)

Auxiliary Bldg. Slabs, Columns, and Walls	
Specified Strength	4,000 psi
Average Strength	6,136 psi
Standard Deviation	704 psi
No. Samples	500
Crib House	
Specified Strength	3,500 psi
Average Strength	5,603 psi
Standard Deviation	606 psi
No. Samples	200

TABLE 3-2

ZION REINFORCING STEEL TEST RESULTS

(Reference 15)

Number 14 and 18 bars	
Average Strength	72.2 ksi
Standard Deviation	7.7 ksi
No. Samples	23
Number 3 to 11 bars	
Average Strength	67.2 ksi
Standard Deviation	5.5 ksi
No. Samples	3,500
Number 14 and 18 bars (elongation)	
Average Elongation	16.5%
Standard Deviation	1.8%
No. Samples	13

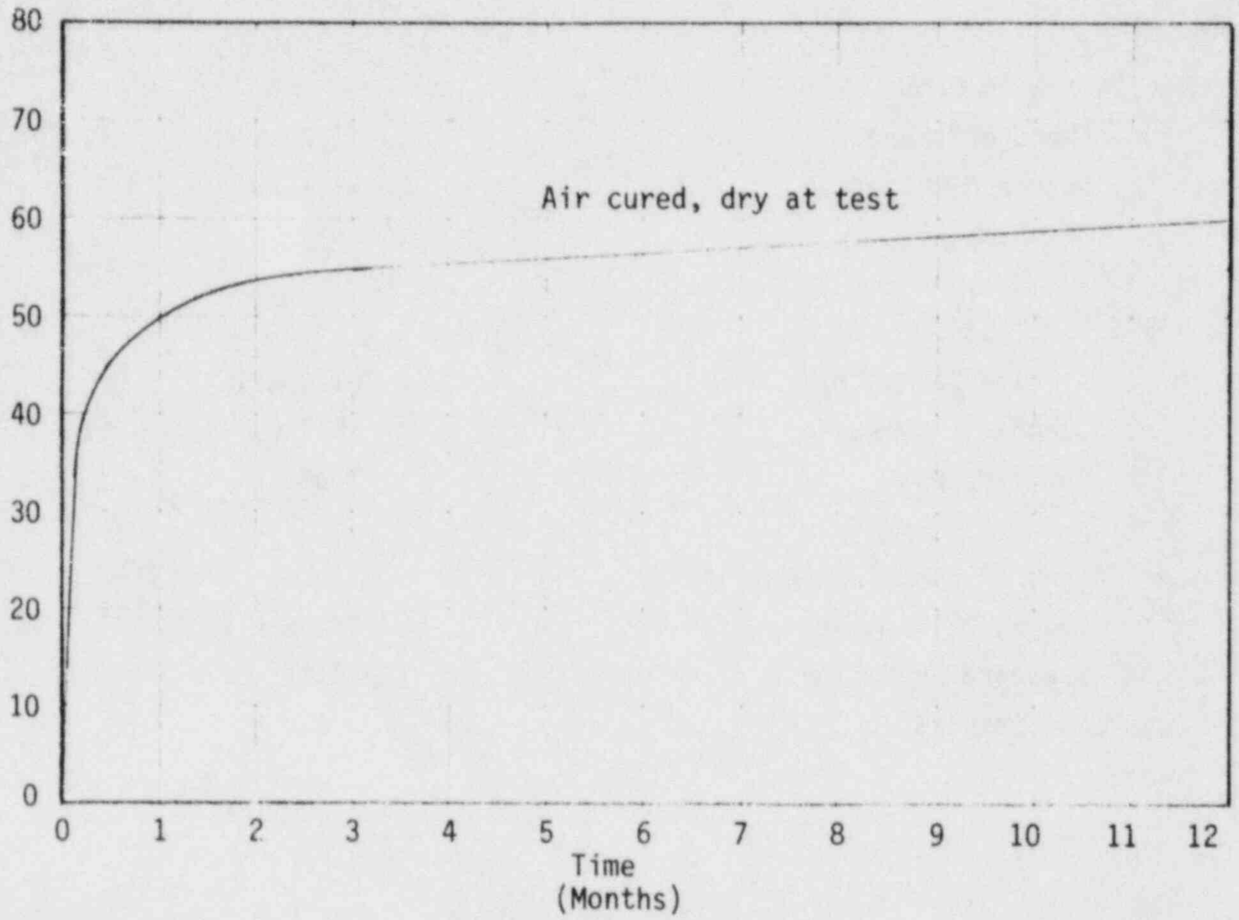

FIGURE 3-1. EFFECTS OF TIME AND CURING CONDITIONS ON CONCRETE STRENGTH (AFTER REFERENCE 16)

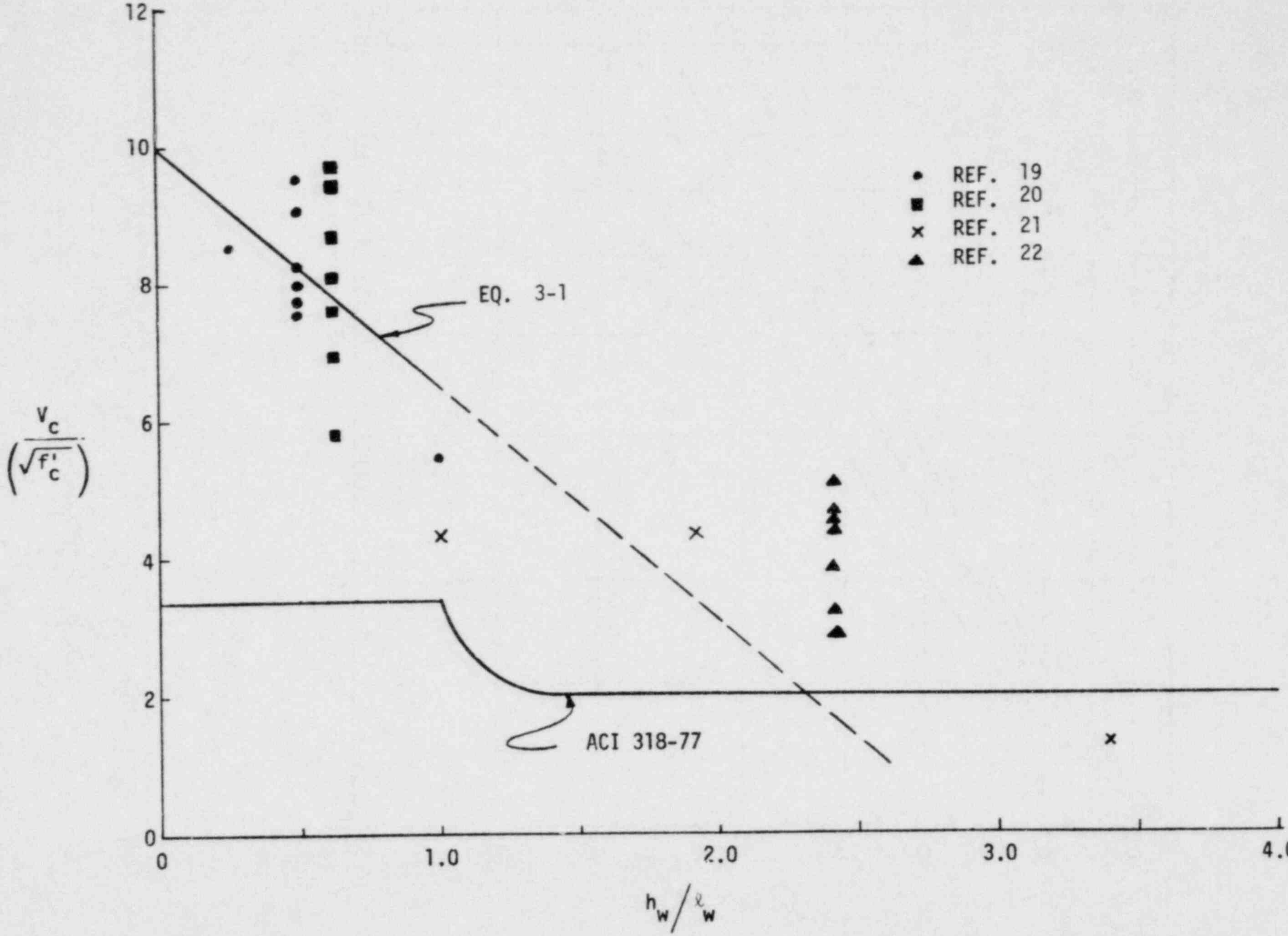

FIGURE 3-2. STRENGTH OF CONCRETE SHEAR WALLS

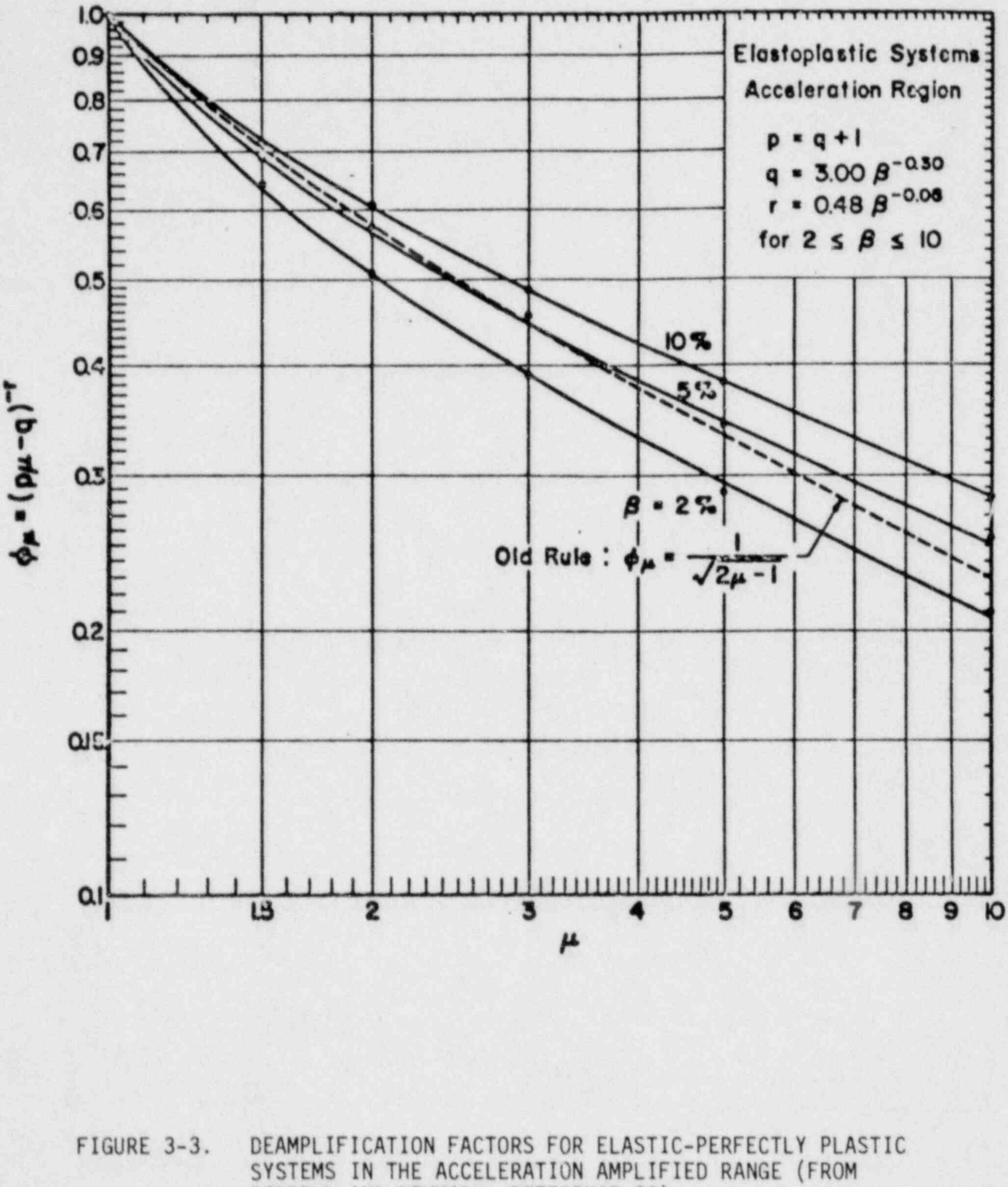

FIGURE 3-3. DEAMPLIFICATION FACTORS FOR ELASTIC-PERFECTLY PLASTIC SYSTEMS IN THE ACCELERATION AMPLIFIED RANGE (FROM RIDDELL AND NEWMARK, REFERENCE 23)

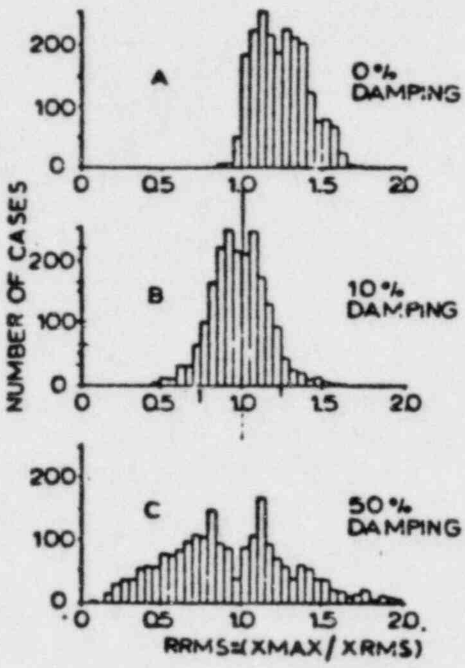

FIGURE 3-4. HISTOGRAMS OF RATIO OF PEAK RESPONSE TO SRSS COMPUTED RESPONSE FOR FOUR-DEGREE-OF-FREEDOM DYNAMIC MODELS (FROM MERCHANT AND GOLDEN, REFERENCE 24)

4. REACTOR BUILDING

4.1 CONTAINMENT VESSEL DESCRIPTION

The reactor containment buildings for Zion Units 1 and 2 are vertical circular cylinders with shallow domed roofs. They enclose the concrete internal structures, the reactor vessels, and reactor coolant systems. The containment vessels and the concrete internals are supported by independent flat circular foundation slabs which include a sump near the center to house the reactor vessel. The cylindrical portion of the containment vessel is prestressed by a post-tensioning system which consists of horizontal and vertical unbonded tendons. The horizontal hoop tendons terminate in one of the six equally spaced vertical buttresses which extend from the base slab to above the spring line of the vessel. The dome is prestressed by a three-way post-tensioning system. Vertical and circumferential reinforcing steel is placed in the cylinder and the dome contains radial and circumferential reinforcing steel toward the outside diameter and reinforcing steel in a rectangular grid near the center. The foundation slab is conventionally reinforced with high-strength steel. Other than the vertical containment vessel tendons which extend through the base slab, no prestressing is used for the base slab. The entire structure is lined with 1/4 inch welded steel plate to provide vapor tightness.

The containment structures for Units 1 and 2 are essentially identical in design and construction. The dimensions for the containment are:

Outside diameter	147'-0"
Wall thickness	3'-6"
Vessel Height	214'-8"
Dome Thickness	2'-8"
Base Slab Thickness	9'-0"
Base O.D.	157'-0"

A vertical section of the containment vessel excluding the concrete internals and equipment is shown in Figure 4-1. Grade elevation is 591'-0" and the top of the base slab is located at elevation 565'-0". Near the center of the slab, a sump which houses the reactor vessel extends from elevation 565'-0" down to elevation 539'-0". The inside diameter of the sump is 21 feet and the wall thickness at this location is 16 feet. The floor slab under the sump is 9 feet thick. A three foot thick reinforced concrete slab was poured on top of the foundation slab. The purpose of this slab is to protect the 1/4 inch steel liner from being damaged by missile impact and provide protection for ducts and piping. However, this slab also extends vertically downward inside the reactor vessel sump and provides additional horizontal shear capacity for the concrete internal structure.

The cylindrical wall of the containment vessel is 3'-6" thick and is prestressed by post-tensioned vertical and horizontal tendons. The horizontal hoop tendons are anchored at the six equally spaced vertical buttresses and the vertical tendons are anchored at the ring girder and bottom of the base slab. The horizontal tendons are located just inside of the outer reinforcing steel as shown in Figures 4-2 and 4-3. The vertical tendons are located in two planes 1'-5" to 2'-0" apart. One plane is just inside the horizontal tendons and the other just outside the inner reinforcing steel. The vertical tendons are staggered in the circumferential direction as shown in Figure 4-4. Nominal bonded reinforcing steel is provided in the wall to distribute strains due to shrinkage and thermal effects. Figure 4 2 also shows the intersection of the wall and the foundation slab. Additional reinforcing steel and stirrups were provided at the intersection to handle the discontinuity stresses.

The configuration of the tendons in the dome is based on a three-way tendon system consisting of three groups of tendons each oriented 120 degrees with respect to each other. These tendons are anchored in the concrete ring girder at the intersection of the dome and cylindrical wall as shown in Figure 4-3. One group of tendons is located in the mid-plane of the 2'-8" thick dome. The second group is located half on the inside and half on the outside of the first group, and the third group is located half on the inside and half on the outside of group 2.

The 1/4 inch thick steel liner plate is fabricated from A442 Grade 60 carbon steel. This provides for leak tightness of the containment building and is anchored to the vessel structure by means of a horizontal and vertical steel angle grid system. The liner was designed for concrete creep and shrinkage, prestress, thermal, and internal pressure loadings.

The minimum gap existing between the reactor buildings and the auxiliary building is 1 inch. Three typical places are: a) roof of the purge system room at elevation 642 ft and roof of the cable penetration vault at elevation 643 ft, b) the floor slab of the pipe chase at elevation 568 ft, and c) between the containment shell and the fuel transfer channel wall of the fuel handling building. At high levels of structure response, the potential for impact between structures exists.

4.2 CONCRETE INTERNAL STRUCTURE DESCRIPTION

Located within the containment vessels are the concrete internal structures. These structures are conventionally reinforced and support the reactor vessel, the steam supply system, the fuel handling pool, and the polar crane. The concrete internal structure consists of a ring wall, operating floor, fuel handling pool, and the reactor biological shield wall. The ring wall is 3'-9" thick with an outside diameter of 106 feet and extends upward from the floor slab at elevation 568 ft to the operating floor at elevation 617 ft. On the operating floor immediately above the ring wall is located the polar crane. Figure 4-5 shows a vertical section through the internals and containment vessel. Figure 4-6 shows the location of the major items of equipment including the reactor vessel, the steam generators, the reactor coolant pumps, and the polar crane.

Inside the ring wall, the reactor biological shield, which is a 8'-6" thick wall with a 34 ft outside diameter, extends downward from approximately elevation 591 ft through the base slab to elevation 542 ft. Below the base slab, the well is surrounded by massive concrete shielding as shown in Figure 4-5.

The floor of the fuel handling pool is continuous with the biological shield at elevation 591 ft., and steps down in two levels so that at the edge of the containment vessel adjacent to the fuel handling building, the floor of the fuel pool is at the same elevation as the bottom of the fuel transfer channel in the fuel handling building as shown in Figure 4-7. Short concrete walls extending upward from the base slab support the floor of the fuel pool (Figure 4-8). The vertical walls rising from the floor of the pool are continuous with the operating floor slab and form the pool boundaries.

The only location where the concrete internals are structurally connected to the containment vessel is at the base of the internal structure (Elevation 568 ft). One foot square by 2 inch deep shear keys connect the ring wall to the 3 foot thick slab above the liner, and 1-3/8" diameter anchor bolts tie the wall into the 9 foot thick foundation slab. A detail of this connection is shown in Figure 4-9. This detail is designed to transmit loads from the internals to the foundation directly without affecting the liner.

There are three major floors inside the containment building. At elevation 568'-0" is located the 3 foot thick reinforced concrete slab poured on top of the liner and foundation slab. There is a 1 inch gap between this slab and the vessel wall which is filled with self-expanding cork. The floor plan is shown in Figure 4-8. At elevations 590 ft. and 617 ft. (operating floor), the floor slabs are constructed of poured-in-place concrete slab, steel grating, or concrete slab supported by steel framing. For the floor slabs located between the ring wall and the containment wall, a 2 inch radial gap exists. Thus, the floor slabs are not designed to act as load transmitting structures between the containment wall and the concrete internal structure.

The 16 inch diameter feedwater pipes and the 34 inch diameter main steam pipes enter the reactor building at elevation 584'-7" through pipe sleeves. The pipes are enclosed in the underground pipe tunnel before entering the containment.

4.3 REACTOR BUILDING FRAGILITY LEVELS

Using the methodology and factors of safety for the contributing effects developed as described in the previous sections, the median fragility levels corresponding to failure can be determined for a number of potential failure modes. Fragility parameters for the reactor building consist of in-structure response accelerations at several locations together with other response parameters as appropriate for the various modes of failure. Since these various response parameters may have different relationships to each other depending on the modal combinations, earthquake dynamic characteristics, etc., it is not possible to provide a direct deterministic correlation between these response parameters. Again, it should be emphasized that failure is defined as occurring when inelastic seismic deformations increase to the extent that the operability of the safety related equipment cannot be guaranteed and does not necessarily imply collapse of the structure. Also, as previously discussed, many of the failure modes are expected to occur only at earthquake levels far in excess of any which can be rationally expected.

4.3.1 Pressurizer Enclosure Failure

One of the lower capacity failure modes resulting from inertia loading within the reactor building is the failure of the pressurizer enclosure and collapse of the enclosure roof. A reinforced concrete structure at the operating floor encloses a portion of the pressurizer which is above the operating floor (Figure 4-10). The pressurizer enclosure has 1 foot thick poured-in-place concrete walls on three sides.

The walls are approximately 39 ft. tall. The fourth wall consists of several pieces of removable concrete panels. The roof is constructed of a 1 foot thick removable concrete slab bolted down to the two walls which are perpendicular to the roof slab span (Figure 4-11).

No diaphragm action is provided by the roof slab due to lack of roof connection to the other two walls and the discontinuity at the center of the roof slab. Because of the open section, considerable torsional response results. The failure mode of the wall will be mainly due to yielding and failure of the wall reinforcing and eventual collapse of the roof and removable panels. This mode of failure is not expected to cause liner damage or result in damage of any of the remainder of the building structure. However, damage to the pressurizer and its associated piping including possible rupture of the reactor coolant pressure boundary should be expected following collapse of the enclosure.

The median effective capacity for this substructure is approximately 1.4g at the reactor building operating floor. Figure 4-12 shows the fragility curves for this failure mode including the upper and lower confidence limits.

4.3.2 Containment Vessel Failure

The containment building will respond to lateral seismic excitation with combined flexure and shear in the structure. Axial stresses resulting from flexure are distributed according to the first harmonic as long as the response of the structure remains linear and discontinuities such as the equipment hatches are neglected. The tangential shear through the cylindrical shell is also distributed according to the first harmonic for elastic lateral response although the location of maximum shear stress is rotated 90° from the location of maximum tension/compression stresses. Axial stresses are reacted by the concrete in compression and by the vertical prestressing tendons and reinforcing steel in tension once the preload has been overcome. Transverse shear is reacted by both radial and tangential shear components in the shell which result from vertical reinforcing steel dowel action and concrete aggregate interlock.

In the Zion containment vessels the tendons are stressed to approximately 60 to 65% of ultimate strength over the life of the structure. For low levels of seismic response, the wall will behave essentially elastically. The concrete is effective in resisting shear and flexural tensile stress in this case. Only after the applied flexural tensile stress exceeds the prestress and the concrete cracks will the bonded reinforcing steel experience any seismic load. The increase in load in the tendons will be small due to the very small increase in strain compared to the preload strain. This occurs because the strain resulting from a crack width is distributed over the length of the unbonded tendon. As the load is increased and the cracks widen, yielding will occur in the reinforcing steel and liner. When the inertia loads are reversed buckling of the reinforcing steel and liner can occur and failure of the liner integrity can result since the steel alone must resist the compressive forces. Local spalling of the concrete outside of the reinforcing steel will result in loss of confinement for the steel and accentuate the failure.

As inelastic response levels are reached, the tangential shear distribution changes. This shear "yielding" occurs due to reduction in dowel stiffness and loss of aggregate interlock as the cracks widen. Any loss of prestress will result in a significant reduction of shear resistance capacity since only the gravity and vertical response loads are available for aggregate "friction". The tangential shear must then be resisted to a larger extent by the bonded reinforcing steel. The dowel action of the reinforcing steel depends on whether the concrete can confine the steel bars. Failure of dowel action can result from either crushing of the concrete or bond splitting along the bar. Initial consequences of shear type failure will be potential failure of the liner and possibly some pipes. This level of failure is expected to occur when the equivalent elastic response at the location of the containment vessel ring girder reaches a median value of approximately 4g. The fragility curves for this mode of failure are shown in Figure 4-13.

Axial (VQ/It) shear stress is resisted by horizontal reinforcing steel and concrete aggregate interlock. This shear must be transferred across the vertical buttress plates which extend the entire length of the cylinder. Shear anchors are located on one side of the buttress plates. However, since the circumferential prestress tendons overlap at the buttress, the preload is essentially doubled through the buttress and the axial shear capacity along the buttress plates is not significantly reduced compared to the remainder of the wall. Vertical shear failure with corresponding loss of liner integrity is expected to occur at a median equivalent acceleration at the ring girder of approximately 4.2g. The fragility curves for vertical shear failure are shown in Figure 4-14.

Flexural failure of the containment vessel wall, shear failure of the containment building base slab, and vessel wall buckling are other possible modes of failure which can result in containment liner failure followed by further degradation and eventual NSSS damage and structural collapse. These failure modes are expected to occur only at incredibly high median levels of response. Median capacity values of equivalent elastic response accelerations at the ring girder of approximately 9g for flexural failure and 13g for base slab failure are indicated. The corresponding fragility curves for these modes of failure are shown in Figures 4-15 and 4-16.

It should be noted, however, that the containment vessel is one structure where the addition of other dynamic loads can significantly influence the seismic capacity. If Loss of Coolant Accident (LOCA) internal pressure is present during the earthquake (or aftershock) a very substantial amount of the prestress capacity will be required to withstand the pressure loads. Consequently, a much lower strength capacity will be available to withstand the seismic loads. This is true not only for the capacity of the vertical system required to resist flexure and transverse shear but also the horizontal system. Typically the horizontal preload system does not need to resist large increases in load as the result of flexural loads. However, in the Zion reactor buildings the circumferential preload is required to transfer the VQ/I shear across the vertical buttress plates. In view of the low probability of a concurrent LOCA, however, these effects were not investigated as part of the current study.

4.3.3 Concrete Internal Structure Failure

The concrete internal structures of the Zion reactor buildings consist of a ring wall, the reactor biological shield wall, the fuel handling pool, and the operating floor. The reactor coolant system which consists of the reactor vessel, the steam generators, the pressurizers, and the reactor coolant pumps are located within the ring wall and laterally supported by the ring wall and the shield wall. Figures 4-7, 4-8, and 4-17 show the plan views at several elevations, and Figure 4-17 shows the location of the major equipment items. The polar crane is also supported by the ring wall.

A major structural failure of the concrete internal structure could lead to a total failure of the reactor coolant system due to loss of support for major components or impact on the coolant system with consequent failure of the pressure boundary. Thus, attention was focused on the failure of any structural elements of the concrete internal structures which could lead to such an event.

The ring wall and shield wall are constructed of reinforced concrete with wall reinforcing in two perpendicular directions. No helical seismic shear reinforcing was observed from the structural drawings. Thus, the seismic induced shear will be resisted by aggregate interlock of the concrete and dowel action of the wall reinforcing steel across any concrete cracks which form. The concrete internal structures were designed to withstand jet force and pressure differential resulting from a LOCA, and seismic loads were not controlling.

The controlling seismic failure mode for the internal structures is shear failure. The internals do not bear against the containment wall but are separated by a 1-inch gap filled with cork at the base slab elevation and 2-inch gaps at higher elevations. The shear transfer path between the concrete internal structure walls and the foundation slab is shown in Figure 4-9. There are 12" x 12" x 2" deep keys at 2'-0" on center at the base of the concrete wall. Shear forces from the internal structures are transferred through these keys to the 3-ft. base slab. At high structure response accelerations, the keys may be sheared off. However, the dowels and vertical wall reinforcing still remain effective in providing a clamping force for shear friction. Thus, the shear force from the 3-ft. thick slab will be transferred to the 9-ft. thick foundation slab through the 1-3/8-inch diameter dowels, friction, and the shear capacity of the vertical (1-ft. thick) continuation of the 3-ft. thick slab at the sump. The lowest capacity failure mode for the internals is the shear failure of the weld for the 1-3/8-inch diameter dowels at the interface of the 3-ft. slab and 9-ft. slab and simultaneous shear failure of the vertical portion of the 3-ft. thick slab in the sump. This will result in loss of liner integrity and possibly pipe and conduit failure. The median expected equivalent elastic response capacity for shear failure of the concrete internals is approximately 5.0g at the operating floor elevation. Figure 4-18 shows the corresponding fragility curves.

4.3.4 Miscellaneous Reactor Building Failure Modes

There are a number of possible failure modes associated with degradation and failure of the soil foundation material beneath the reactor building. Among these are soil liquefaction, surface faulting, sliding, and others which were not considered as part of the structures fragility evaluation. A preliminary investigation of the effect of base slab uplift was conducted, however.

Base slab uplift is initiated at slightly less than the DBE (0.17g) level. As the input ground motion is increased and the base slab-soil contact area decreases, the contact pressure increases significantly. The contact pressure eventually reaches the point where the soil strength is inadequate to support the toe loading condition and is deformed such that relative motions can increase above those which would result if the soil remained elastic. The strength of the soil is inadequate to cause failure of the tendon gallery, even after large base slab uplift, so that the prestressing tendon anchorage system is not expected to be damaged. The reactor building structure and liner are likewise not expected to be damaged directly from this level of input. However, relative vertical motion between the reactor buildings and the adjacent pipe tunnels may reach the point that potential damage to the piping and control cable penetrations needs to be considered. No nonlinear response analysis was conducted to determine the uplift for the Zion reactor building base slabs. However, based on nonlinear analyses of other reactor systems (Ref. 26) which included the effect of uplift, possible vertical motion in the range of 1 to 2 inches is estimated to be possible in conjunction with soil failure at the toe of the base slab. Overturning instability is not a credible mode of failure. This is because the rocking period of the structure becomes very long at large excursions compared to the earthquake forcing frequencies. Resonance cannot occur and the structure tends to become an isolated dynamic system rocking about its c.g. rather than overturning. The fragility curves associated with toe pressure failure are shown in Figure 4-19.

Although the soil failure is not expected to result in failure of the structure directly, the resulting increased relative displacement of the reactor building can lead to impact between the reactor and auxiliary building. Even without the increased deformation from soil failure, impact between the two structures of sufficient magnitude to cause liner failure is expected at response levels comparable to other failure modes investigated in this study. In the Zion reactor containment vessels, no tangential (or hoop) reinforcing steel was included for the inside faces of the vessels in the areas of impact. Although the liner is anchored by a network of embedded angles, relatively little capacity exists to resist external line or point load conditions such as can result from impact with the auxiliary building shear walls. Consequently, concrete spalling and subsequent liner damage is expected at relatively low levels of additional displacement once the circumferential prestress is overcome.

No analysis of the phasing of motion between the reactor buildings and the auxiliary building was conducted during Phase I of the SSMRP. The relative motion between adjacent structures was assumed to consist of the SRSS of the displacements of the individual structures moving independently. No impact is expected to occur for reactor building displacements less than approximately 0.8 inch at elevation 642 ft., regardless of of phasing. The fragility curves associated with impact between the reactor buildings and auxiliary buildings are shown in Figure 4-20.

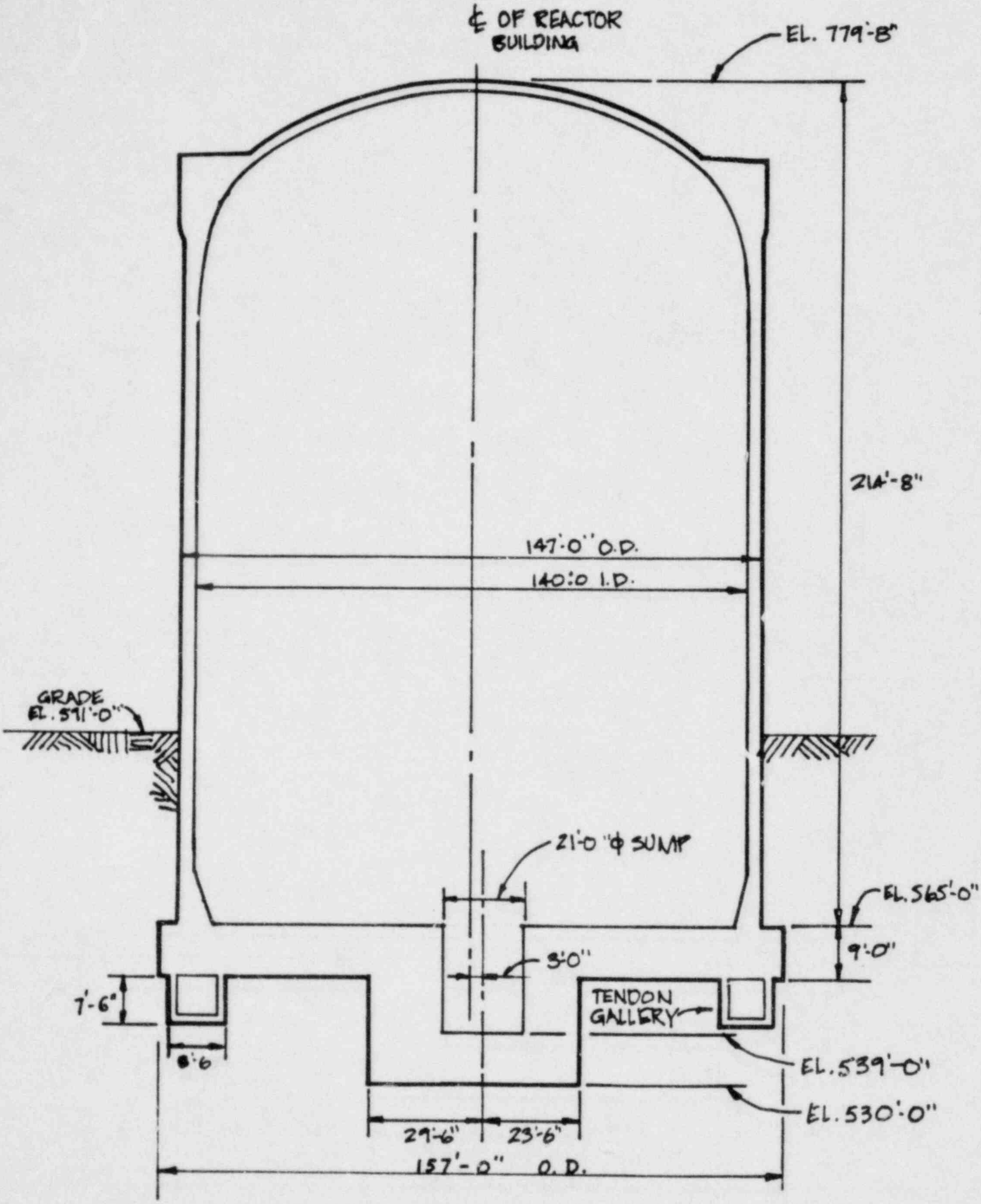

FIGURE 4-1. SECTION OF REACTOR CONTAINMENT BUILDING

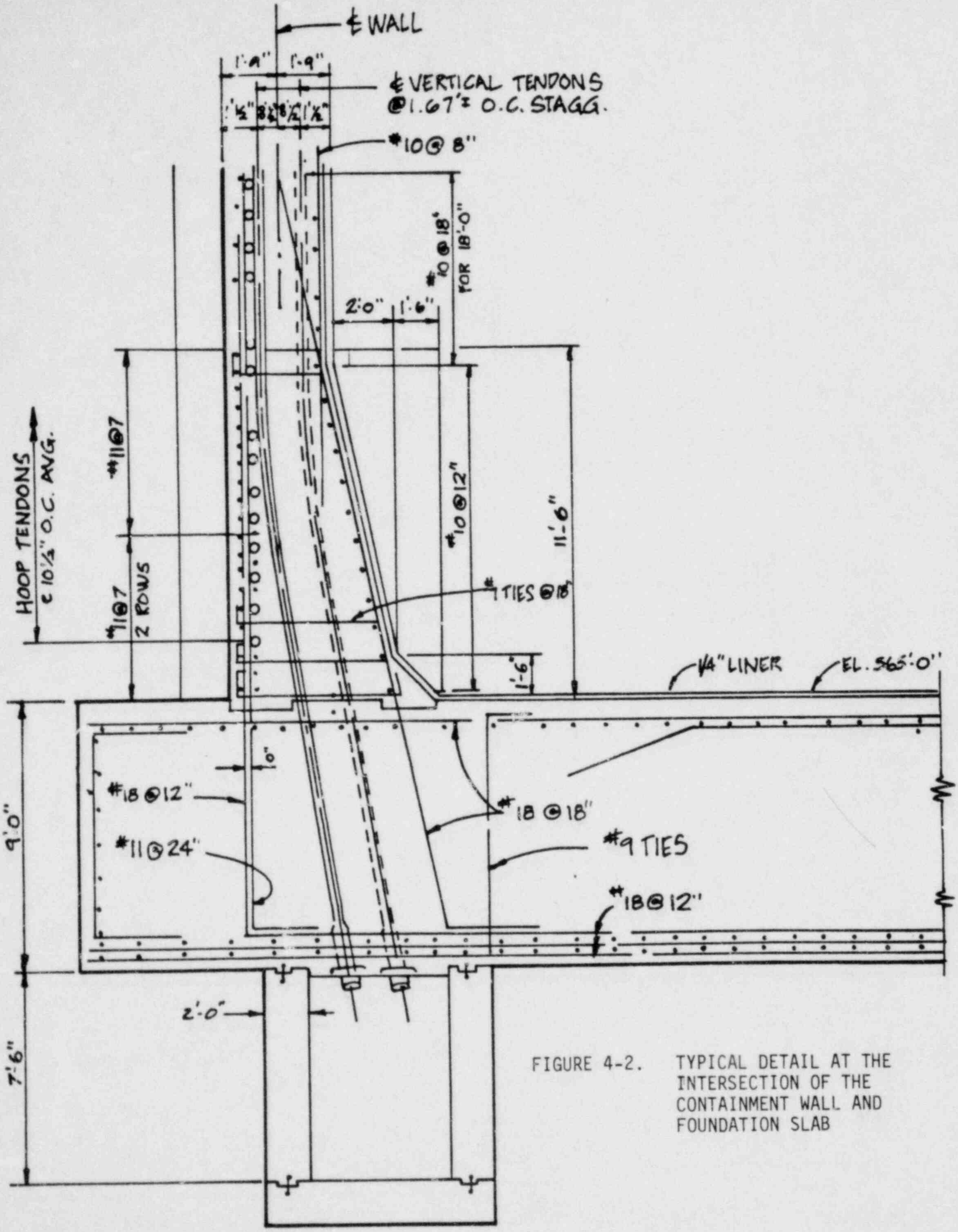

FIGURE 4-2. TYPICAL DETAIL AT THE INTERSECTION OF THE CONTAINMENT WALL AND FOUNDATION SLAB

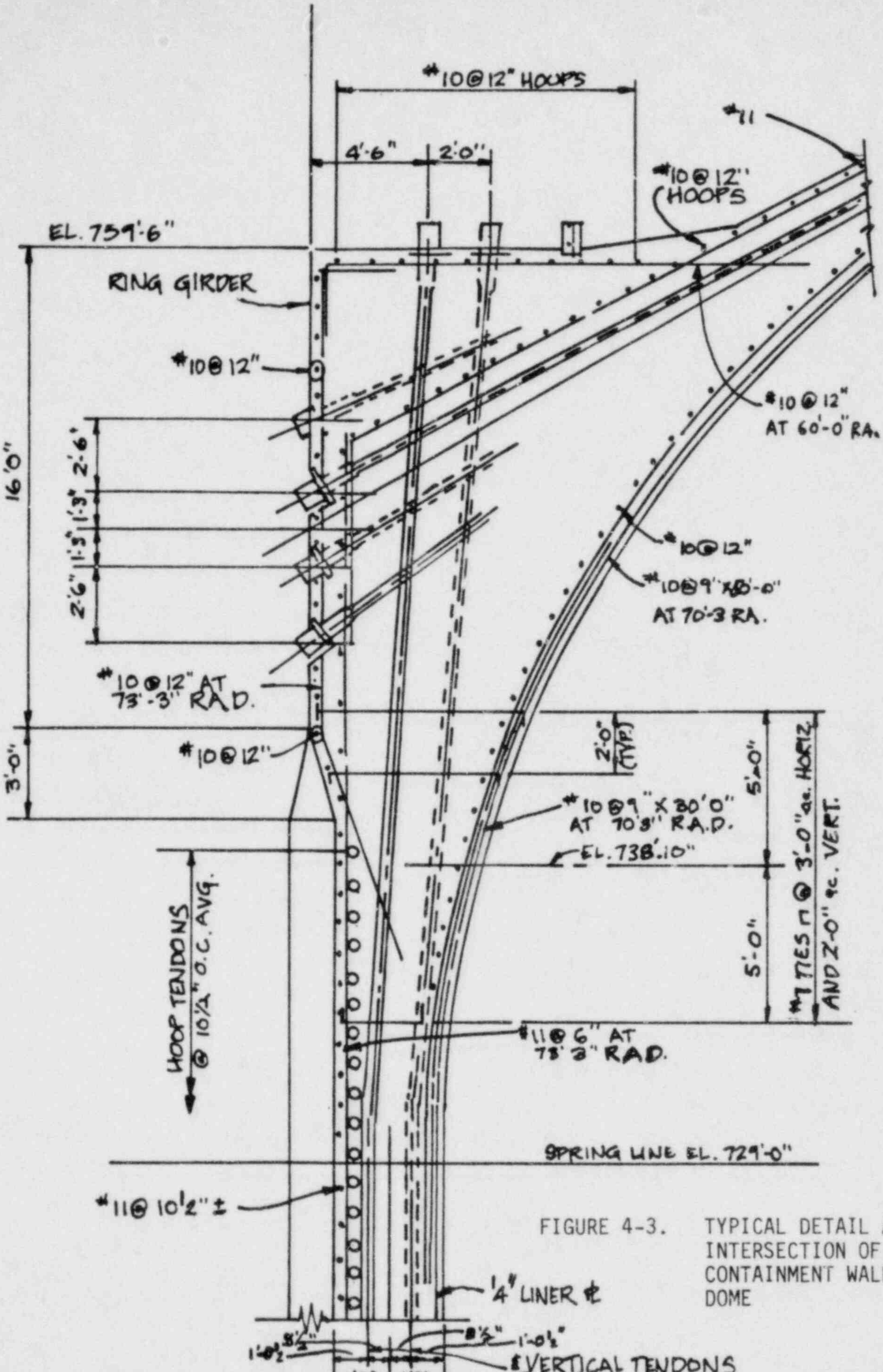

FIGURE 4-3. TYPICAL DETAIL AT THE INTERSECTION OF THE CONTAINMENT WALL AND DOME

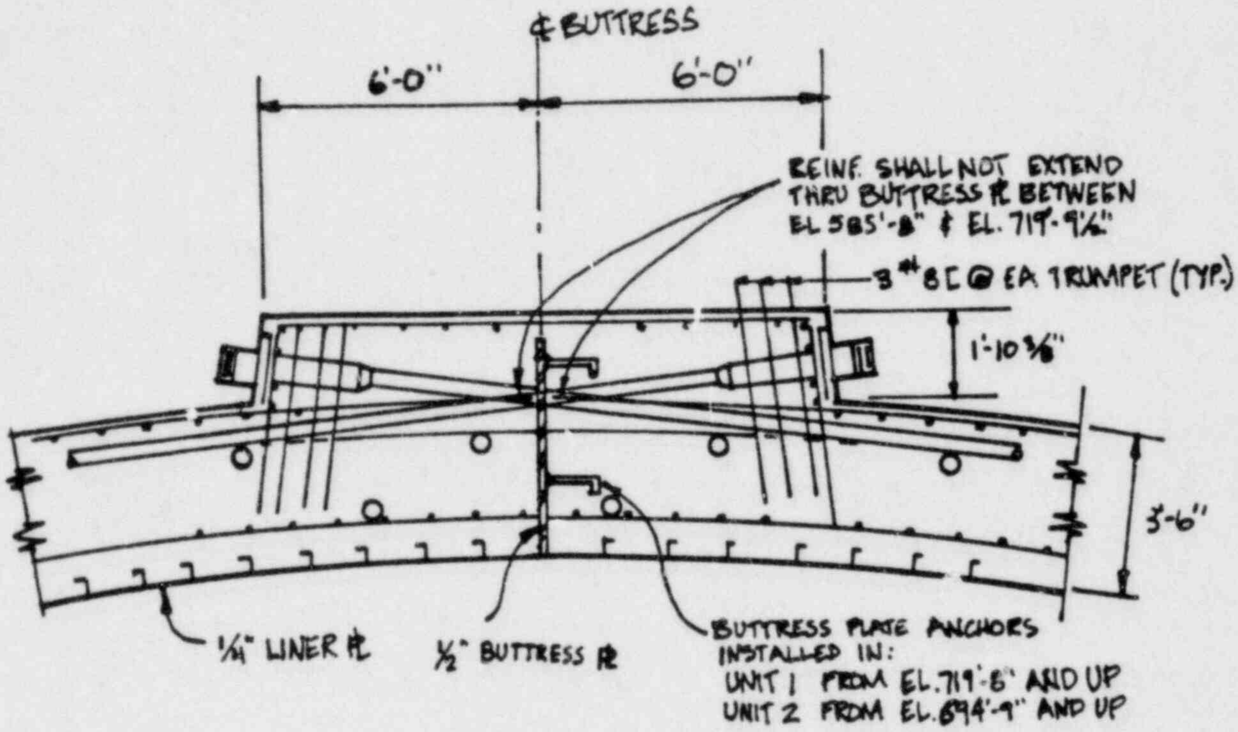

FIGURE 4-4. SECTION OF CONTAINMENT WALL BUTTRESS

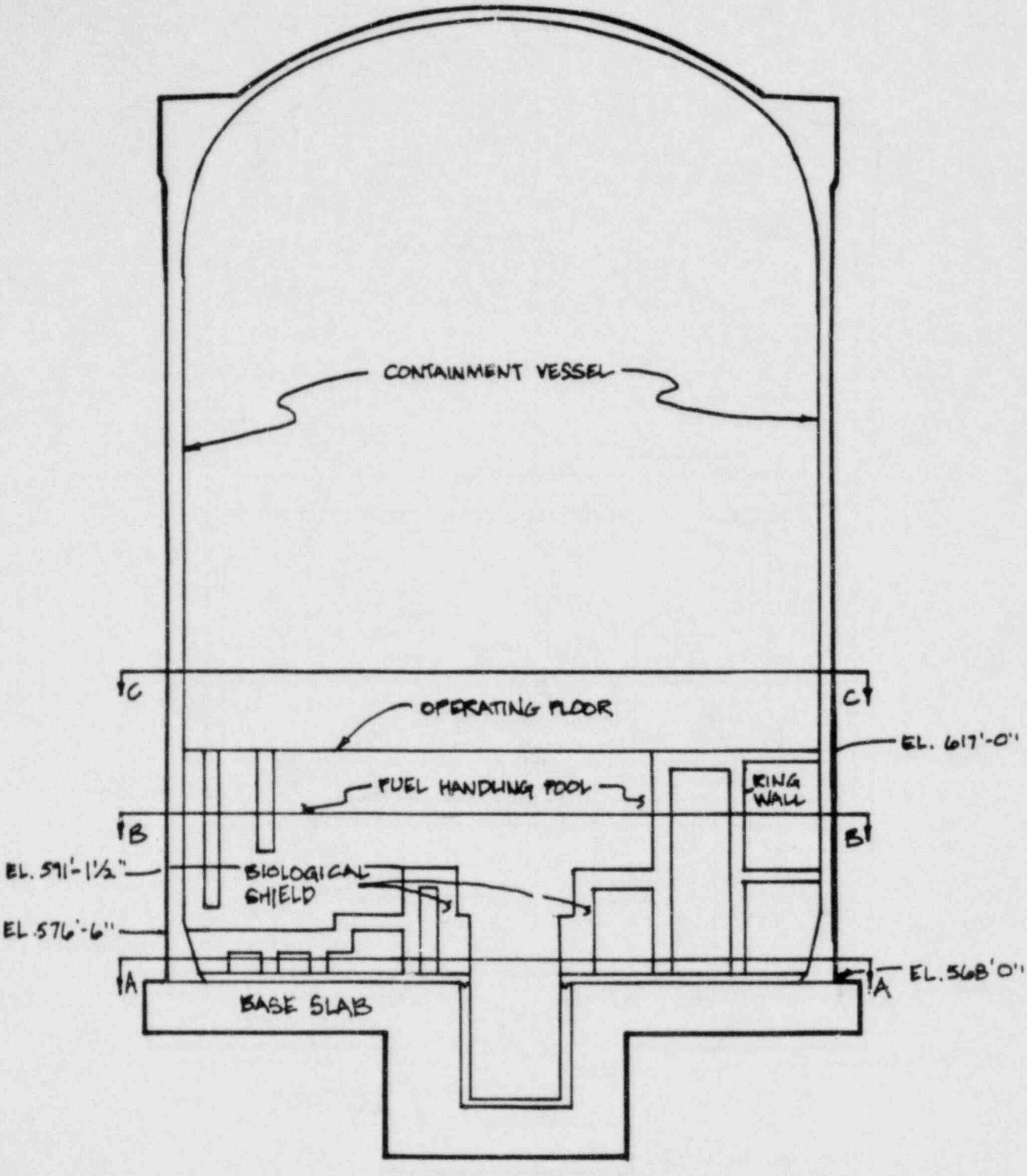

FIGURE 4-5. ZION REACTOR BUILDING AND INTERNAL STRUCTURES

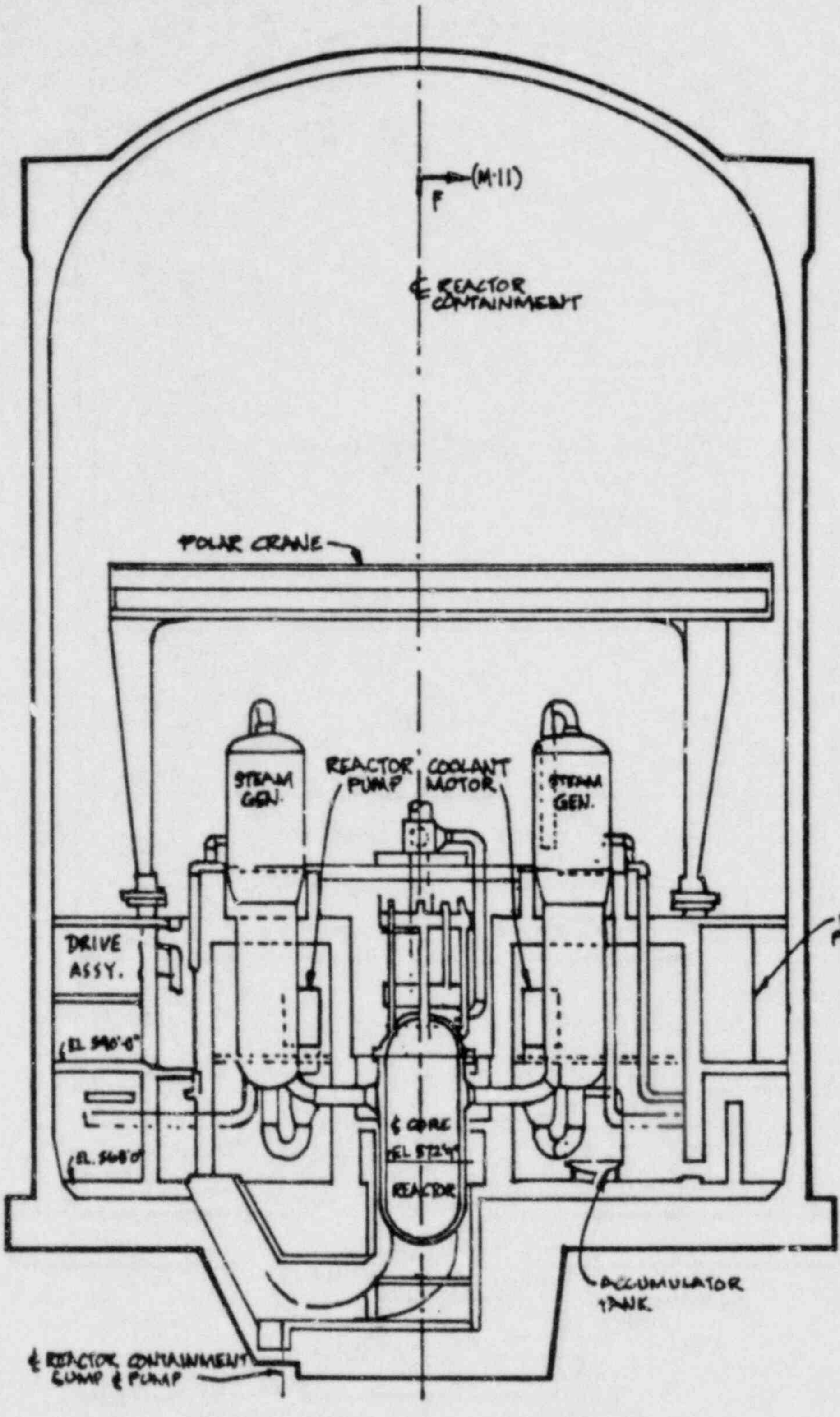

FIGURE 4-6. E-W SECTION OF CONTAINMENT BUILDING

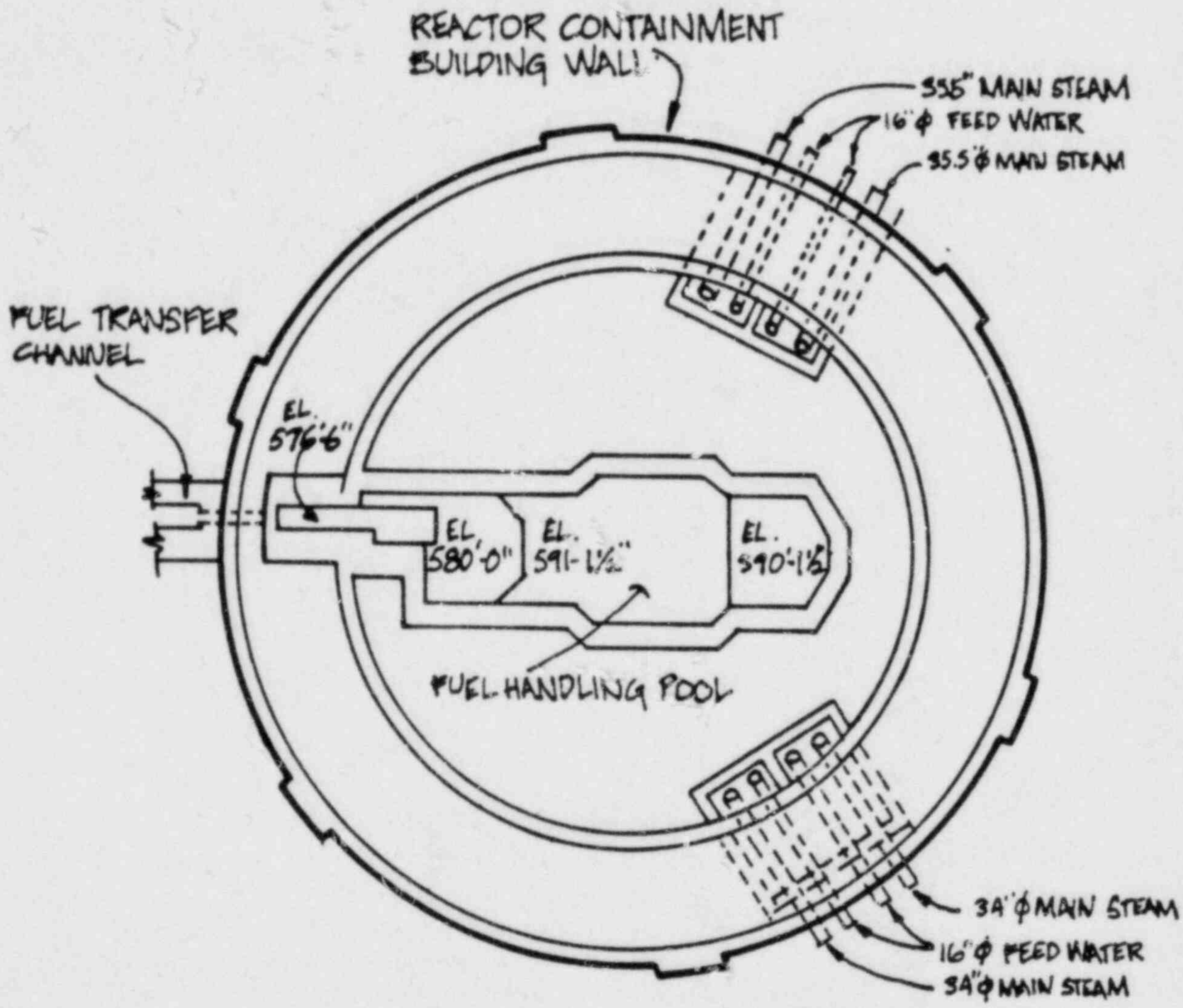

FIGURE 4-7. PLAN OF THE FUEL HANDLING POOL

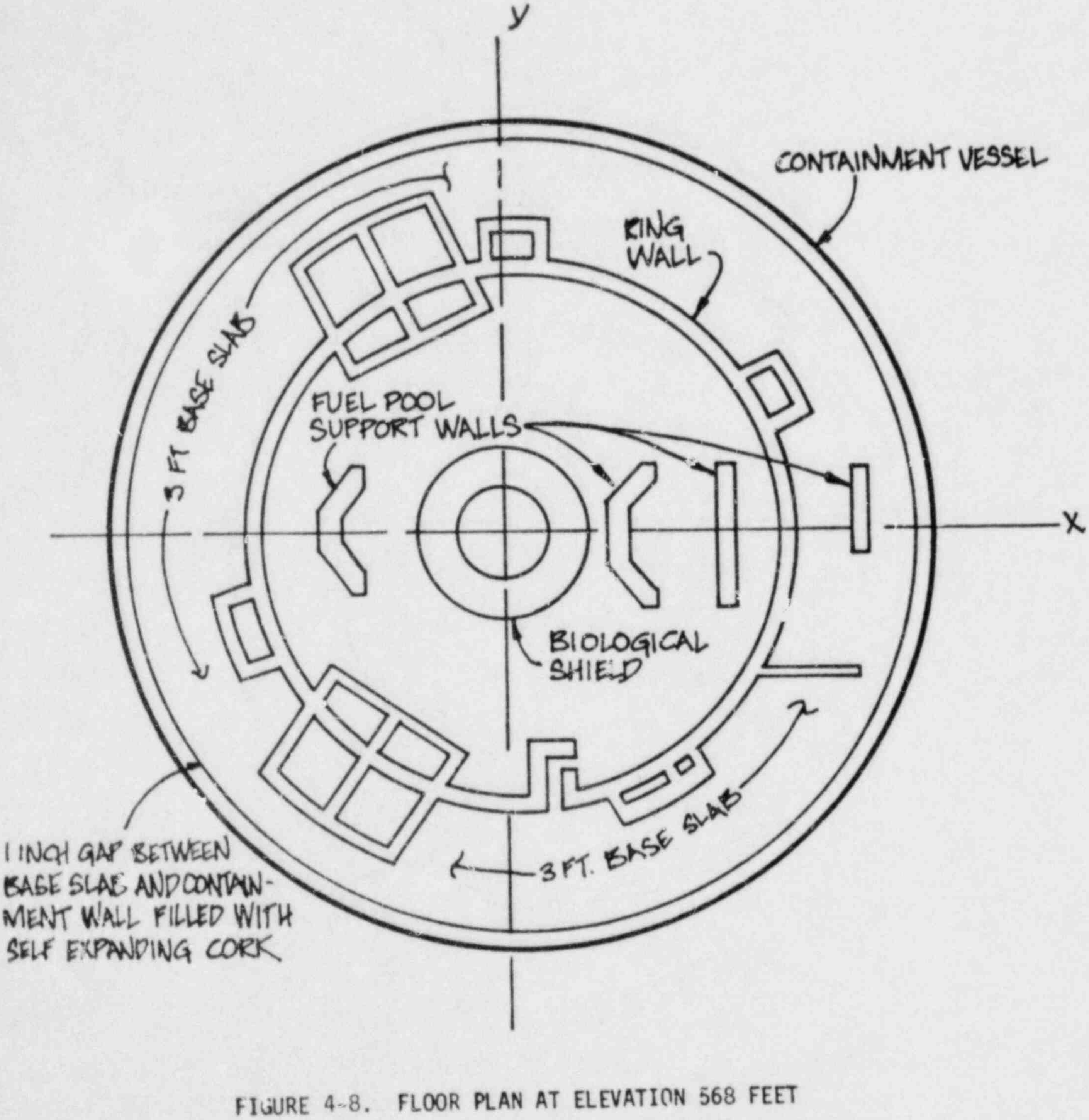

FIGURE 4-8. FLOOR PLAN AT ELEVATION 568 FEET
(SECTION A-A OF FIGURE 5-5)

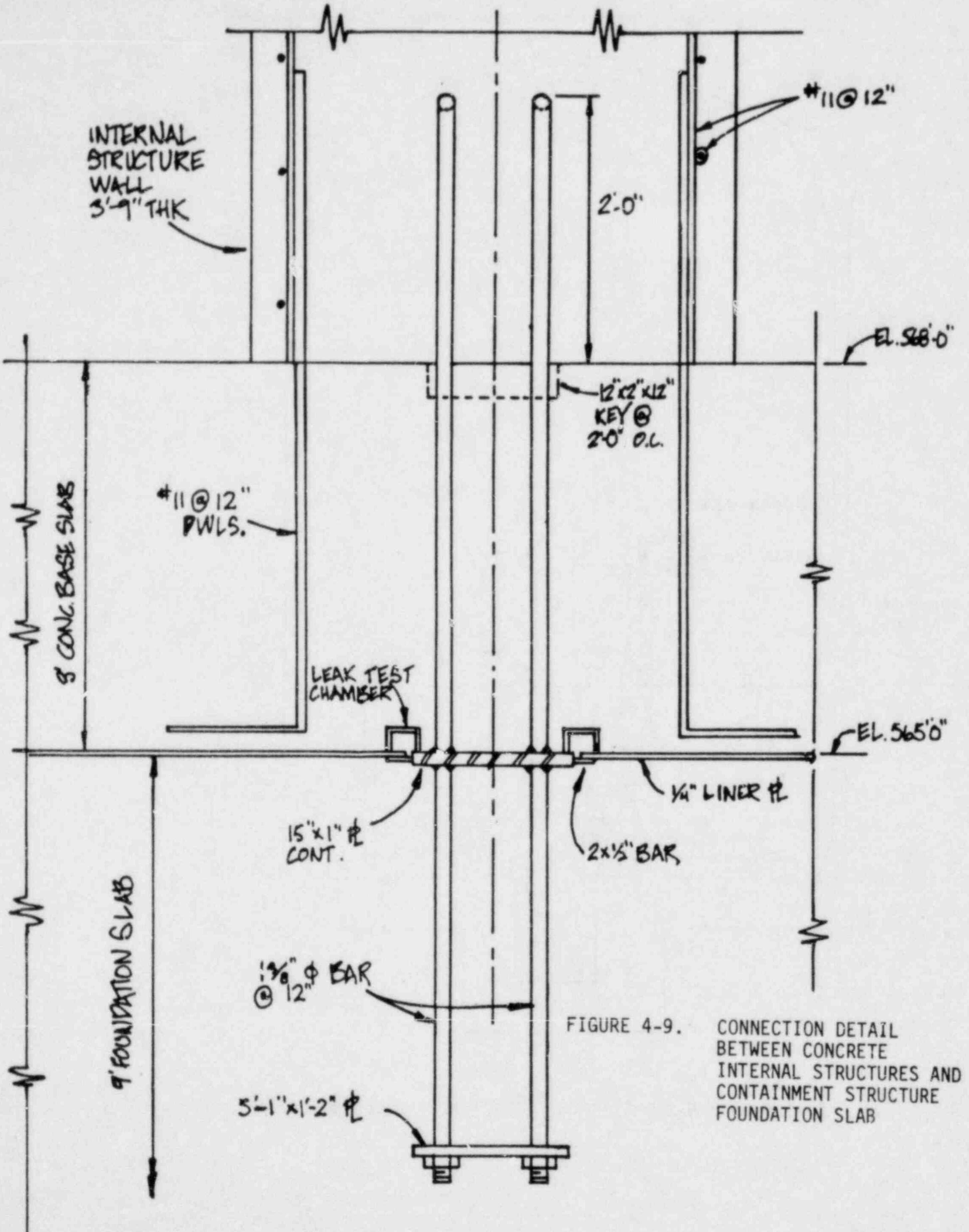

FIGURE 4-9. CONNECTION DETAIL BETWEEN CONCRETE INTERNAL STRUCTURES AND CONTAINMENT STRUCTURE FOUNDATION SLAB

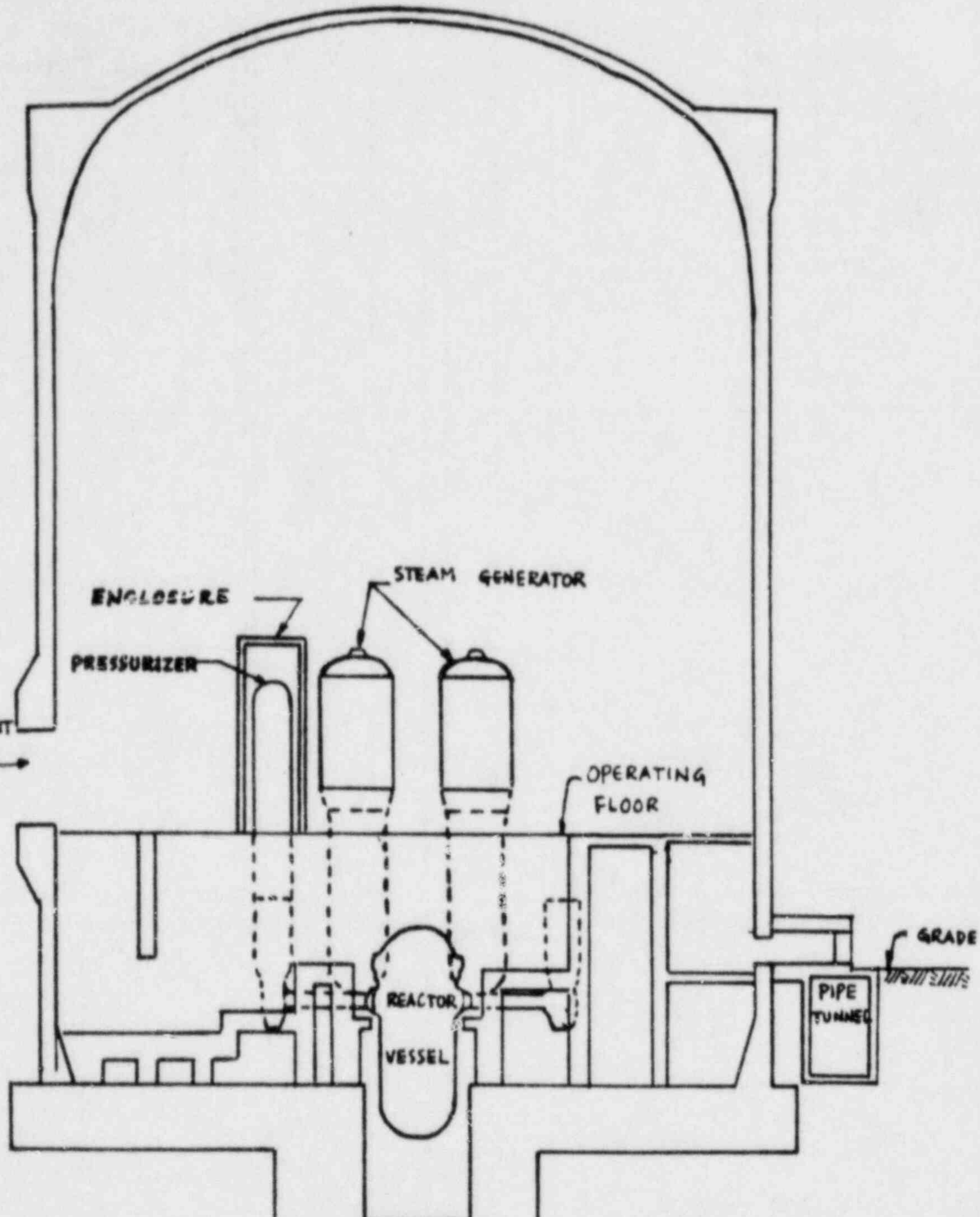

FIGURE 4-10. N-S SECTION OF CONTAINMENT BUILDING

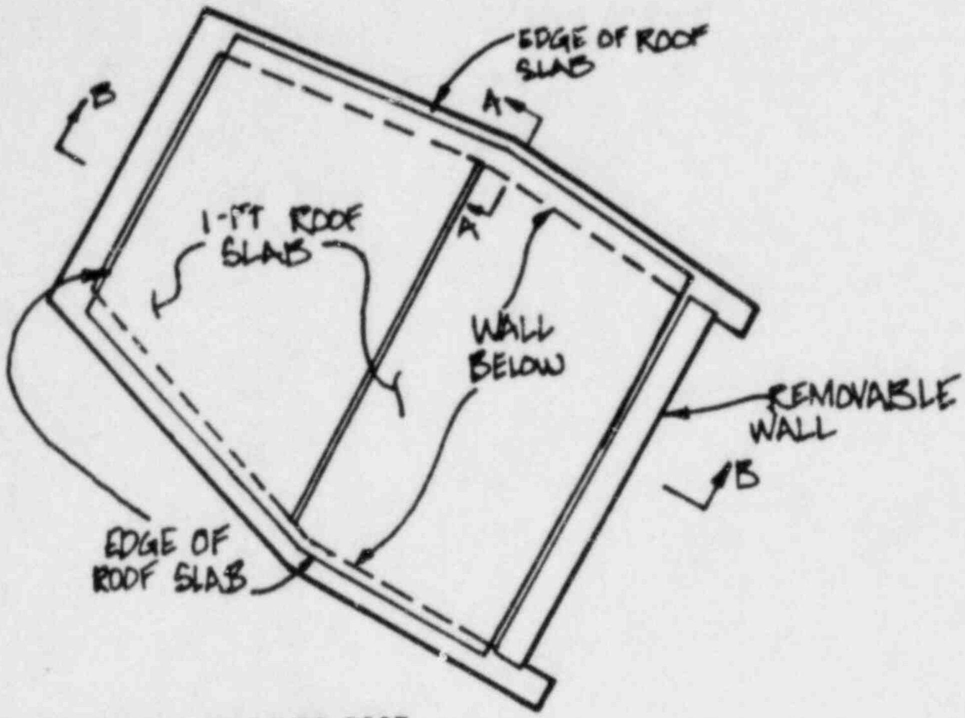

PRESSURIZER ENCLOSURE ROOF

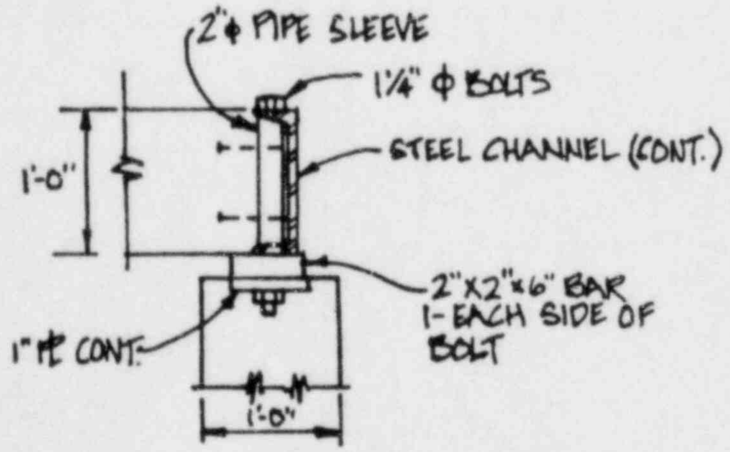

SECTION A-A

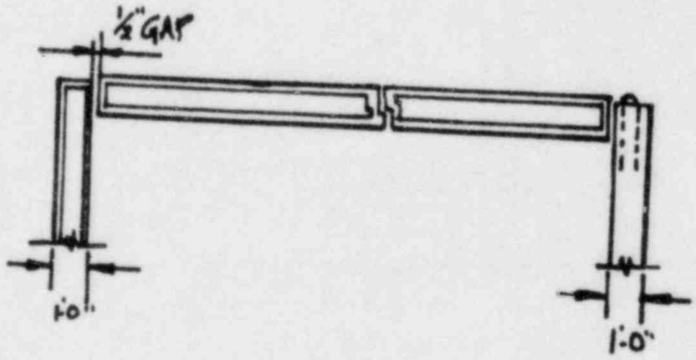

SECTION B-B

FIGURE 4-11. PLAN AND SECTIONS OF PRESSURIZER ENCLOSURE

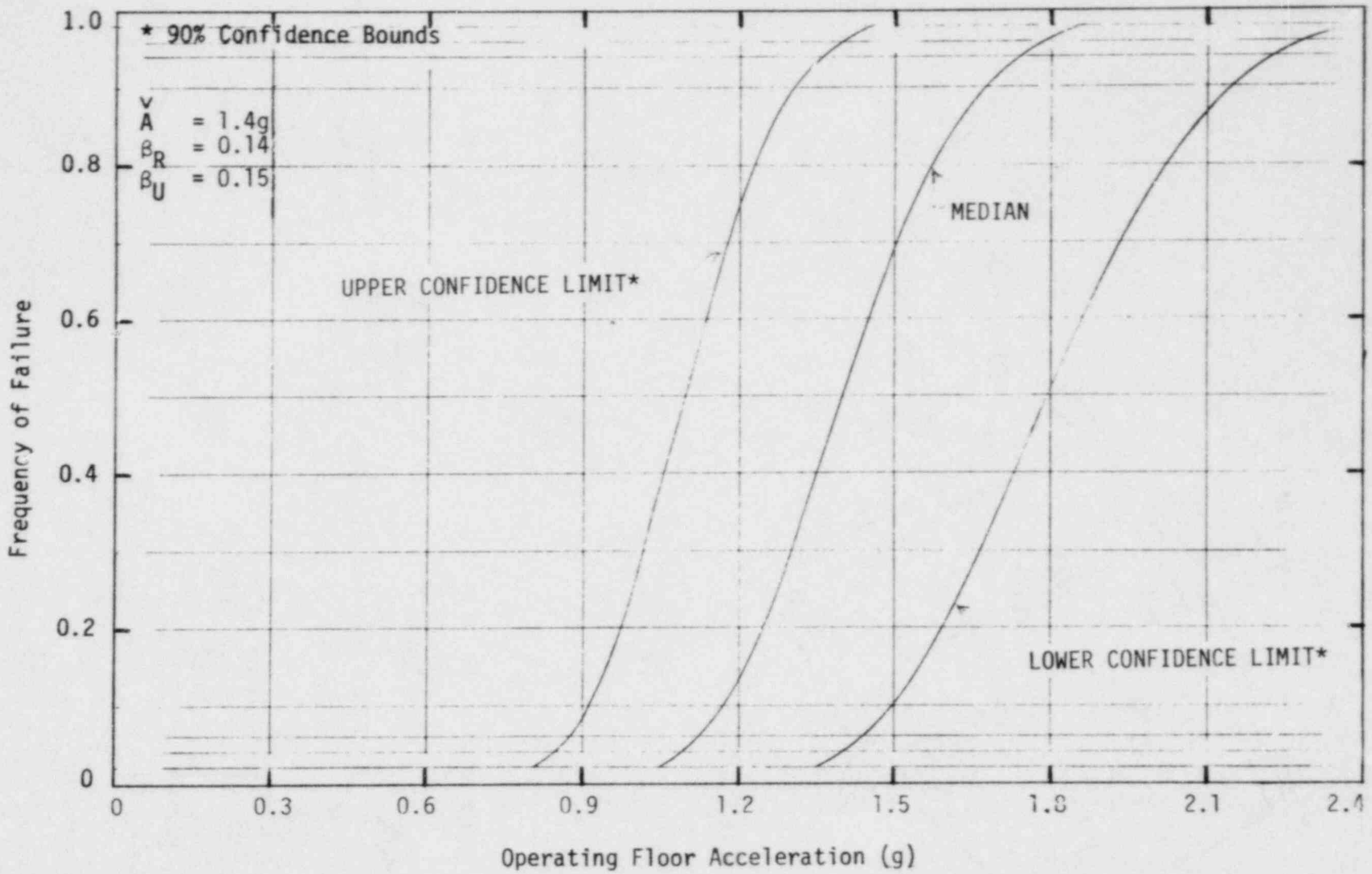

FIGURE 4-12. COLLAPSE OF REACTOR BUILDING PRESSURIZER ENCLOSURE

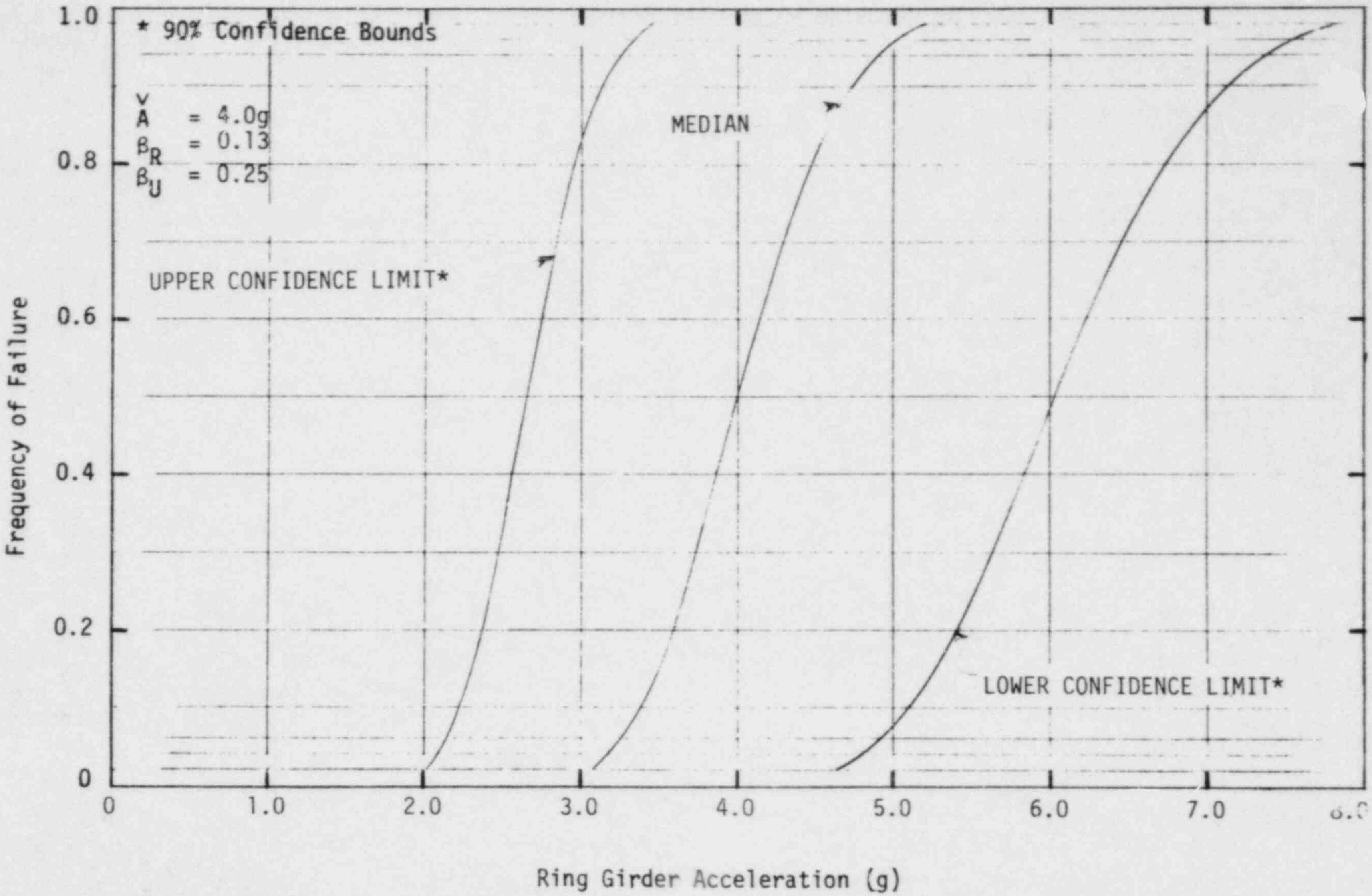

FIGURE 4-13. SHEAR FAILURE OF REACTOR BUILDING CONTAINMENT WALL

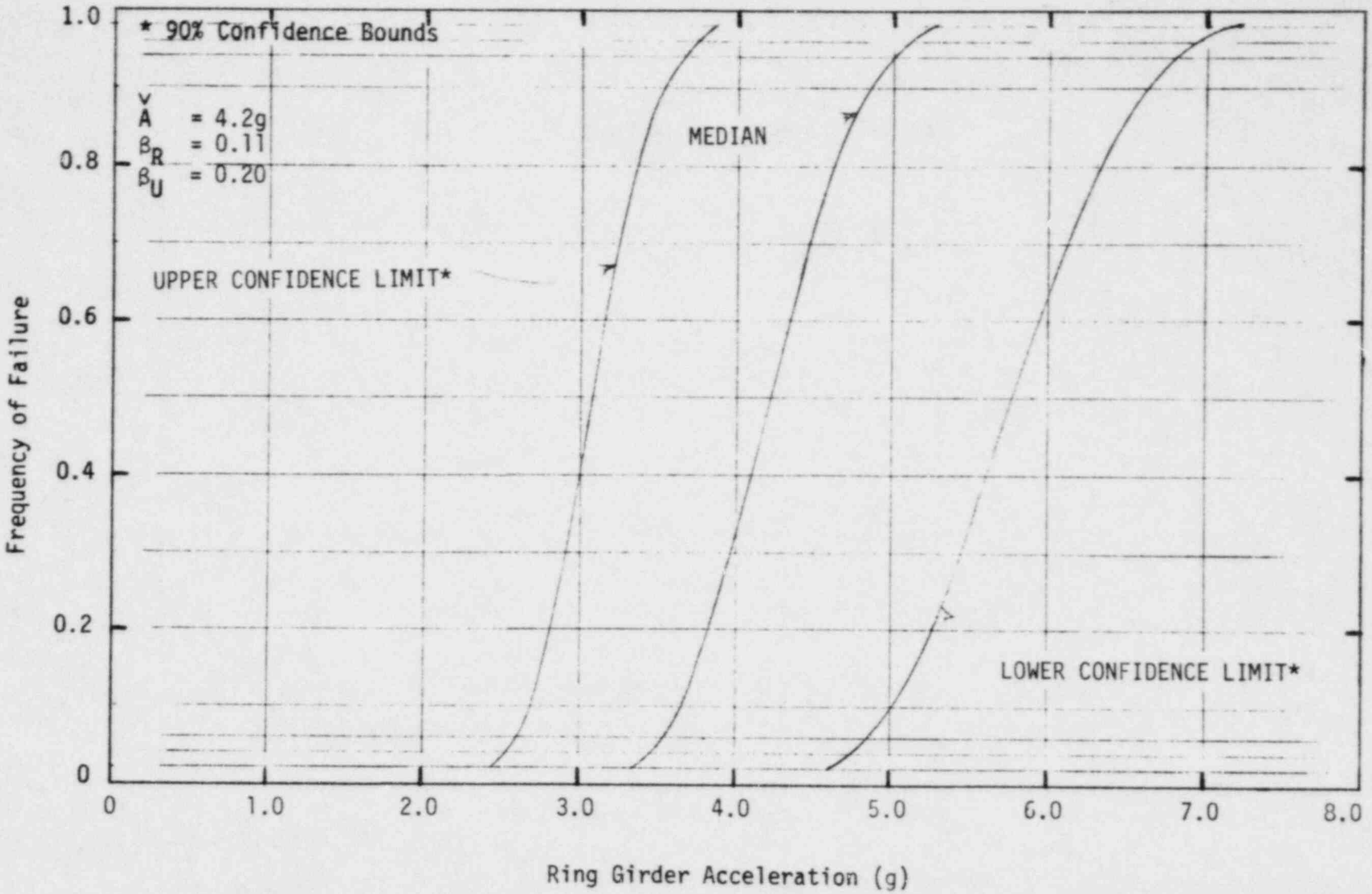

FIGURE 4-14. VERTICAL SHEAR FAILURE AT REACTOR BUILDING BUTTRESS PLATES

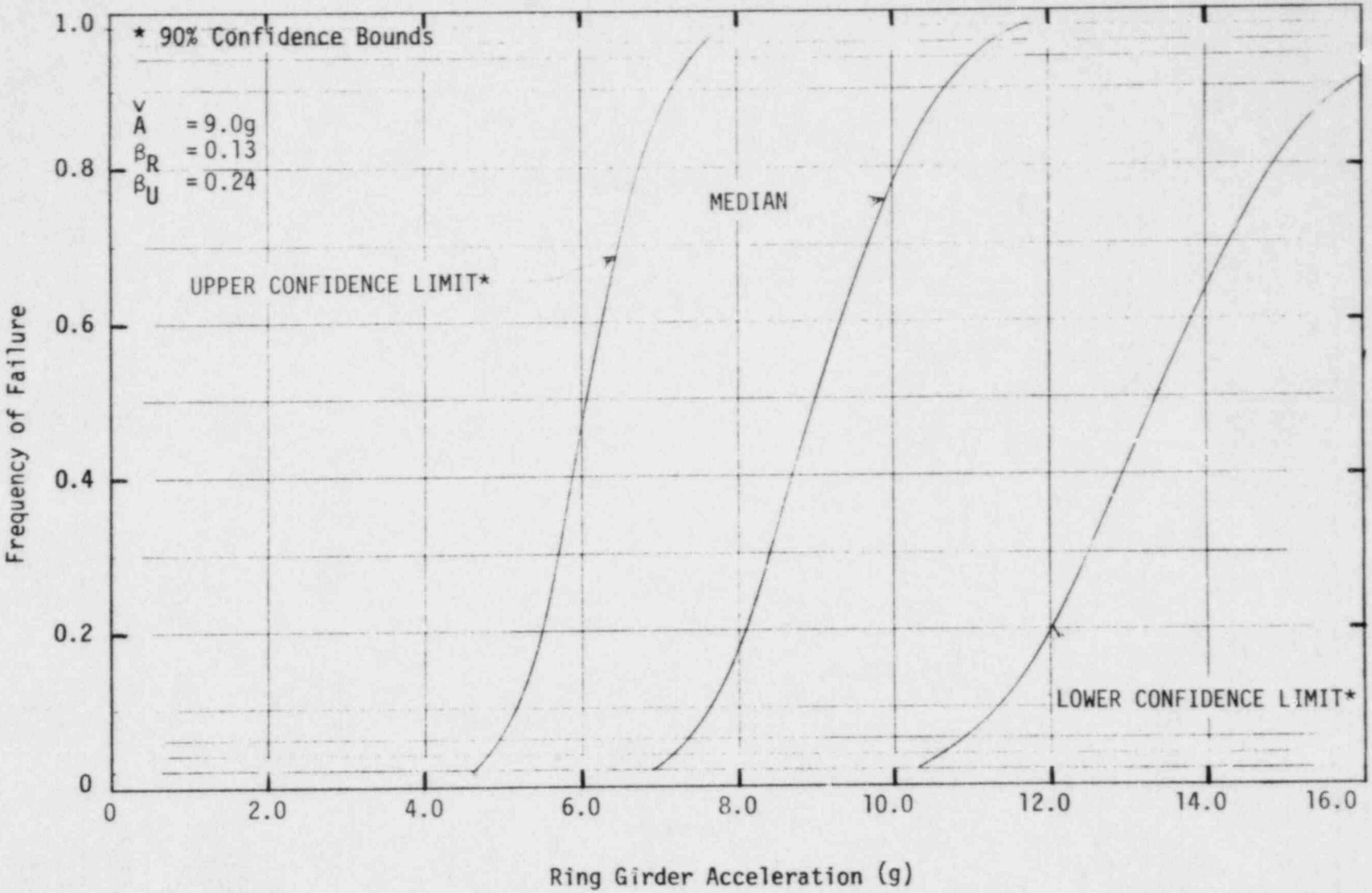

FIGURE 4-15. FLEXURAL FAILURE OF REACTOR BUILDING CONTAINMENT WALL

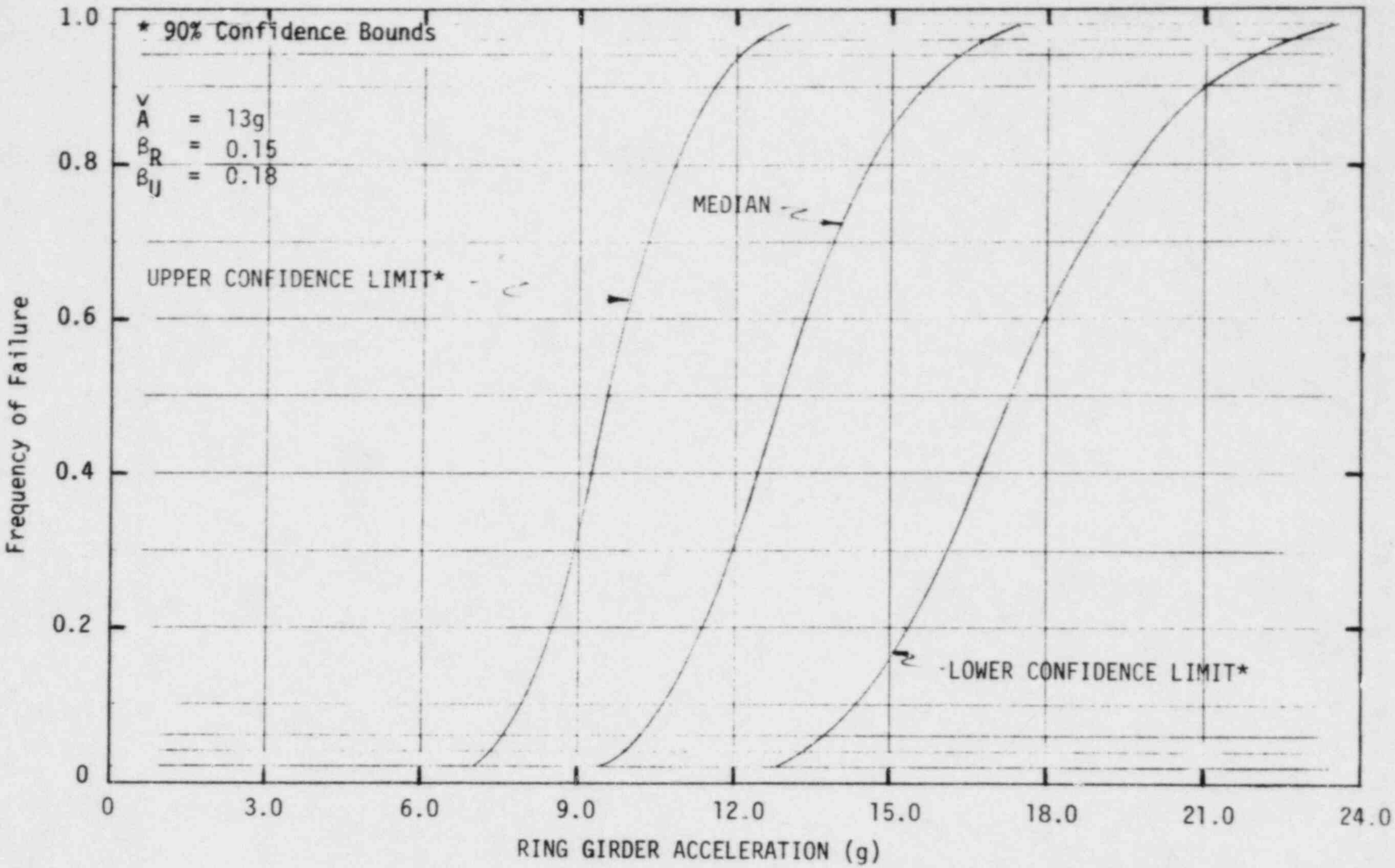

FIGURE 4-16. SHEAR FAILURE OF REACTOR BUILDING BASE MAT

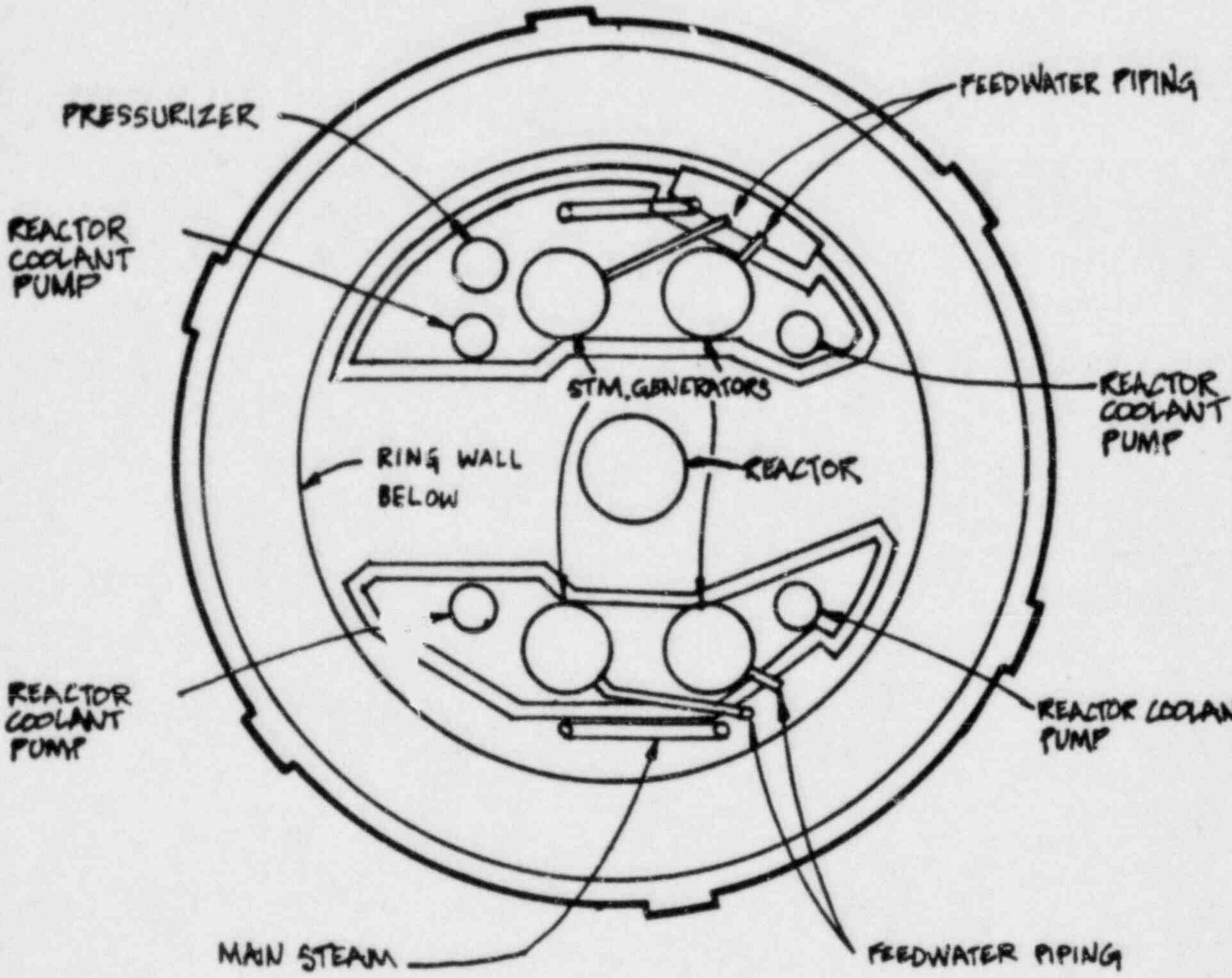

FIGURE 4-17. LAYOUT OF CONTAINMENT COOLANT SYSTEM AT OPERATING FLOOR

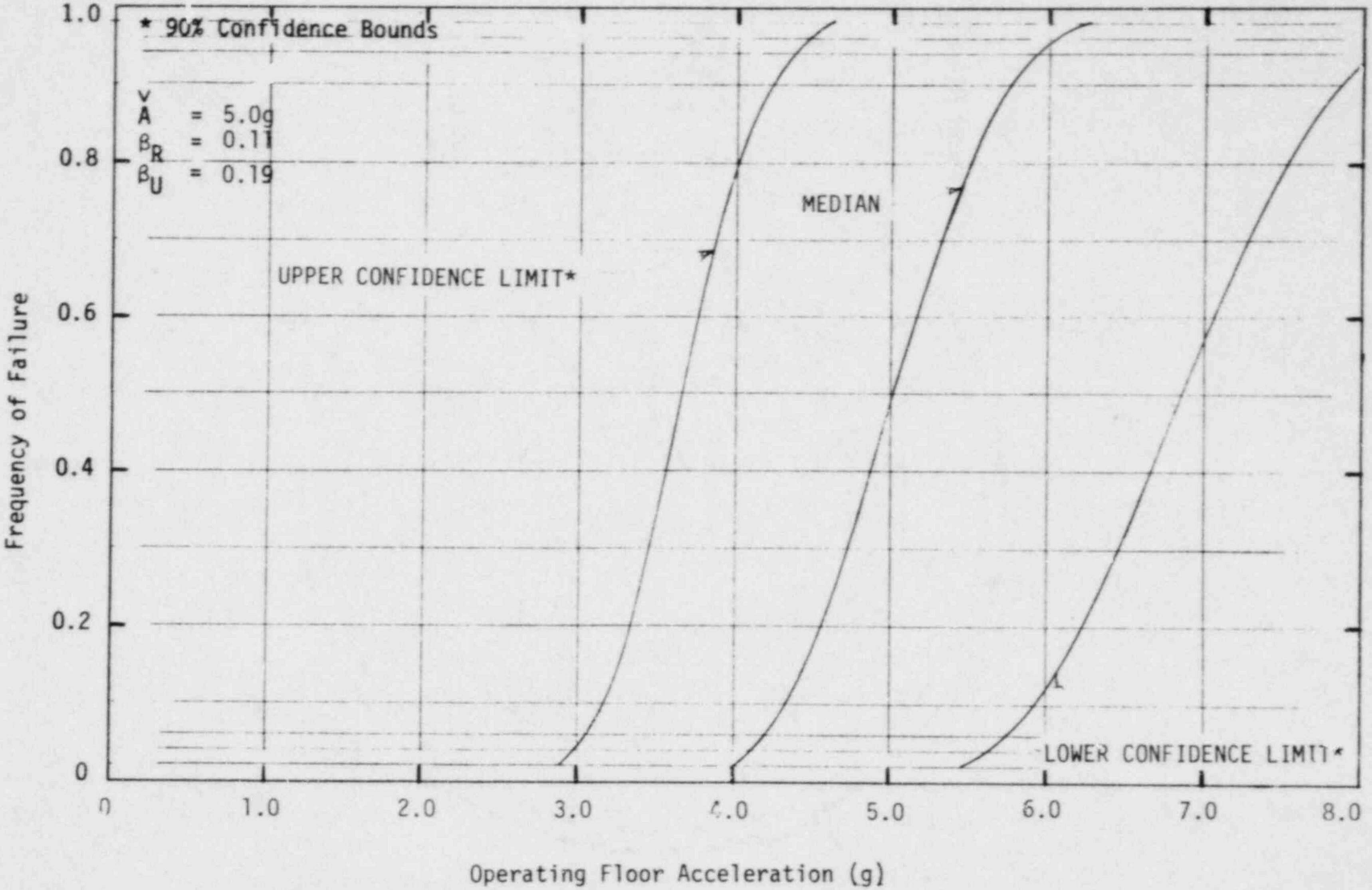

FIGURE 4-18. FAILURE OF REACTOR BUILDING INTERNAL SHEAR ANCHORS

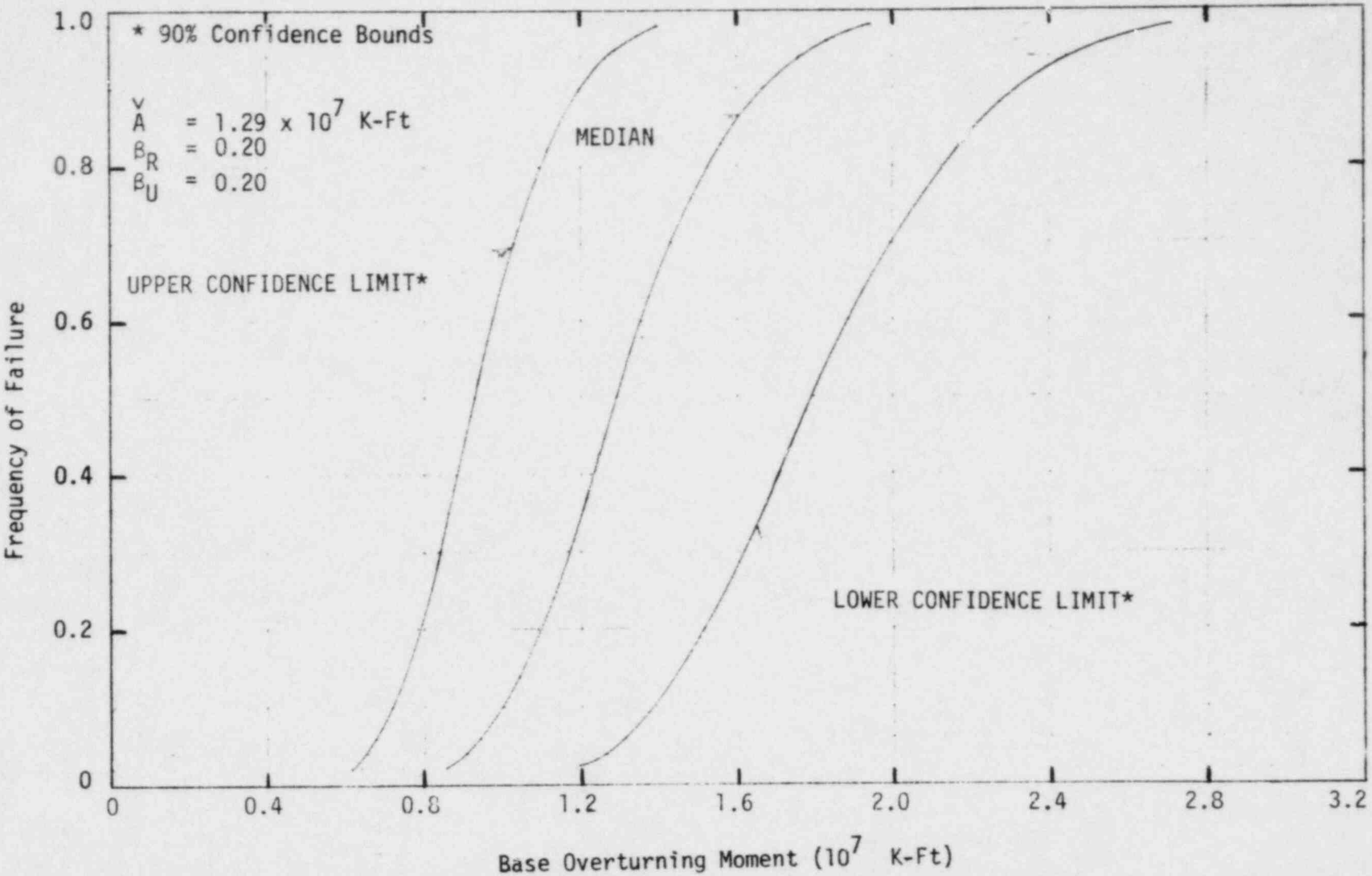

FIGURE 4-19. FAILURE OF SOIL BENEATH REACTOR BUILDING BASE MAT

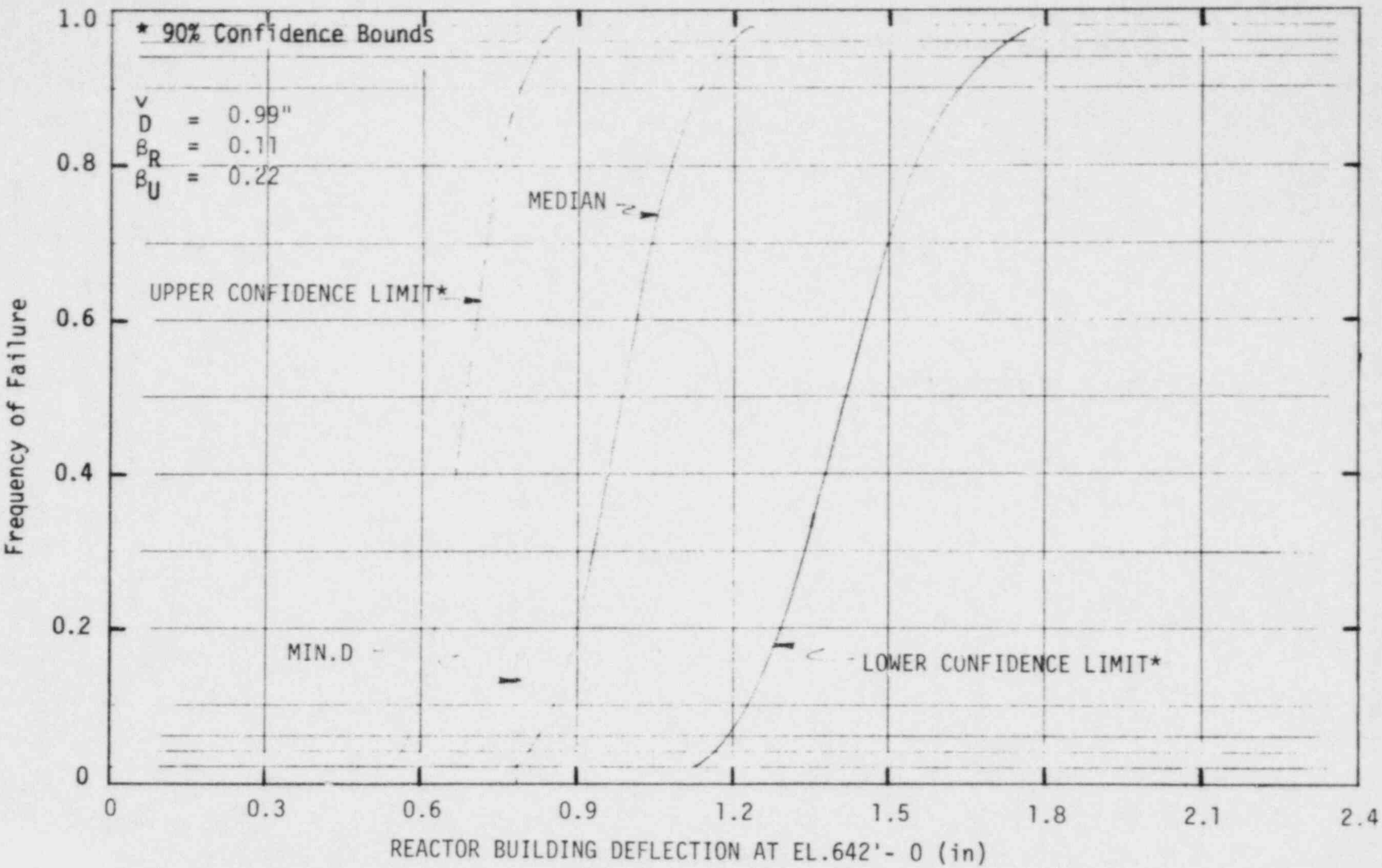

FIGURE 4-20. **IMPACT BETWEEN REACTOR AND AUXILIARY BUILDINGS**

5. AUXILIARY/TURBINE BUILDING

The turbine/auxiliary building complex of the Zion nuclear power plant consists of the following buildings: the turbine building, the auxiliary building, the fuel handling building and the diesel generator rooms. All four buildings are structurally interconnected at different levels through walls, roofs, and floor slabs. The general layout of the complex is given in Figure 5-1. It is observed that the complex is nearly symmetric about the east-west axis but is highly unsymmetric about the north-south axis. The reactor containment buildings of Unit 1 and Unit 2 are located symmetrically on each side of the fuel handling building but are not structurally coupled to the adjacent structure.

Among these four buildings, the auxiliary building, the diesel generator rooms, and the fuel handling building were designed as Class I structures. The turbine building is non-Class I. All buildings are founded on either reinforced concrete foundation slabs or spread footings. The lateral force resisting systems used are structural steel braced frames and reinforced concrete shear wall systems. All Class I buildings in the complex have the latter (shear wall) lateral force resisting system.

5.1 TURBINE BUILDING DESCRIPTION

The turbine building, a 678 ft by 130 ft structure, is symmetrical about an approximate east-west centerline. The south part of the building houses the turbine of Unit 1 and the north part of the building houses the turbine of Unit 2. Most of the turbine building (i.e., turbine and condenser supporting structures) is founded on a reinforced concrete foundation mat with varying thickness (Figure 5-2). The top of the foundation mat elevation is at approximately elevation 560 ft. The remainder of the turbine bulding which is not located over the foundation mat is supported by concrete columns which extend downward to the spread footings. Centrally located in the turbine building below the turbines are the condenser well slabs at elevation 560 ft. A 14-ft thick continuous slab is located between the condenser well slabs of Unit 1 and Unit 2 (Figure 5-2). At the west edge of the condenser well slabs, a 3-ft 4-in thick continuous slab connects the foundation mat to the floor slab at elevation 560 ft in the auxiliary building (Figure 5-3).

Rectangular reinforced concrete piers rise from the top of the condenser well slabs to elevation 592 ft where continuous haunched girders connect the piers along each side of each condenser well. The turbine foundations are massive reinforced concrete space frames which are continuous with the piers of the condenser wells and rise from elevation 592 ft to the main floor of the turbine building at elevation 642 ft. The turbine foundations are isolated from the major turbine building floors at elevations 617 ft and 642 ft by a one-inch gap (Figure 5-4).

The ground floor, a 3-ft thick reinforced concrete slab, is continuous with the floor slab at the same elevation (elevation 592 ft) in the auxiliary building (Figure 5-3). At elevations 617 ft and 642 ft, the floors were constructed of poured-in-place concrete slabs supported by vertical and horizontal braced steel framing. A typical floor slab support detail is shown in Figure 5-5. The slabs are continuous, through the steel floor framings and concrete slabs, with the floor slabs at the same elevations in the auxiliary building (Figure 5-6). The west side vertical braced frame along column Line G, located between the turbine building and the auxiliary building and diesel generator rooms, is encased in reinforced concrete walls (Figure 5-5) from ground level up to the auxiliary building roof level at elevation 668 ft. The other walls above ground including the wall above the auxiliary building roof level are constructed of fluted metal sidings (Figure 5-7). Two 110 ton capacity cranes are located at elevation 689 ft 10 in (one for each turbine). The cranes run in the north-south direction. A typical transverse section of the turbine building is shown in Figure 5-8.

The roof was constructed of 3-1/2 inch thick precast concrete channel slabs covered with 1-inch rigid insulation and is supported by braced steel roof framing. The elevation of the main roof over the turbines is 712 ft and the roof elevations of the heater bay are 666 ft and 642 ft. The roof framing consists of steel roof girders, wide flange roof beams, and double angle diagonal bracings. A minimum of three 7/8-inch diameter bolts and 3/8-inch thick gusset plates were used for the connections of the diagonal bracings. No detail information was available for the connections between the individual precast roof slabs and between the roof slabs and steel framing. It was assumed that only nominal metal clips were used to restrain the roof slabs against uplift due to wind.

The vertical lateral force resisting systems of the turbine building are the steel braced frames along all four sides of the building. Schedule 40 pipes were used as diagonal bracing elements for the braced frames. The braced frames at the north and south ends of the turbine building are shown in Figures 5-9 and 5-10. Fluted metal sidings were attached to the girt system of each vertical braced frame to enclose the turbine building.

5.2 TURBINE BUILDING FAILURE

The turbine building, auxiliary building, fuel handling building and diesel generator buildings form a single combined structure. Failure of one part of the structure, while not necessarily resulting in failure of the entire complex, will at least influence the dynamic response characteristics of the overall building. Since no Seismic Category I equipment is located in the turbine building with the exception of the 48-inch diameter service water pipes which are embedded in the turbine building base slab, turbine building failure modes were investigated only to the extent they could directly cause damage or failure to Category I structures or equipment.

The lowest capacity potential mode of failure consists of failure of the turbine building roof system. There are two horizontal lateral force resisting systems in the turbine building roof which are effective in collecting and transmitting lateral inertia forces to the vertical shear resisting systems. The first system consists of the precast concrete channel slabs. The second system is the braced steel roof truss. No positive connection of the roof channel slabs is provided. Thus the roof inertia force can be collected and transferred to the vertical resisting systems by the roof channel slabs only through the friction forces developed between the channel slabs and supporting steel members. The channel slabs span in the east-west direction. Thus, under the east-west direction ground excitations, only half of a channel slab weight is effective in producing friction forces and resulting couples to transfer the roof inertia force to the end vertical braced frames (Figure 5-11). Therefore, the diaphragm capacity of the first horizontal force resisting system is very low and sliding between adjacent concrete channel slabs and between the slabs and roof beams will occur at a low response acceleration level. However, sufficient restraint will be provided by the parapet walls to limit motions of the roof slabs and prevent them falling provided the horizontal roof braced frame remains effective.

The roof braced frame will resist the roof inertia force as soon as sliding begins to occur in the roof channel slabs. The steel roof framing system consists of roof girders, roof beams, and double angle diagonal bracing members. Due to the high aspect ratio (approximately 5) of the turbine building, the roof frame is quite flexible. For N-S response, sliding of the roof slabs is restrained by the parapet wall as shown in Figure 5-11. Loss of this restraint capacity can be expected at a median acceleration response of the roof of approximately 0.7g. The capacities of the horizontal truss elements and the vertical braced frame systems are somewhat higher so that sliding of the channel slabs followed by falling of various individual slabs is expected before total failure and collapse of the total roof system is expected. As the individual roof slabs fall, the inertia loads on the braced frame system are proportionately reduced so that the steel frame system is expected to remain intact after most of the roof slabs have fallen for N-S excitation.

For E-W excitation, a somewhat similar failure mode is anticipated. In this case, the parapet wall has somewhat higher relative capacity so that the slabs will be restrained at the walls. In this case, buckling of the roof slabs as rigid links loaded end to end is expected at a median roof acceleration of over one g. Once buckling has occurred, relatively little sliding motion at one end of a slab is required before that end of the slab slips off the flange of the supporting steel beam and the slab will then fall to the operating floor. Loss of the restraint at the parapet wall or failure of the 3/4" diameter tie rods and subsequent failure of the horizontal roof truss are expected at slightly higher roof acceleration levels.

For both N-S and E-W excitation, it is expected that virtually all the roof slabs will fall inside the turbine building. This may be expected to result in loss of the turbine units as well as possible loss of equipment which is located under any open hatches or those with light steel gratings under the operating floor. It is not considered possible that falling roof slabs could damage the service water pipes. Although the steel framing in both the roof frame and the vertical braced frames may be expected to be damaged, it is expected to remain standing after loss of the concrete roof slabs. This relatively lightweight structure is then expected to withstand substantially higher excitation levels.

Other modes of failure involving impact between the turbine pedestal and the turbine building floor slabs or shear wall failures at the lower elevations of the turbine building, while resulting in structural damage to the turbine building and equipment within this structure, are not expected to result in damage to any safety related equipment. Therefore, no fragility curves are provided for any of the turbine building failure modes.

5.3 AUXILIARY BUILDING DESCRIPTION

The tee-shaped auxiliary and fuel handling building is located west of and is structurally continuous with the turbine building. A common wall joins the two structures below grade as shown in Figure 5-3, and a 24-inch thick reinforced concrete common wall is located between the two buildings from ground floor up to the auxiliary building roof level as shown in Figures 5-5 and 5-6. Structural connectivity between the two buildings is further provided by continuous floor slabs at various levels. The diesel generator rooms are an integral part of the structural complex. The auxiliary building, the fuel handling building, and the diesel generator rooms were all designed as Class I structures.

The auxiliary building is founded on a 5-ft thick soil-supported reinforced concrete mat at elevation 542 ft. The grade elevation is 591 ft. A reinforced concrete mat foundation was also used for the fuel handling building. The elevation of the mat at the spent fuel pit is 576 ft and the rest of the fuel handling building foundation mat is at the grade level (Figure 5-12). The diesel generator rooms at the north and south ends of the auxiliary building are founded on walls extending to a strip footing at elevation 557 ft 4 in. Reinforced concrete foundation walls of the auxiliary building are laterally supported by concrete floor slabs at elevations 560 ft, 579 ft and 592 ft. The floors are reinforced concrete slabs supported by concrete beams, columns, and foundation walls.

Above grade, the lateral force resisting system is a combination of braced structural steel frames and concrete slabs and walls. Vertical braced steel frames were erected on foundation walls around the periphery of the auxiliary-fuel handling building and diesel generator rooms. Various diameter steel pipe was used for the diagonal bracing. The entire vertical braced frames were then encased in reinforced concrete walls which form the shear wall system. The floors at elevations 617 ft, 630 ft, and 642 ft are reinforced concrete slabs supported by horizontal braced steel framing. At places where heavy floor loads were expected, shear studs were used at the top flange of the steel floor beams to achieve a composite action. The roofs of the auxiliary building and diesel generator rooms were constructed of a poured concrete slab supported by braced steel roof framing at elevations 668 ft and 658 ft.

The fuel handling building houses the spent fuel storage which is a rectangular concrete tank which extends from elevation 576'-0" to elevation 617'-0". Reinforced concrete walls rise on the three exterior sides from elevations 576 ft and 592 ft to the roof at elevation 663'-11-1/2". There are partial floor slabs at elevation 602'-0" and 617'-0" in the fuel handling buidling (Figure 5-12). A discontinuity between the auxiliary building and the fuel handling building is formed by the fuel transfer channel (Figure 5-13). The only structural connection is at the base slab and the roof level (Figure 5-14). The roof of the fuel handling building was constructed of 4-1/2" deep corrugated metal decking with a 12-inch concrete slab supported by steel roof framing (Figure 5-15).

Locations of some of the safety-related equipment and piping in the auxiliary building are given from Figures 5-16 to 5-18. These important equipment and piping are identified as: safety injection pumps, containment spray pumps, diesel generator oil storage tanks, feedwater pump seal water collection tank, motor driven and turbine driven steam generator feedwater pumps, auxiliary motor driven and turbine driven steam generator feedwater pumps, diesel generators, and condensate storage tanks. These locations are noted in relation to their proximity to structural walls.

5.4 AUXILIARY BUILDING FAILURE

Since the turbine and auxiliary buildings form a common structure, failure of any portion of the turbine building will affect the dynamic response characteristics of the auxiliary building. Thus, the loss of the turbine building precast roof slabs will result in different overall structure frequencies and seismic load distribution. A sequential analysis to account for various structural changes was not conducted during Phase I of the SSMRP nor was any nonlinear seismic response analysis. All failure modes evaluated in this investigation were based on the elastic response loads obtained from the finite element model of the combined turbine/auxiliary building developed by LLL as part of Project IV of the SSMRP. These loads were obtained from a number of LLL time history analyses selected to provide both the median loads and the variabilities of these loads. The fragility parameter selected for the auxiliary building failure modes is the equivalent elastic response of Node 3006 of the LLL model which is located at the approximate cg of the control room floor slab at elevation 642 feet.

At elevations above ground level, structural steel braced frames are encased in the concrete shear walls and floor and roof slabs. With one or two exceptions, no shear connectors or reliable bond between the steel members and concrete exists. Thus, instead of having a reliable composite force resisting system, the concrete and steel tend to behave as a redundant system. Due to its relative flexibility, the steel frame structure carries little load as long as the concrete wall and floor system remains intact. Once failure of the concrete occurs, load is transferred to the braced frame system. However, the capacity of the steel framing is significantly less than that of the concrete so that once failure of the concrete occurs, failure of that part of the structure will rapidly follow provided there is no redundant structure available to carry the redistributed seismic loads. In addition to the failure modes discussed below, a number of other modes of failure were investigated and found to have significantly higher capacity levels or relatively minor effects. Typical of the latter is vertical floor slab response which may be expected to result in local flexure failure and spalling of concrete near the walls. This is not expected to substantially reduce the diaphragm capacity of the slabs however, and damage to equipment from the relatively small size concrete fragments generated is not expected to seriously damage most components.

5.4.1 N-S Auxiliary Building Shear Wall Failure

The lowest level significant structural failure mode within the auxiliary building consists of failure of the common shear wall between the auxiliary building and the turbine building. This failure is expected to initiate at El. 592' where the composite wall construction consisting of braced steel framing with in-fill reinforced concrete panels begins. In this wall, shear studs are welded to the steel column webs to ensure a composite action between the concrete penels and the braced steel frame and to provide continuity of the concrete shear wall across the columns. After the common shear wall-braced frame fails, the shear load will be redistributed to the remaining shear walls at this story. However, because this wall resists a major portion of the load and contributes significantly to the story shear capacity, it is expected that failure of the remaining shear walls will immediately follow failure of the common wall. This can be assumed to result in failure of most of the auxiliary building above El. 592'. This will include failure of the diesel generator buildings as they are an integral part of the auxiliary building structure. Failure of the structure and Class I equipment below El. 592' will not necessarily occur at the same acceleration level since the shear wall capacity at the lower elevations exceeds that above El. 592'.

Failure of the shear wall is a complex nonlinear mechanism involving first the failure of the shear studs, redistribution of shear loading to the in-fill panels, and finally flexural failure of the in-fill panels.

The force-deflection curve for the common wall between El. 592' and El. 617' is shown in Figure 5-19. Stiffness of the braced frames is included. The wall behaves elastically until initial shear stud failure occurs. Initial failure occurs when the vertical shear force at a steel column exceeds the vertical shear capacity. The vertical shear force was determined from the elastic shear stress distribution predicted by:

$$\tau = \text{shear stress}$$

$$= \frac{V_h Q}{Ih}$$

where

V_h = horizontal shear force

Q = first statical moment of area above section under consideration

U = moment of inertia

h = wall thickness

The vertical shear capacity was determined using the shear stud capacity given in Section 3.1.5. As the wall is continually divided into panels separated by steel columns, successive shear stud failure will occur as load is redistributed after each failure of an in-fill panel to column joint. As failure progresses the total shear was distributed to the panels in proportion to their stiffnesses and subsequent vertical shear failures determined. Reductions in total shear upon resisted vertical shear failures are due to reductions in total stiffness and flexural yielding of individual panels (those panels not containing embedded steel columns). The wall is completely subdivided into individual panels when the last shear stud failure occurs. The force-deflection curve for increased deflection is then defined by the force-deflection curves of the individual panels, shown combined together in Figure 5-19.

Behavior of individual panels is governed by flexure rather than shear because of the low steel reinforcement ratios. Flexural deformations were determined from moment-curvature relationships for each of the panels. Panels were limited to deflections causing maximum concrete compressive strains of ε_u (Reference 29), where

$$\varepsilon_u = 0.003 + \frac{0.5}{Z}$$

$$= 0.00355 \text{ in/in}$$

Z = span distance from point of maximum moment to point of zero moment (in.)

Panels were assumed to lose their load-resistance at their deflection limits, thus resulting in the discontinuities in the force-deflection curve of Figure 5-19 for drifts greater than 0.06 ft.

The total effective energy available to a structural system subjected to approximately three to five excursions into yield (anticipated for a maximum earthquake) is a combination of the recoverable and non-recoverable energy. Recoverable energy is associated with ductile behavior while non-recoverable energy is associated with non-ductile (brittle) behavior. An example of each is shown in Figure 5-20. The energy enclosed by the force-deflection curve for combined individual panels in flexure is recoverable because the panels can sustain multiple yield excursions without loss of load-carrying capability. It is estimated that 75% of the recoverable energy for a member subjected to monotonic loading is effective during an earthquake having three yield excursions. The energy enclosed by the force-deflection curve corresponding to loading and failure of the shear studs is non-recoverable because load-carrying capability under multiple cycles of the studs is lost once the studs have been loaded to failure. Also, energy associated with individual panels loaded past their deflection limits must be considered non-recoverable. It is estimated that one-third of the non-recoverable energy is effective during an earthquake having three yield excursions. A median effective energy available of 257 k-ft corresponding to the common wall being displaced to the lowest panel deflection limit (7.09×10^{-2} ft) was calculated).

Because the effective energy is essentially a measure of the capacity, it was preferable to determine a median capacity factor directly, then calculate corresponding median strength and inelastic energy absorption factors. An elasto-plastic force-deflection curve with elastic stiffness K_e and yield force V_{eff} was proposed. The initial elastic stiffness was used for K_e since this corresponds to the assumptions of the original design-analysis. For different values of V_{eff}, an equivalent ductility ratio, μ_{eff}, corresponding to the median effective energy was calculated.

E_{eff} = median effective energy

= 257 k-ft

V_{eff} = yield strength

K_e = initial elastic stiffness

Δ_y = yield deflection

$$= \frac{V_{eff}}{K_e}$$

μ_{eff} = equivalent effective ductility ratio

The relationship between energy, yield strength and ductility is:

$$E_{eff} = V_{eff}\,\Delta_y\,(\mu_{eff} - 0.5)$$

$$= \frac{V_{eff}^2}{K_e}\,(\mu_{eff} - 0.5)$$

The effective ductility can be expressed as:

$$\mu_{eff} = \frac{E_{eff}\,K_e}{V_{eff}^2} + 0.5$$

Median strength and inelastic energy absorption factors corresponding to combinations of V_{eff} and μ_{eff} that produce the effective energy, E_{eff}, were combined resulting in different median capacity factors. The lowest capacity factor for credible range of V_{eff} thus calculated was selected for determination of the median acceleration capacity. This value, 7.0, resulted from an assumed V_{eff} of 5000 k, the approximate total yield shear force for flexural failure of the individual wall panels.

A median shear strength of 20,000 k, the shear force that causes initial stud failure, was assumed. The resulting median strength factor is 4.4. The median inelastic energy absorption (ductility) factor was then derived as:

$$\check{F} = \frac{\check{F}_c}{\check{F}_s}$$

$$= 1.6$$

The median response acceleration capacity for the common turbine/ auxiliary building shear wall is thus approximately 1.1g at node 3006.

Variabilities of the strength and inelastic energy absorption factors were determined by first calculating the variability of the capacity factor and then finding corresponding variabilities of the strength and inelastic energy absorption faction. The capacity factor was determined using effective values of strength and ductility. Since the effective strength was an assumed value for the purpose of calculation only, there is no variability associated with it. Variability of the capacity factor is thus dependent on variability of the effective ductility ratio.

The effective ductility ratio is seen to be dependent on the total effective energy and the elastic stiffness. Random variability of the total effective energy is a function of the random variabilities of the concrete strength and rotational capacity and the steel yield strength. The random variability of the elastic stiffness is due to variability of the concrete modulus of elasticity. The resulting logarithmic standard deviation associated with randomness of the effective ductility was determined to be approximately 0.29. With this estimate, the logarithmic standard deviation associated with randomness for the capacity factor (equal to that of the equivalent inelastic energy absorption factor) was determined to be 0.12.

Uncertainty of the effective ductility ratio is a combination of the uncertainties of the flexural capacity and limit deflection of the individual wall panels, the percentages of the recoverable and non-recoverable energies effective in resisting cyclic loading, and the elastic stiffness. The uncertainty of the effective ductility ratio was combined with the estimated uncertainty for the response reduction predicted by Reference 23 to give a logarithmic standard deviation associated with uncertainty of the capacity factor of 0.20.

The randomness of the actual strength factor is dependent on the randomness of the concrete compressive strength. The logarithmic standard deviation associated with randomness of the strength factor is thus 0.07 (Section 3.1.5). The uncertainty of the strength factor is a combination of the uncertainty of the stud shear strength and the distribution of shear stress in the wall. The logarithmic standard deviation associated with uncertainty of the strength factor is estimated to be 0.14.

The variabilities of the inelastic energy absorption factor were back-calculated from the variabilities of the capacity and strength factors. The logarithmic standard deviations associated with randomness and uncertainty of the inelastic energy absorption factor are:

$$\beta_R = 0.10$$

$$\beta_U = 0.14$$

The fragility curves associated with this mode of failure are shown in Figure 5-21 The median response acceleration at Node 3006 for failure of this wall is approximately 1.1g.

5.4.2 Diesel Generator Room Shear Wall Failure

At very slightly above the same median capacity, failures of the outermost E-W shear walls (Column Lines 5 and 35) are expected. Failure of these walls is expected to be initiated at elevation 592 ft from N-S excitation. Due to the torsional response in the structure, the E-W shear walls are highly loaded from N-S excitation. There are a number of redundant E-W shear walls between the generator rooms as well as the auxiliary building at Column Lines 10 and 20 and other locations which can be expected to carry additional loads once the maximum capacity of the outermost walls is reached. Thus, although the outermost walls may be expected to reach their ultimate capacity and experience substantial cracking, the load will be transferred to adjacent walls and collapse of a significant part of the diesel generator rooms is not expected until higher levels of response are reached. There will then be a sequential failure of the shear walls from the extremities of the combined auxiliary building and diesel rooms propagating towards the center of the structure. However, in conjunction with the definition of failure described in Chapter 3, functionality of equipment attached to or immediately adjacent to these walls cannot be guaranteed above these levels. The fragility curves for the diesel generator building shear walls from N-S excitation are shown in Figure 5-22. The median response acceleration capacity for this mode of failure is expected to be approximately 1.1g at node 3006. This is based on the assumption that the common wall between the turbine and auxiliary remains functional although in fact, it is expected to fail at essentially the same response level as discussed in Section 5.4.1.

5.4.3 Failure of Masonry Walls

A number of concrete block masonry walls are located throughout the auxiliary building. For the most part, these walls are non-load bearing or at most support an unloaded concrete slab. The walls are typically constructed of 1-foot thick concrete blocks, vertically reinforced, and grouted. The evaluation of these walls was conducted using in-structure response spectra generated in the original design analysis scaled up to the response acceleration level required to cause failure. Typical of these walls are those around the control room and enclosing the 125 V DC batteries. The collapse mechanism for these walls consists of cracking through the mortar near the base, midsection, and top, followed by rigid body rotation of segments of the wall restrained by the reinforcing steel which forms plastic hinges. Typically, some portions of the wall may be dislodged and collapse vertically, but much of the wall can be expected to be retained by the steel although in a shattered condition. Failure of these walls may be expected to result in loss of function of any attached conduit or equipment but will be quite localized and will not affect any other structural members. The fragility curves associated with masonry walls at elevation 592' are shown in Figure 5-23. The median response acceleration capacity at node 3006 associated with failure of the walls is approximately 1.7g. Walls at lower elevations may be expected to have higher equivalent ground motion capacity.

5.4.4 Shear Wall Failure for E-W Excitation

The auxiliary building, including the diesel generator rooms and the fuel storage building, has higher seismic capacity to withstand E-W excitation than if the excitation is primarily in a N-S direction. This occurs in part because the structure is essentially symmetric about the east-west axis and very little torsional response results for E-W excitation.

Failure from E-W excitation is expected to be initiated in the shear walls along Column Lines 17 and 23 at elevation 592 ft. After yielding of these walls occurs, some load redistribution is expected but only marginally higher load capacity may be expected. The structure below elevation 592 ft, as in the case of N-S excitation, has somewhat higher capacity than the shear wall system with the embedded steel structure but yielding in the lower elevations will begin before failure of the walls above elevation 592 ft occurs. Failure of the walls along Column Lines 17 and 23 may be expected to result in failure of the two 400,000 gallon capacity refueling water storage vaults which may result in flooding of some components in addition to other damage. The fragility curves for failure of the auxiliary building shear wall system for E-W excitation are shown in Figure 5-24. The median expected response acceleration capacity at node 3006 for failure due to E-W excitation is approximately 2.7g. This is twice the capacity expected for excitation primarily in the N-S direction.

5.4.5 Auxiliary Building Roof Diaphragm Failure

The roof of the tee-shaped auxiliary building is a 21-inch thick reinforced concrete slab. The lowest capacity failure modes for the auxiliary building consists of a shear failure of this slab along Column Line P due to N-S excitation. The roof slab is supported on a shelf angle so that only the upper reinforcing steel in the slab is effective. A sketch of this detail is shown in Figure 5-14. Loss of the roof diaphragm results in the requirement that the concrete walls resist the lateral inertia force in transverse bending. This capacity is relatively low. Failure of the reinforced concrete walls in bending about the weak axis then leads to the collapse of the roof. The control room equipment at the floor immediately below (elevation 642 ft) will be severely damaged by the collapsed roof. The fragility curves corresponding to this mode of failure are shown in Figure 5-25. The median acceleration response capacity at node 3006 is approximately 3.0g, again assuming no failures associated with the previous failure modes have occurred.

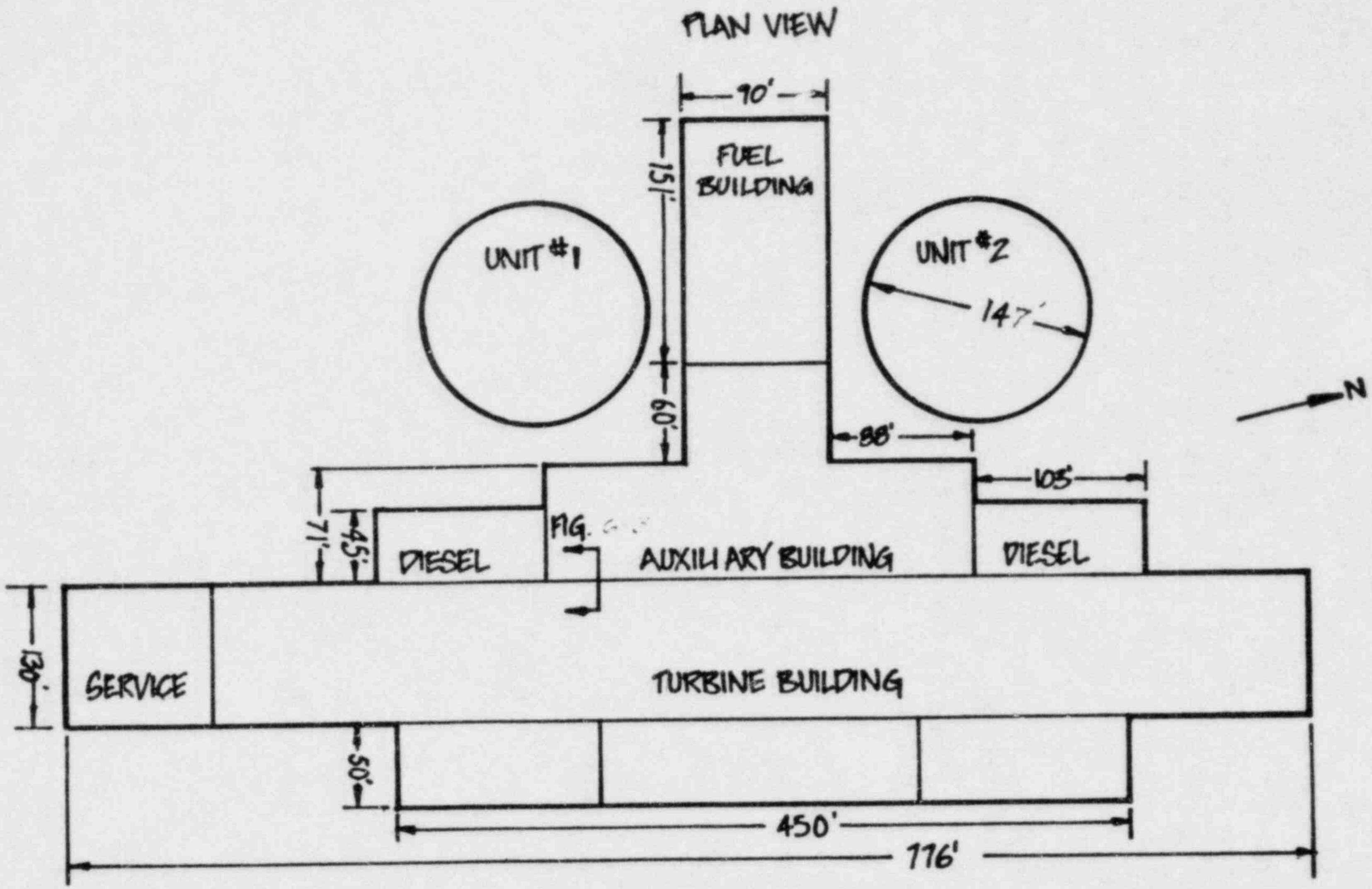

FIGURE 5-1. **ZION STATION PLAN VIEW**

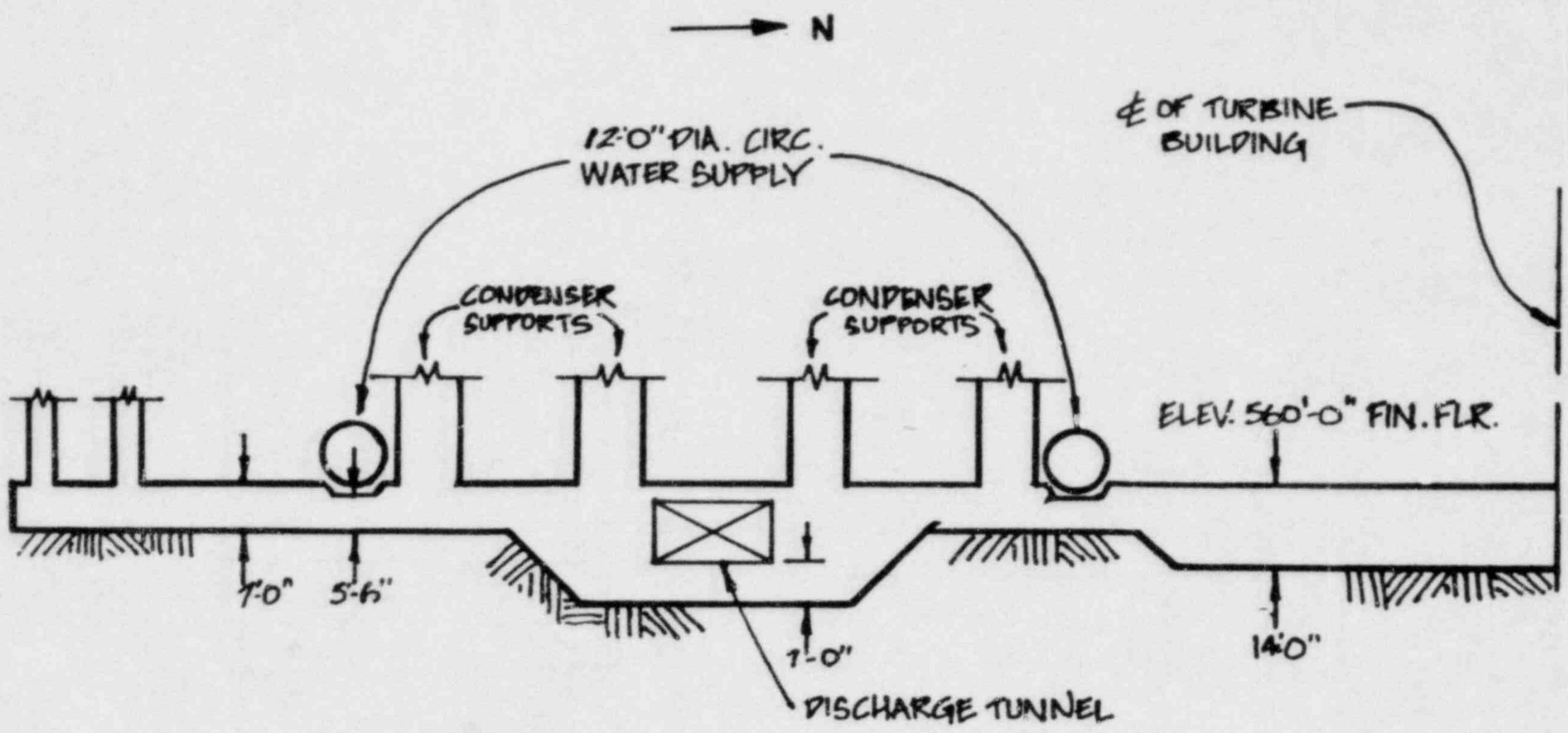

FIGURE 5-2. LONGITUDINAL SECTION OF THE TURBINE BUILDING FOUNDATION MAT

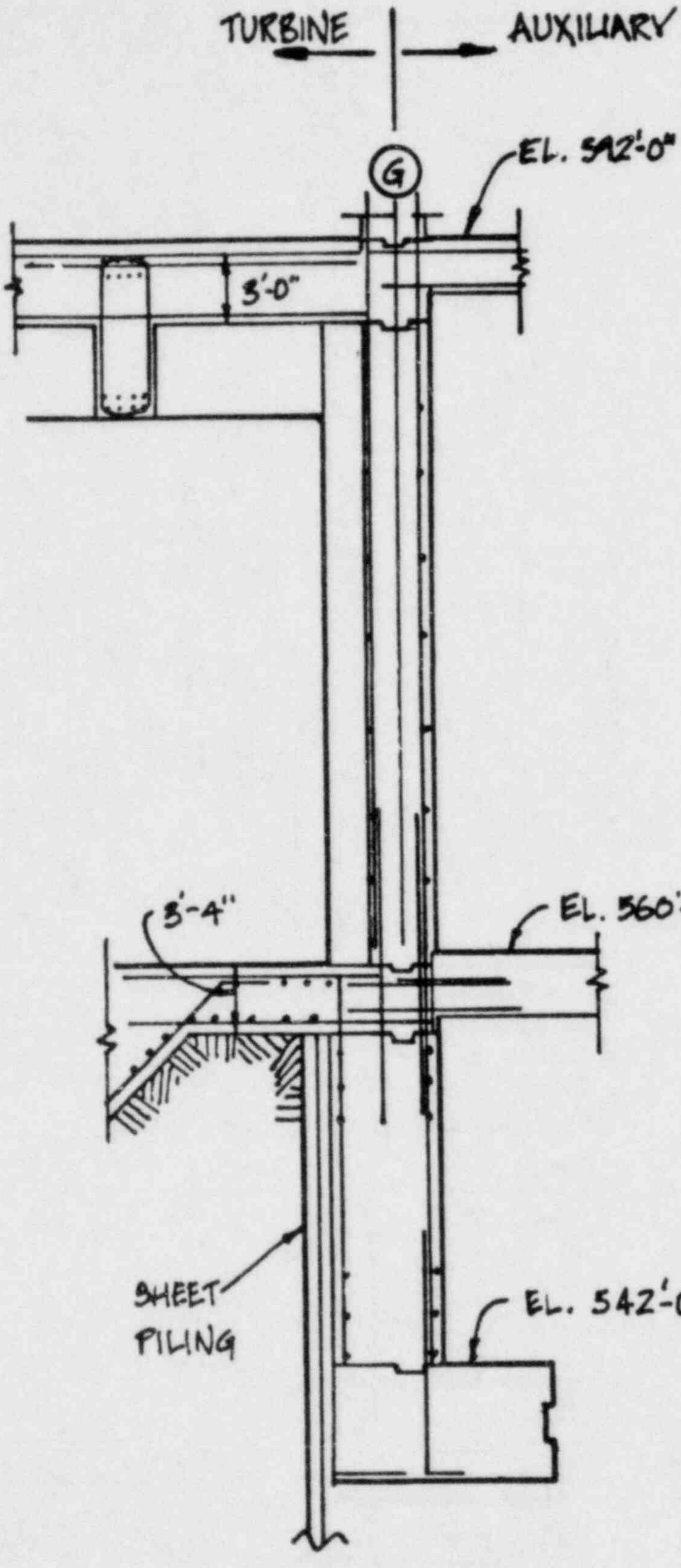

FIGURE 5-3. STRUCTURAL CONNECTIVITY BETWEEN THE TURBINE AND AUXILIARY BUILDING AT EL. 560'-0" and 592'-0"

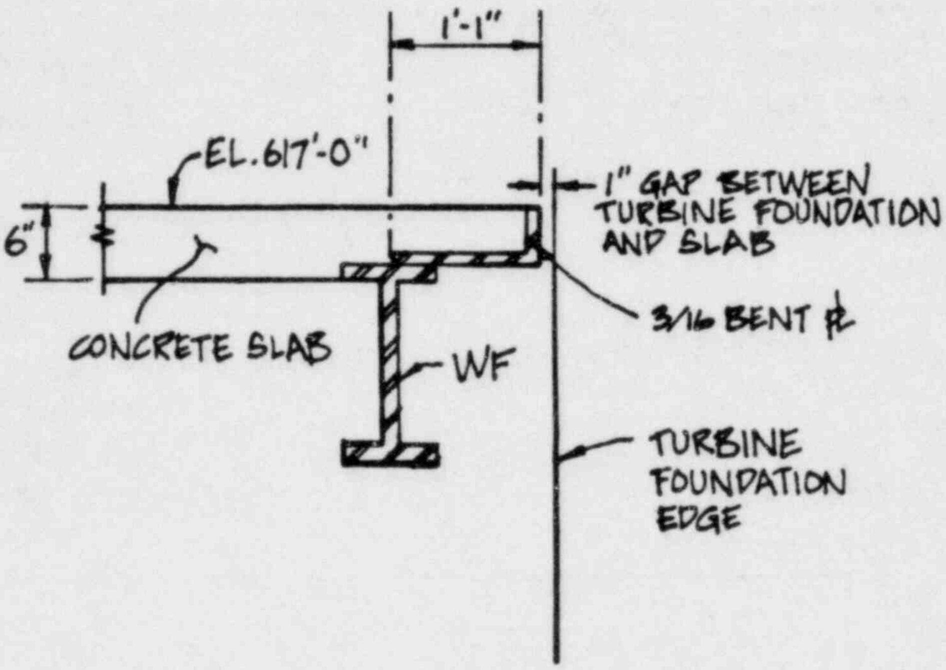

FIGURE 5-4. ISOLATION OF THE TURBINE FOUNDATION (CONCRETE FRAME)

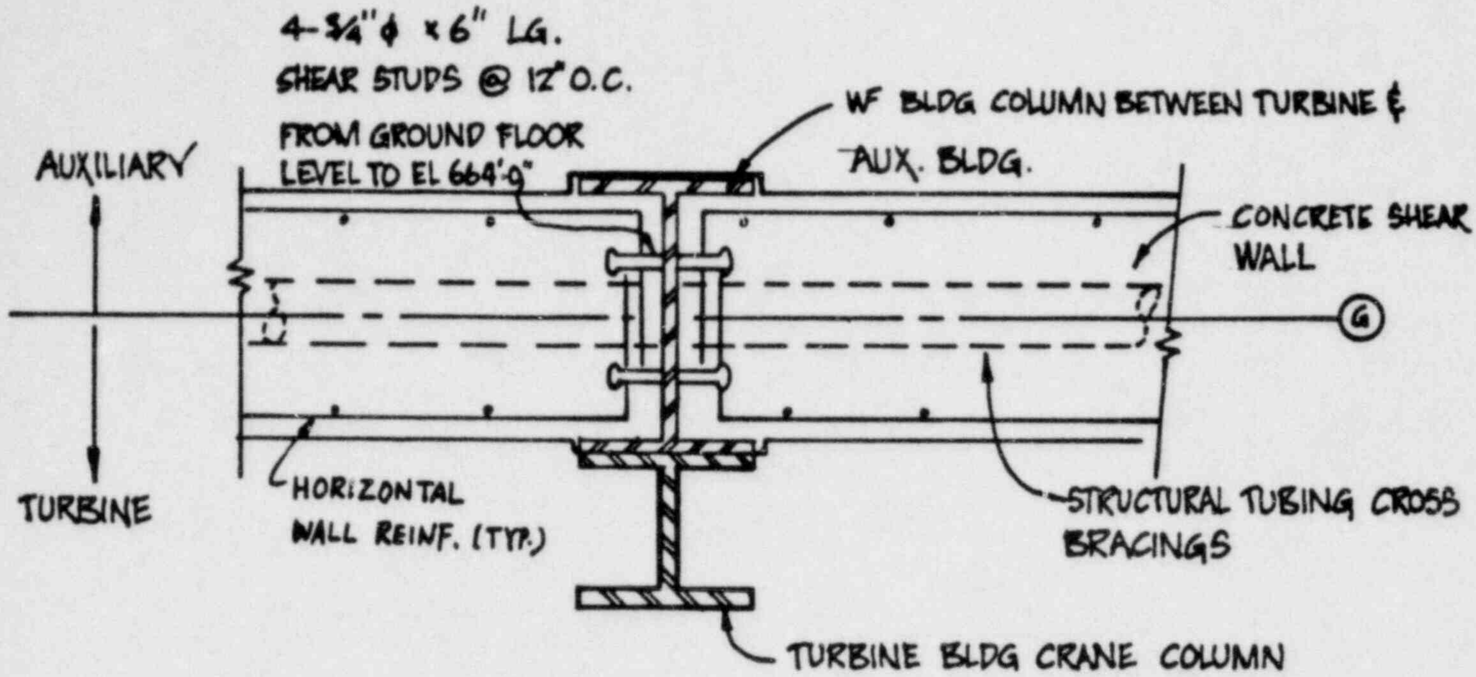

STEEL BRACED FRAME AND SHEAR WALL ALONG LINE (G)

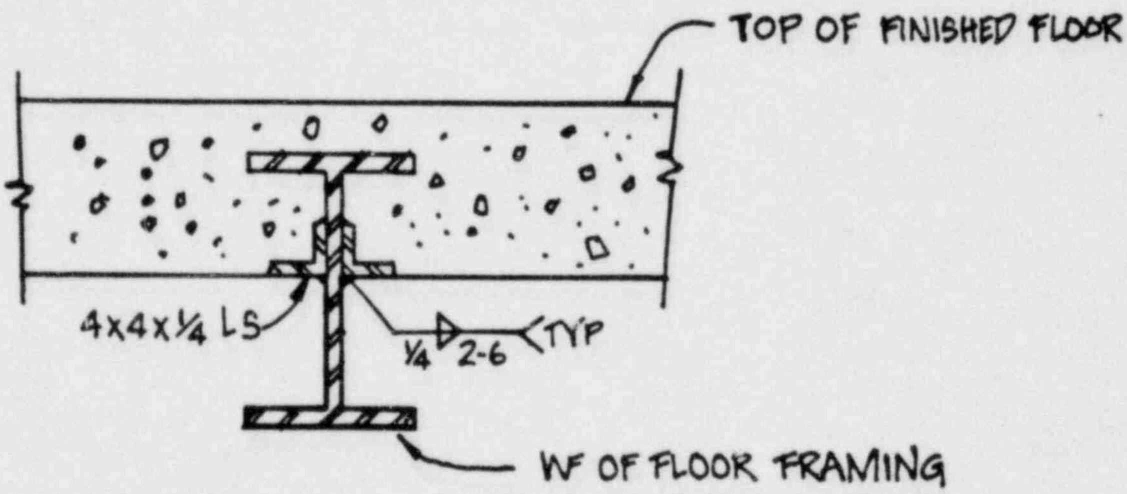

TYPICAL CONCRETE FLOOR CONSTRUCTION

FIGURE 5-5. STRUCTURAL DETAIL OF THE TURBINE BUILDING WEST WALL AND TYPICAL CONCRETE FLOOR SLAB

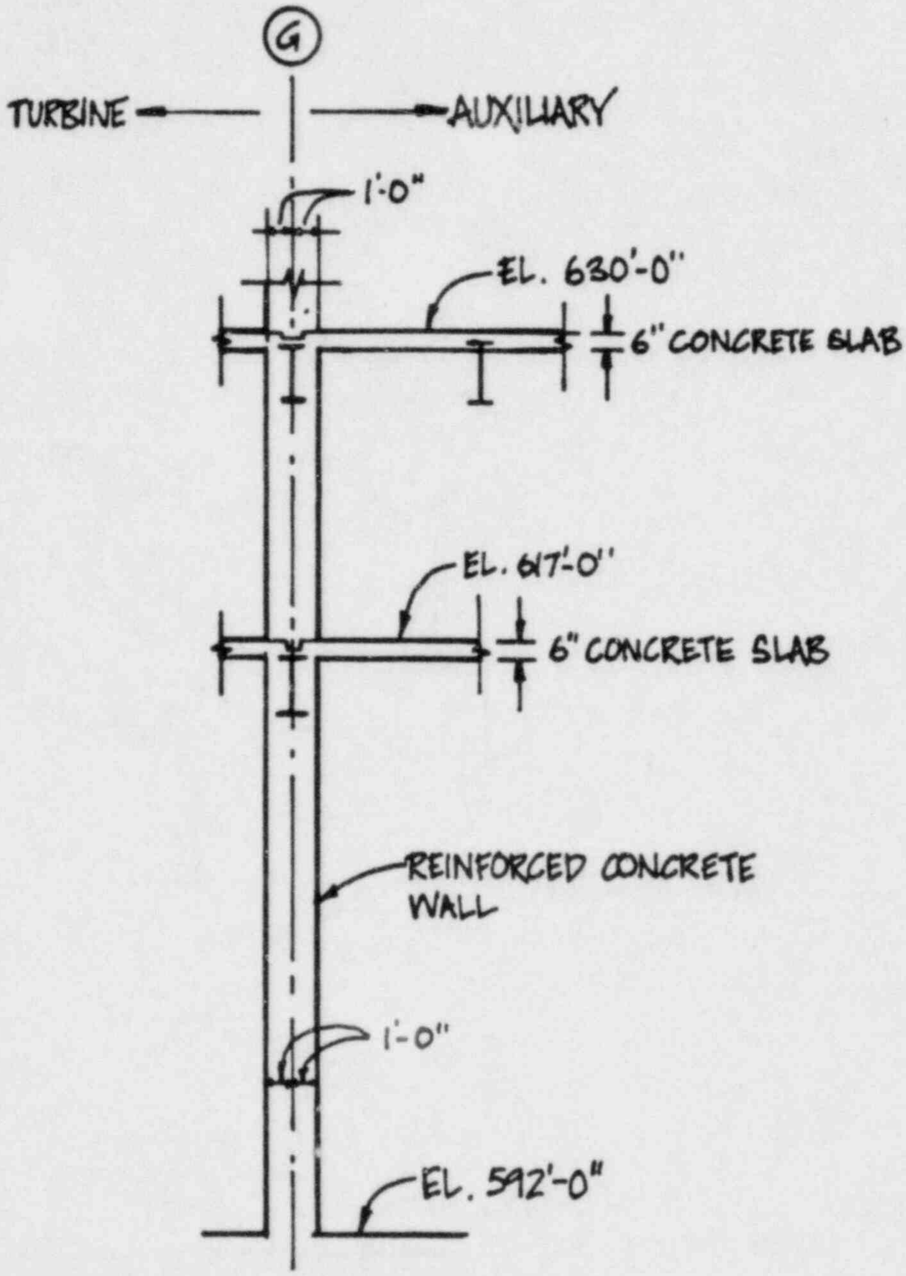

FIGURE 5-6. STRUCTURAL CONNECTIVITY BETWEEN THE TURBINE AND AUXILIARY BUILDING AT ELEVATIONS 617'-0" and 630'-0"

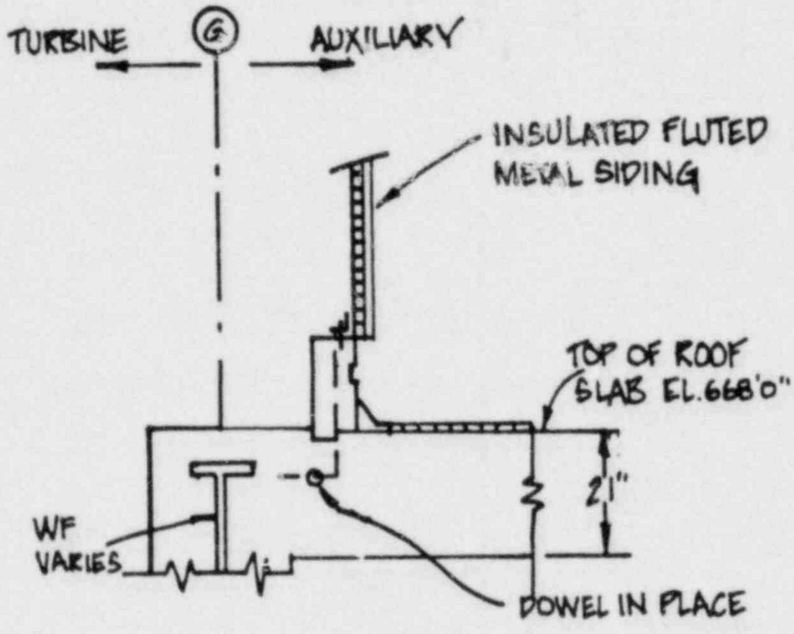

FIGURE 5-7. DETAIL OF TURBINE BUILDING WALL ABOVE THE AUXILIARY BUILDING ROOF LEVEL

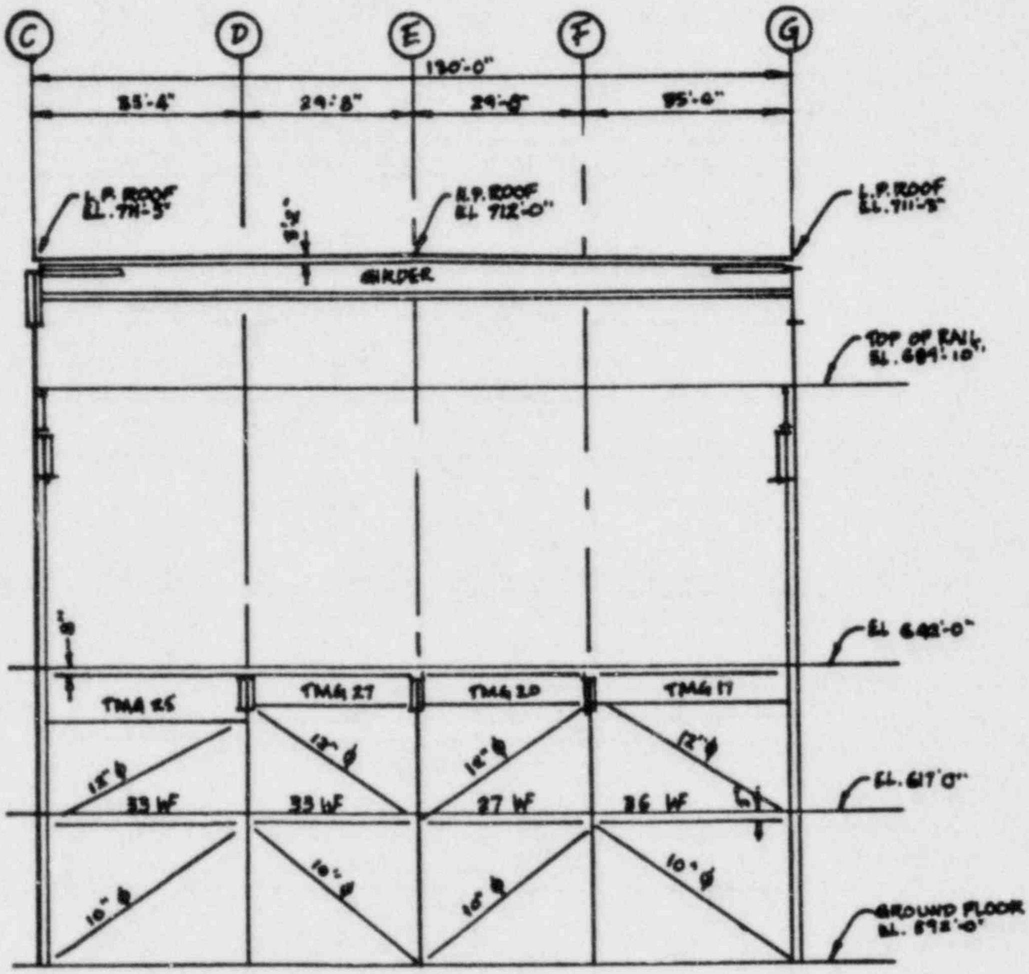

FIGURE 5-8. TRANSVERSE SECTION OF THE TURBINE BUILDING

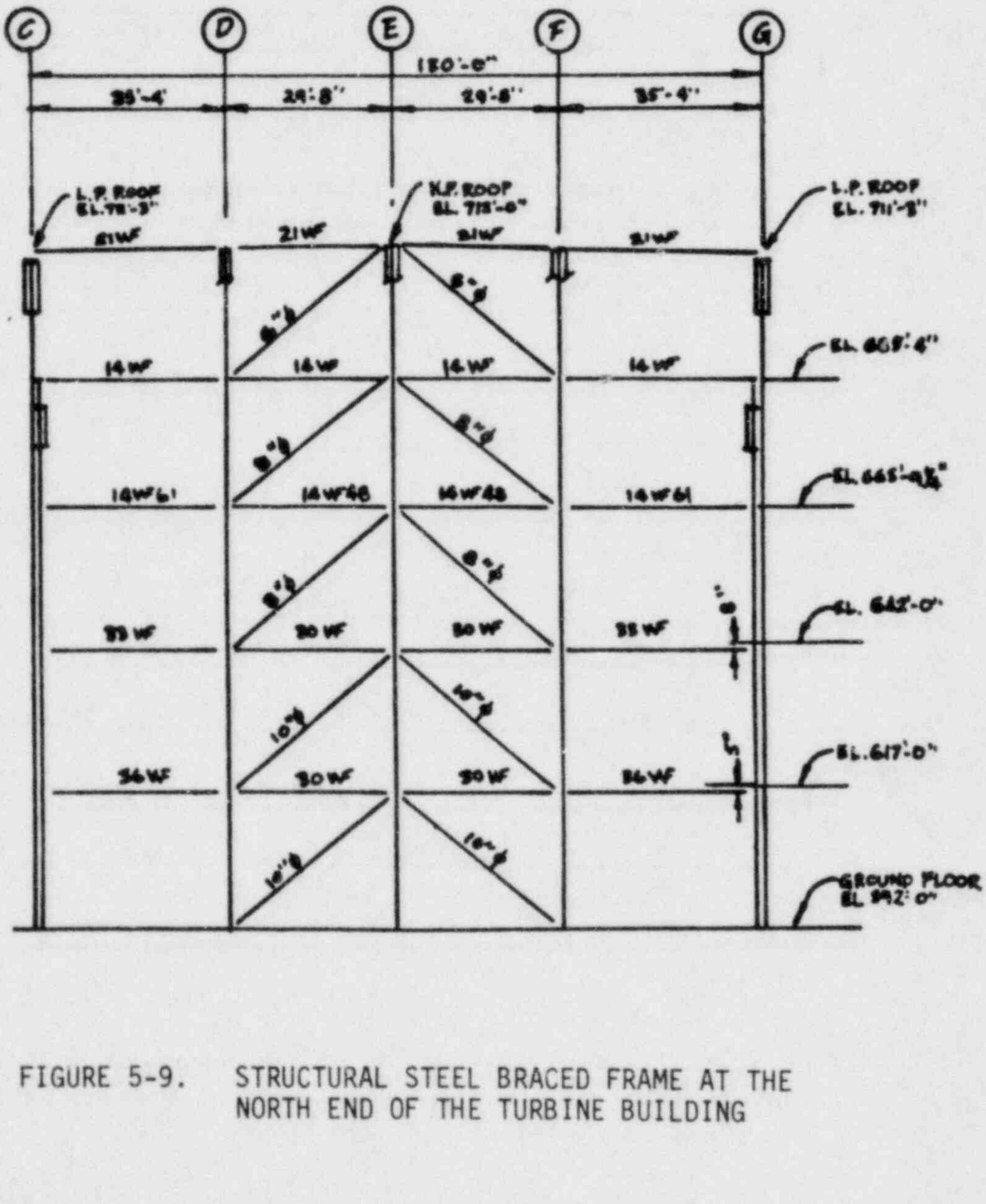

FIGURE 5-9. STRUCTURAL STEEL BRACED FRAME AT THE NORTH END OF THE TURBINE BUILDING

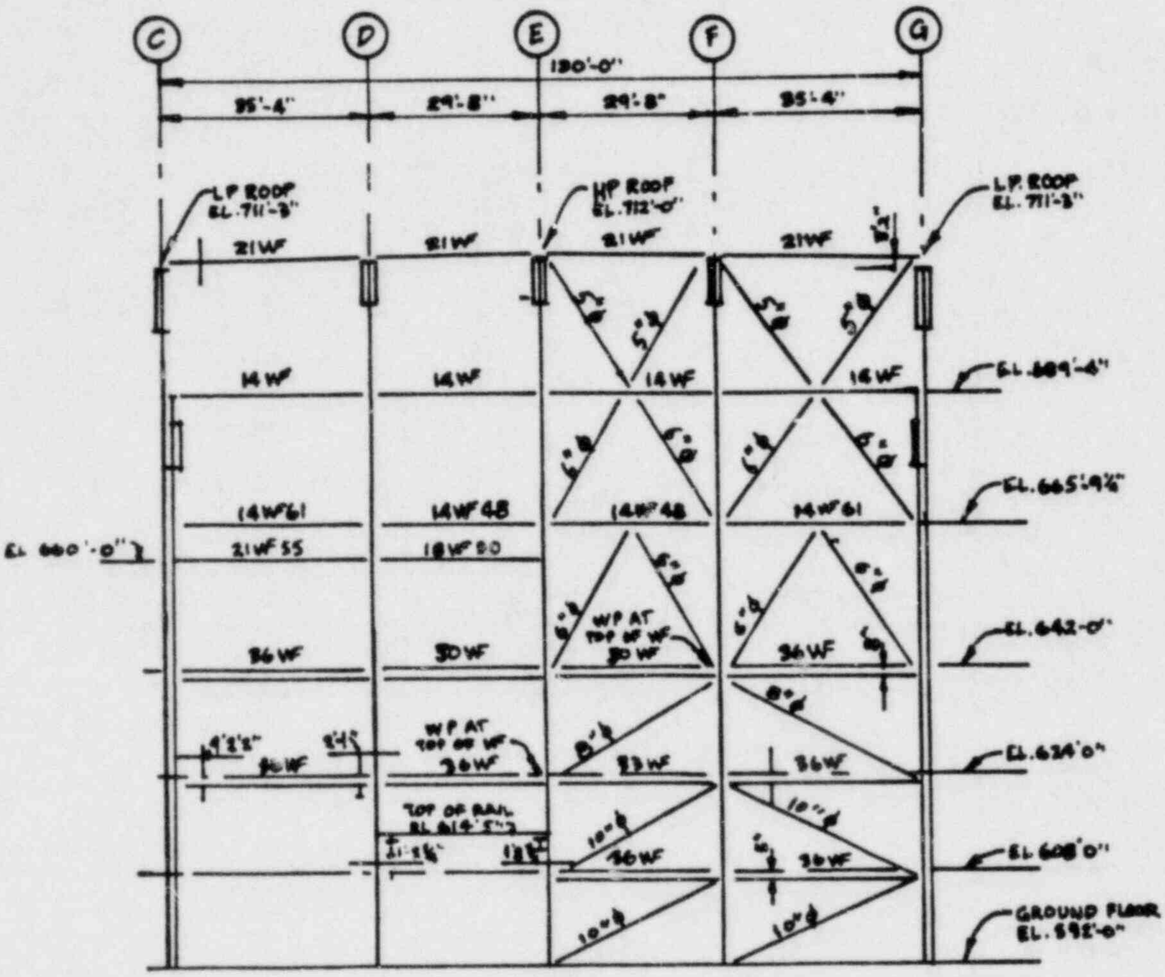

FIGURE 5-10. STRUCTURAL STEEL BRACED FRAME AT THE SOUTH END OF THE TURBINE BUILDING

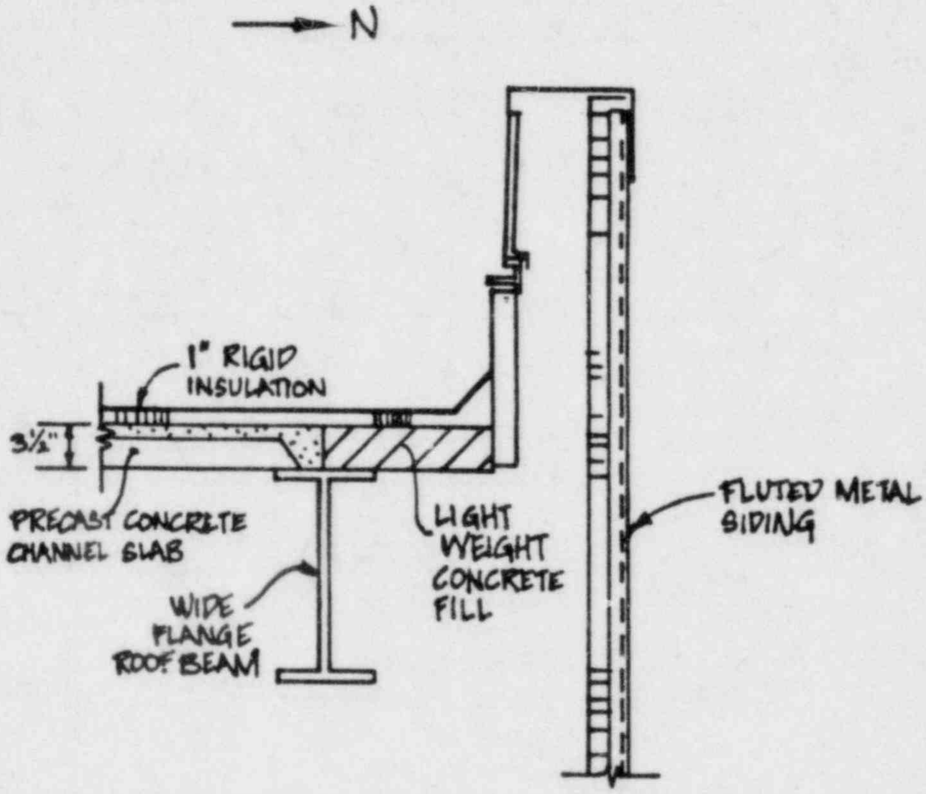

5-11. TURBINE BUILDING ROOF DETAIL AT THE END BRACED STEEL FRAMES

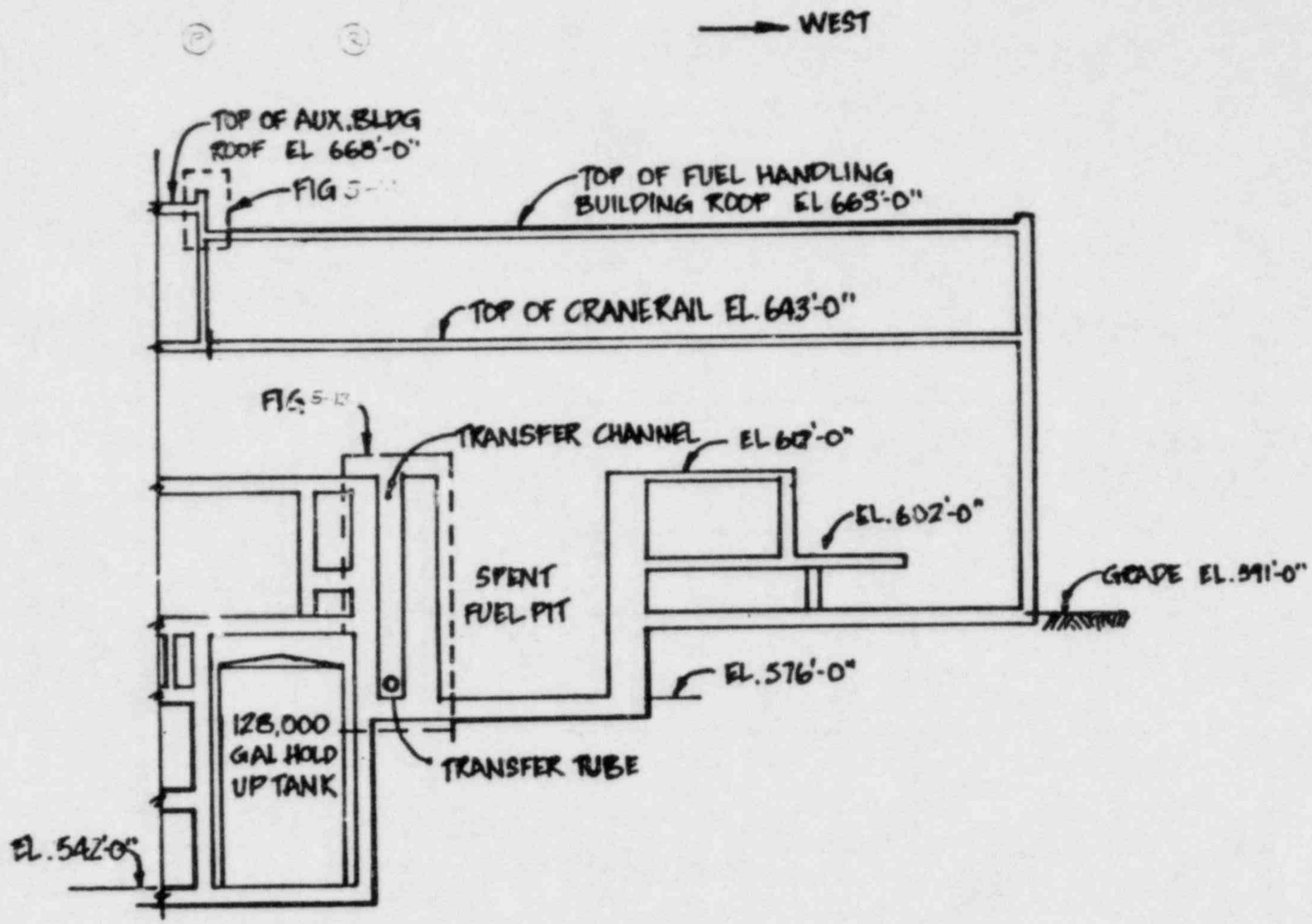

FIGURE 5-12. LONGITUDIN'. SECTION OF THE FUEL HANDLING BUILDING

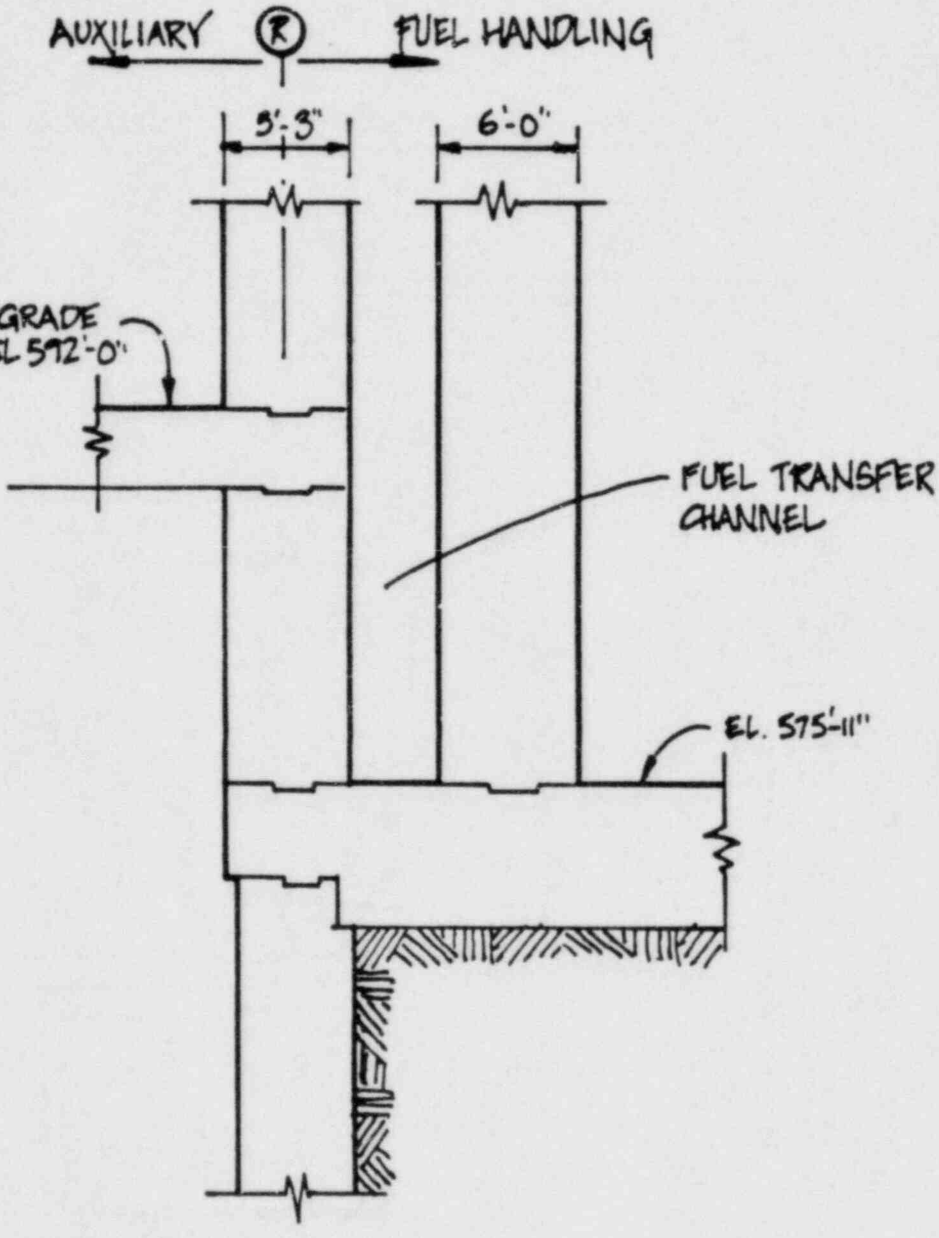

FIGURE 5-13. AUXILIARY-FUEL HANDLING BUILIDNG AT ELEVATION 592'-0"

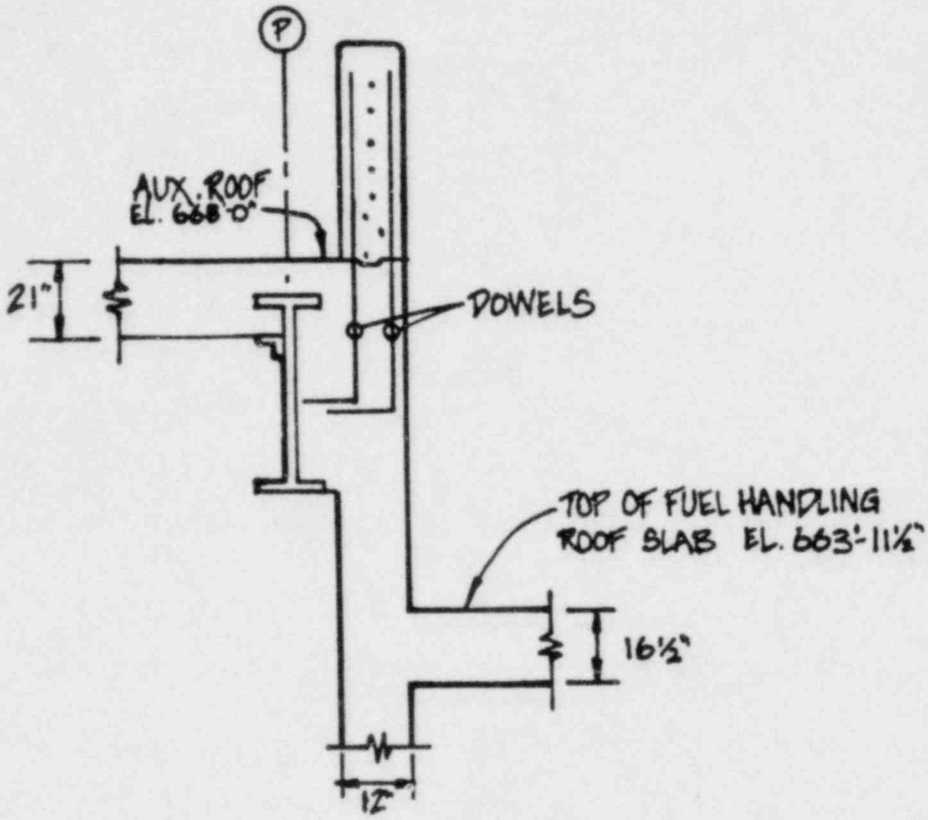

FIGURE 5-14. AUXILIARY-FUEL HANDLING BUILDING AT THE ROOF LEVEL

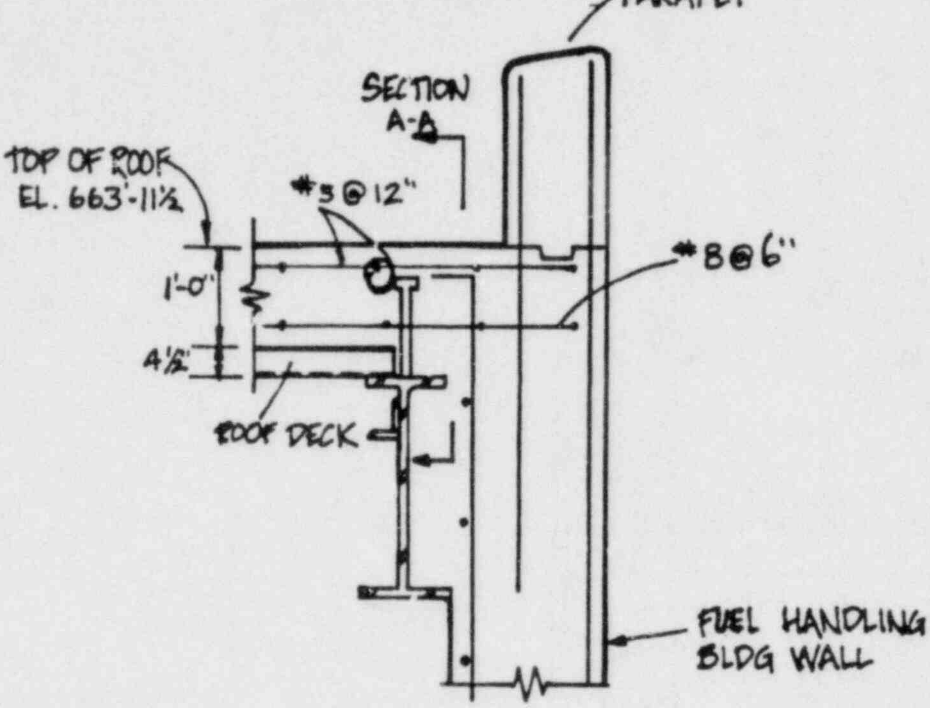

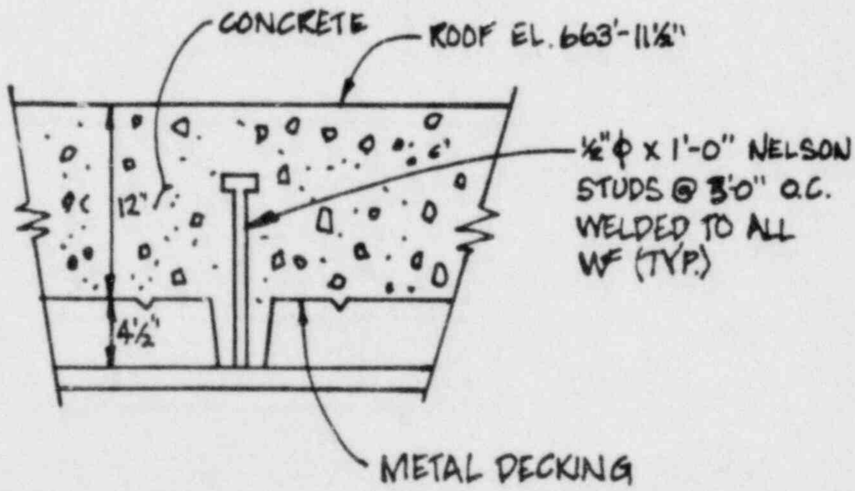

FIGURE 5-15. DETAIL OF THE FUEL HANDLING BUILDING ROOF SLAB

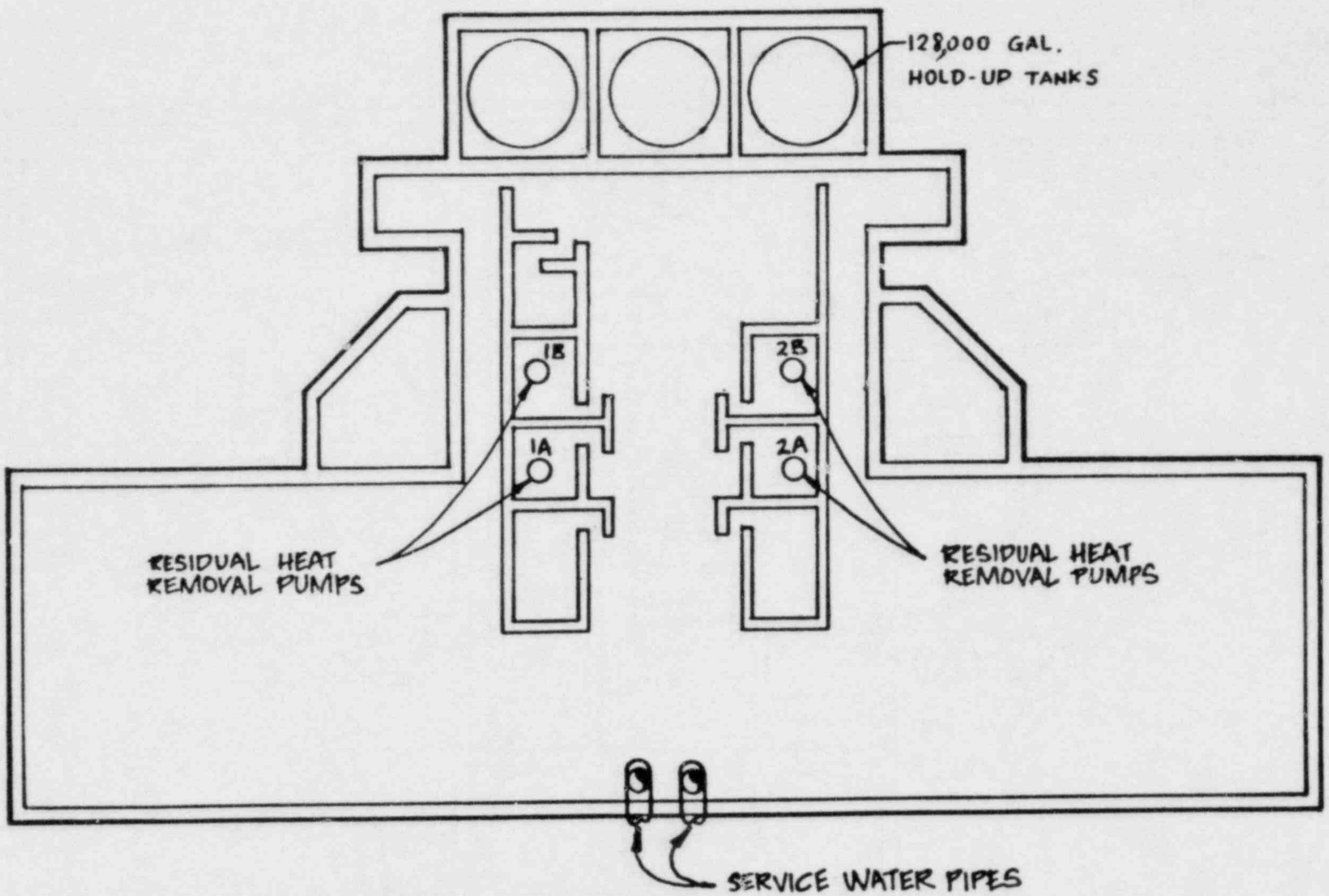

FIGURE 5-16. LOCATION OF SAFETY-RELATED EQUIPMENT AT FLOOR ELEVATION 542 FT. OF THE AUXILIARY BUILDING

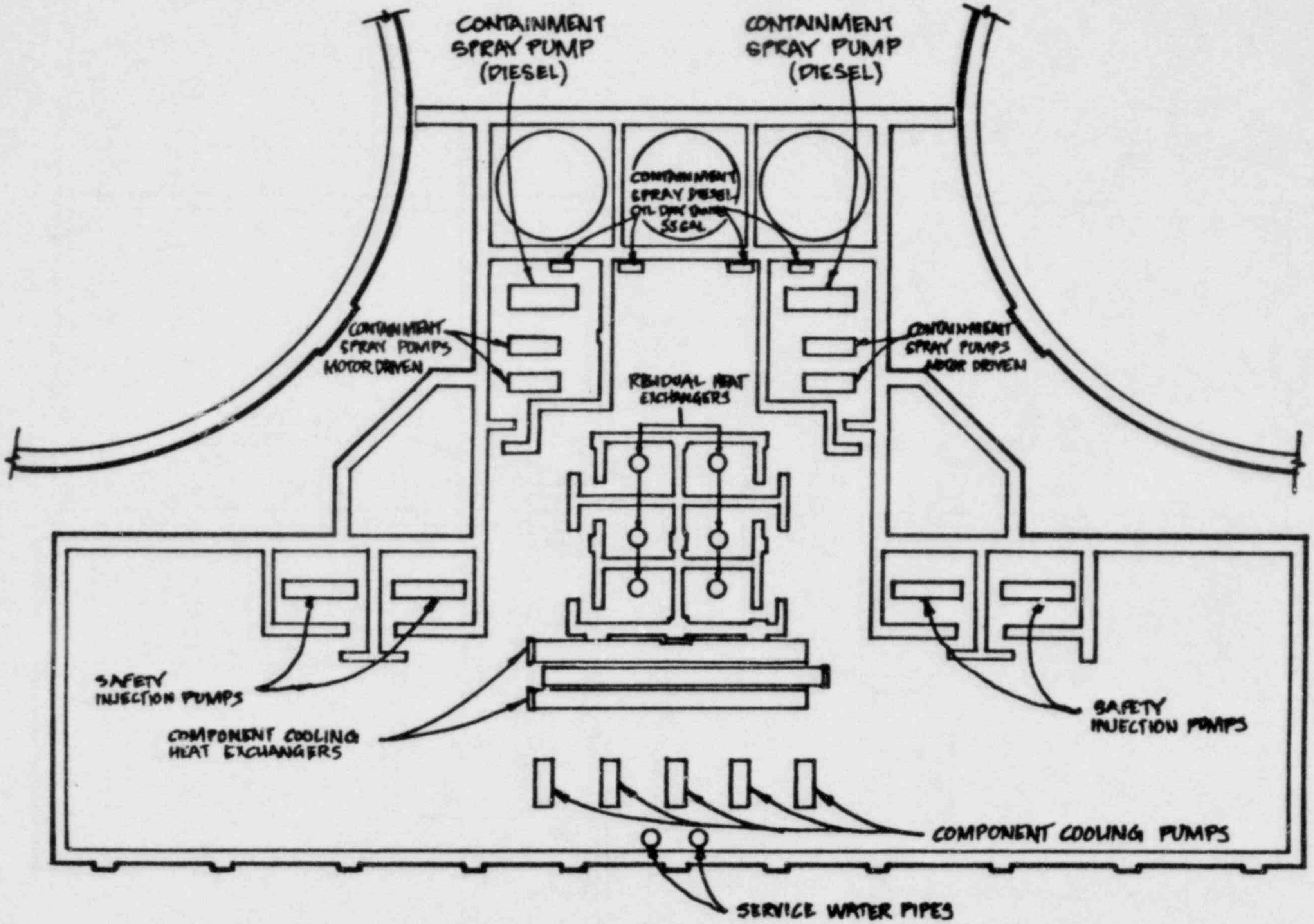

FIGURE 5-17. LOCATION OF SAFETY-RELATED EQUIPMENT AT FLOOR ELEVATION 560 FT. OF THE AUXILIARY BUILDING

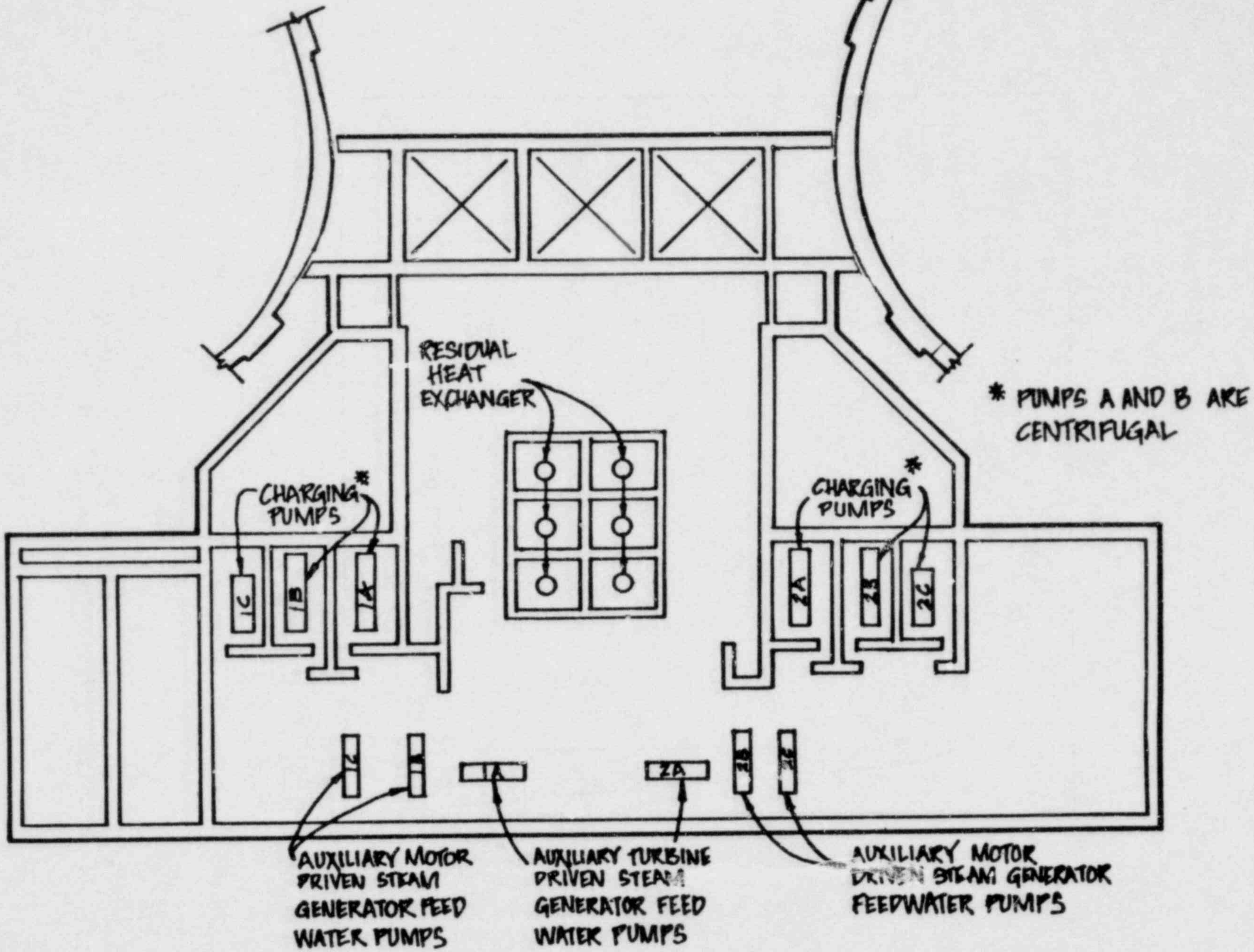

FIGURE 5-18. LOCATION OF SAFETY-RELATED EQUIPMENT AT FLOOR ELEVATION 579 FT. OF THE AUXILIARY BUILDING

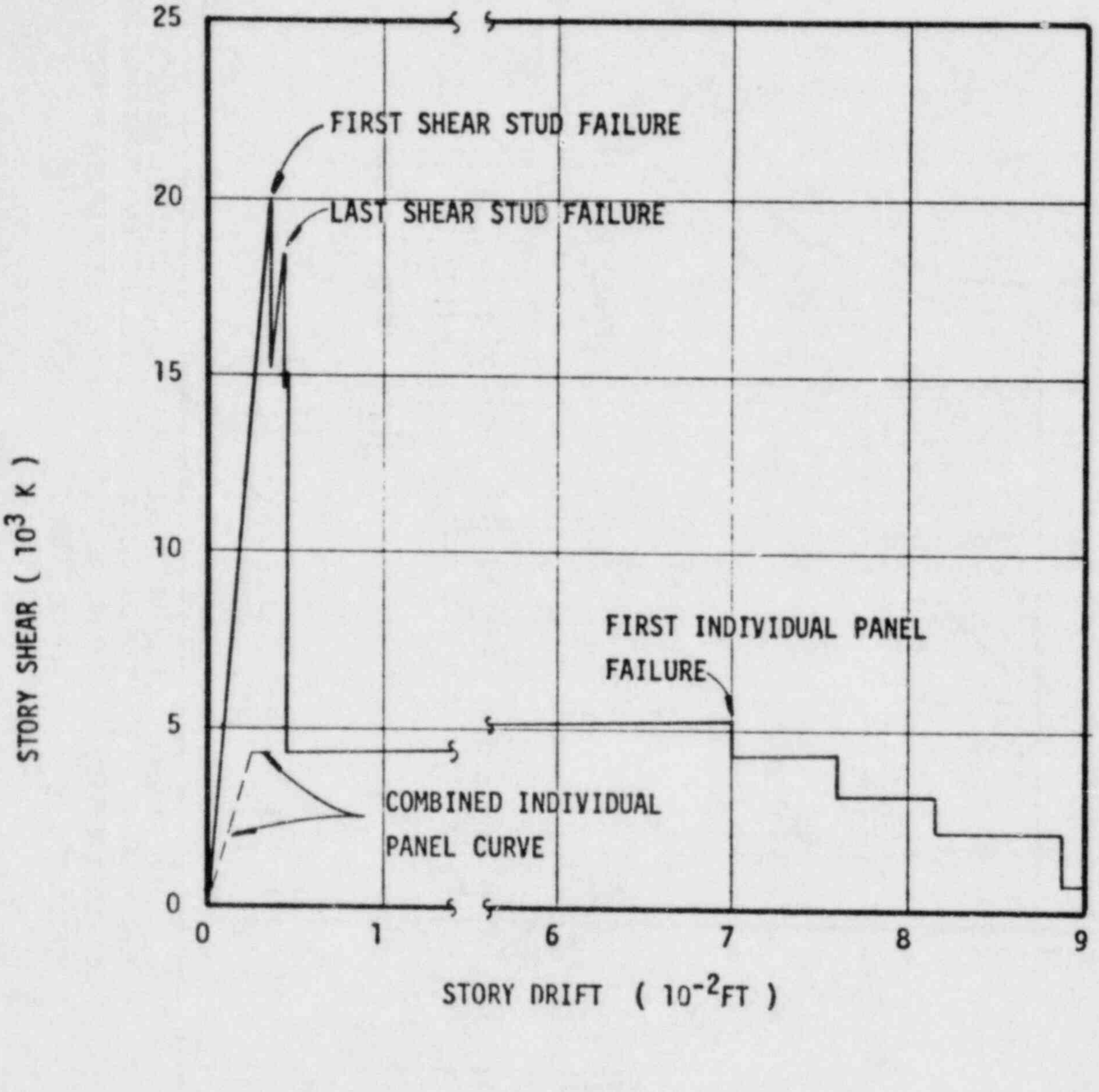

FIGURE 5-19. FORCE-DEFLECTION CURVE FOR COMMON WALL BETWEEN ELS. 592' and 617'

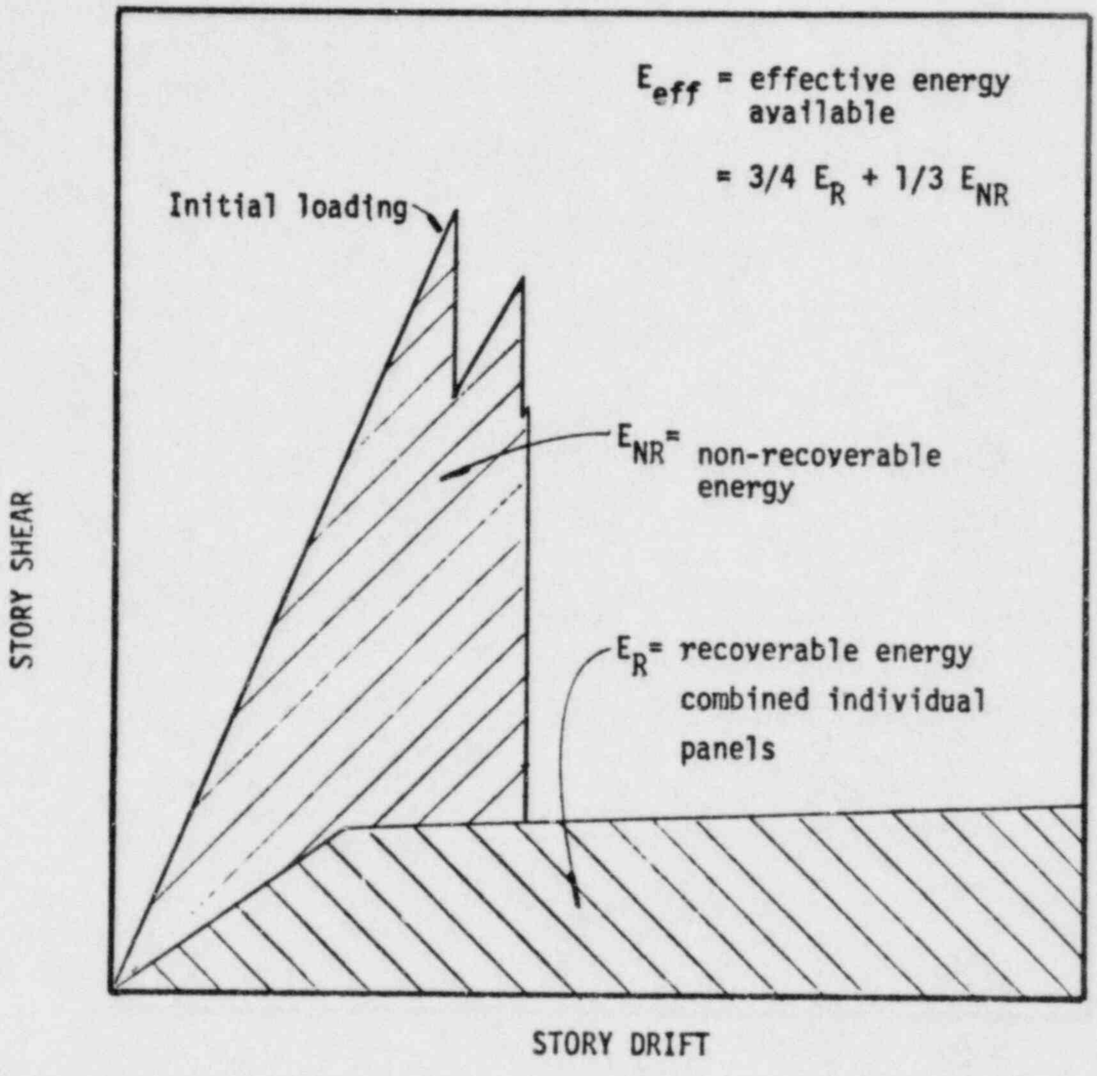

FIGURE 5-20. RECOVERABLE AND NON-RECOVERABLE ENERGY

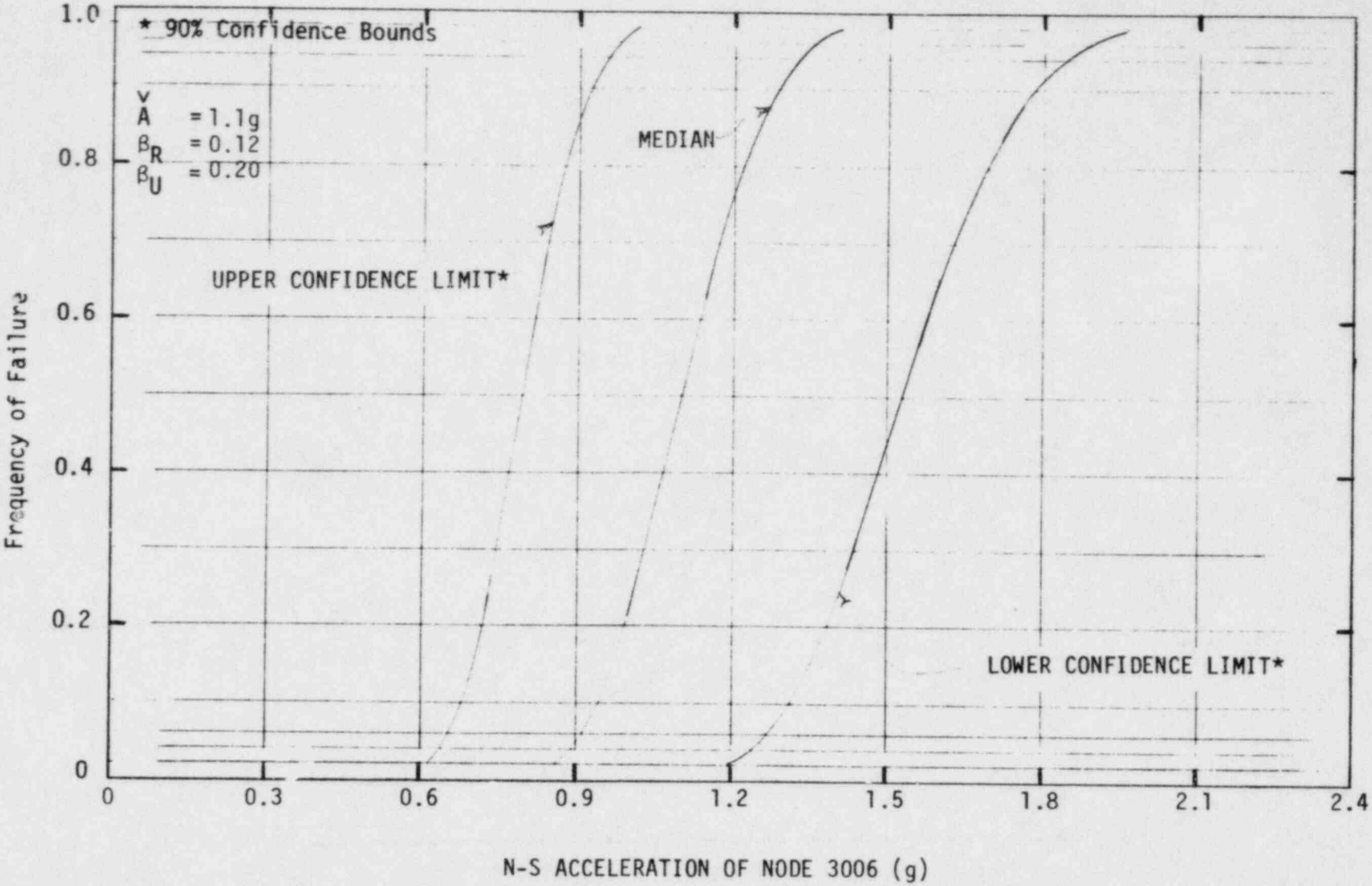

FIGURE 5-21. FAILURE OF AUXILIARY BUILDING SHEAR WALLS DUE TO N-S GROUND MOTION

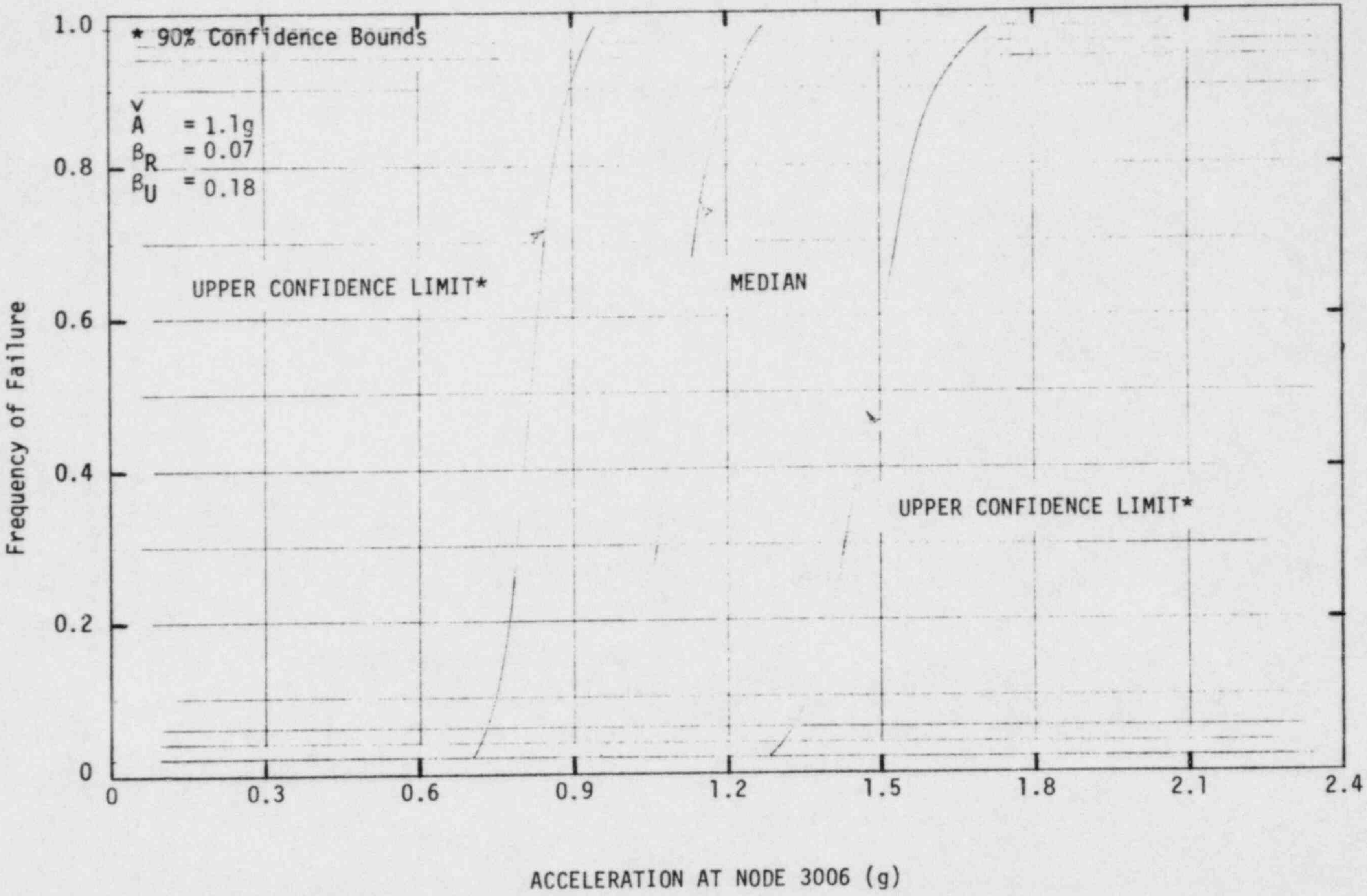

FIGURE 5-22. FAILURE OF DIESEL GENERATOR BUILDING WALLS

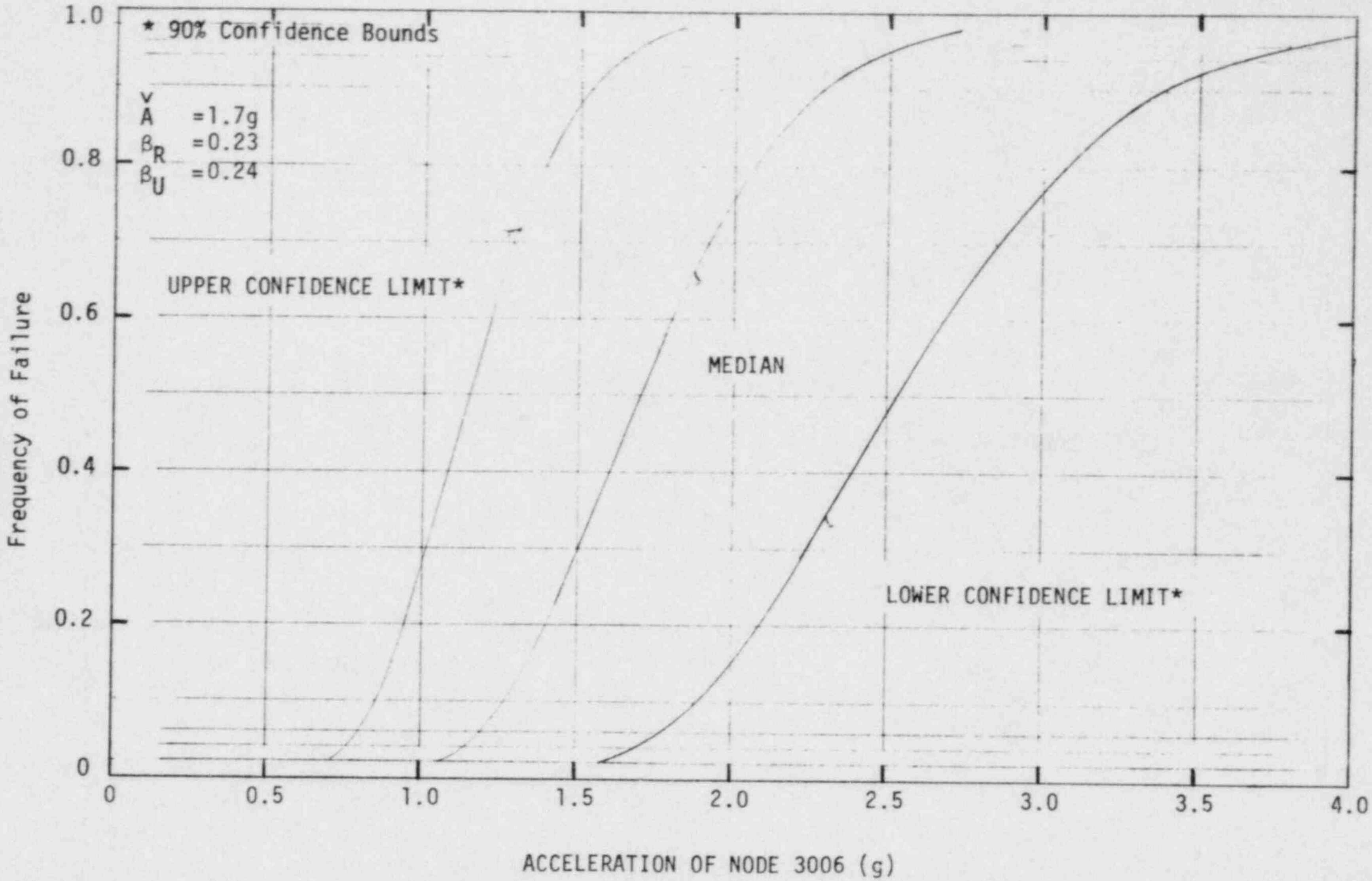

FIGURE 5-23. COLLAPSE OF MASONRY WALLS AROUND CONTROL ROOM

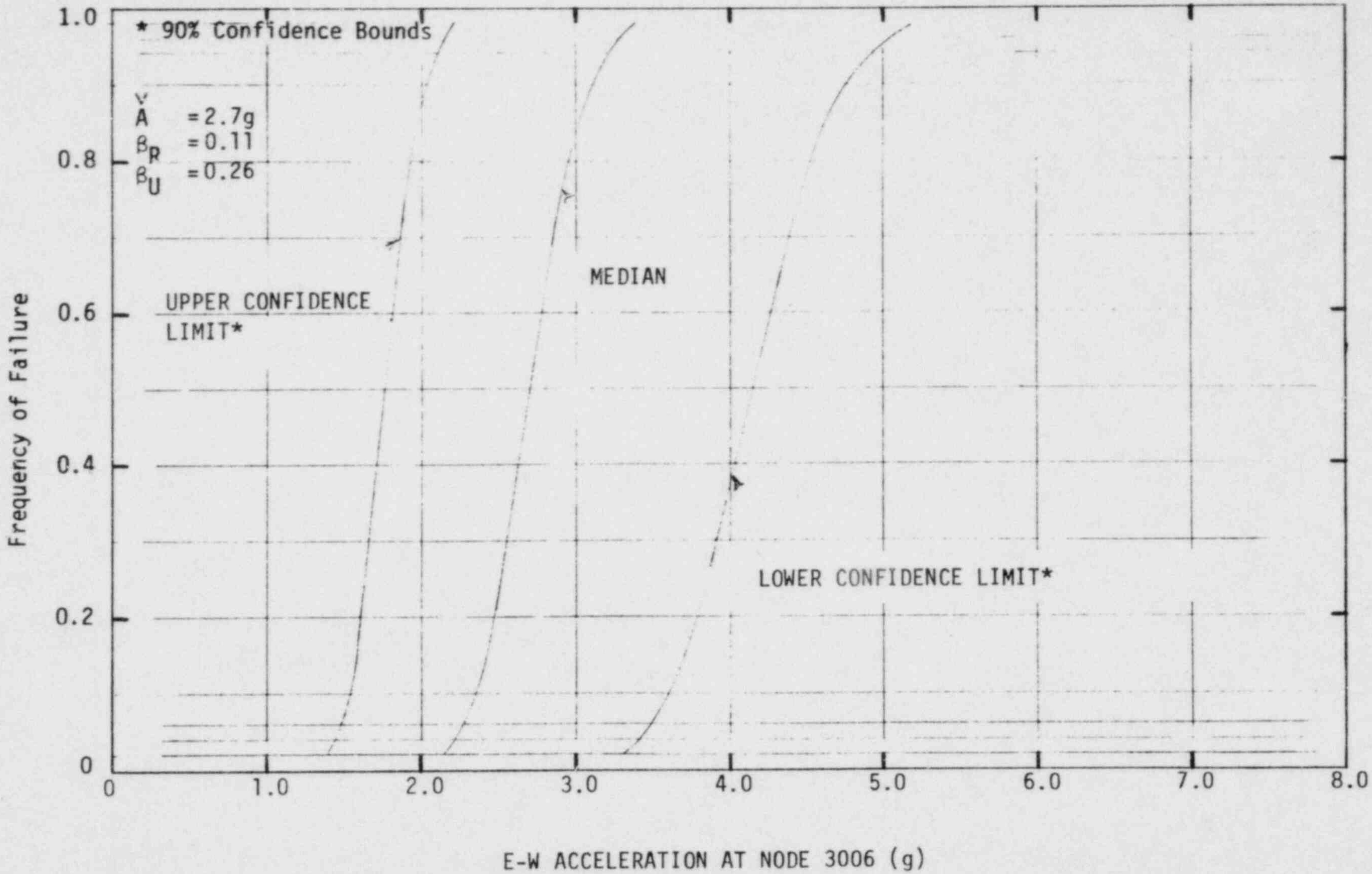

FIGURE 5-24. FAILURE OF AUXILIARY BUILDING SHEAR WALLS DUE TO E-W GROUND MOTION

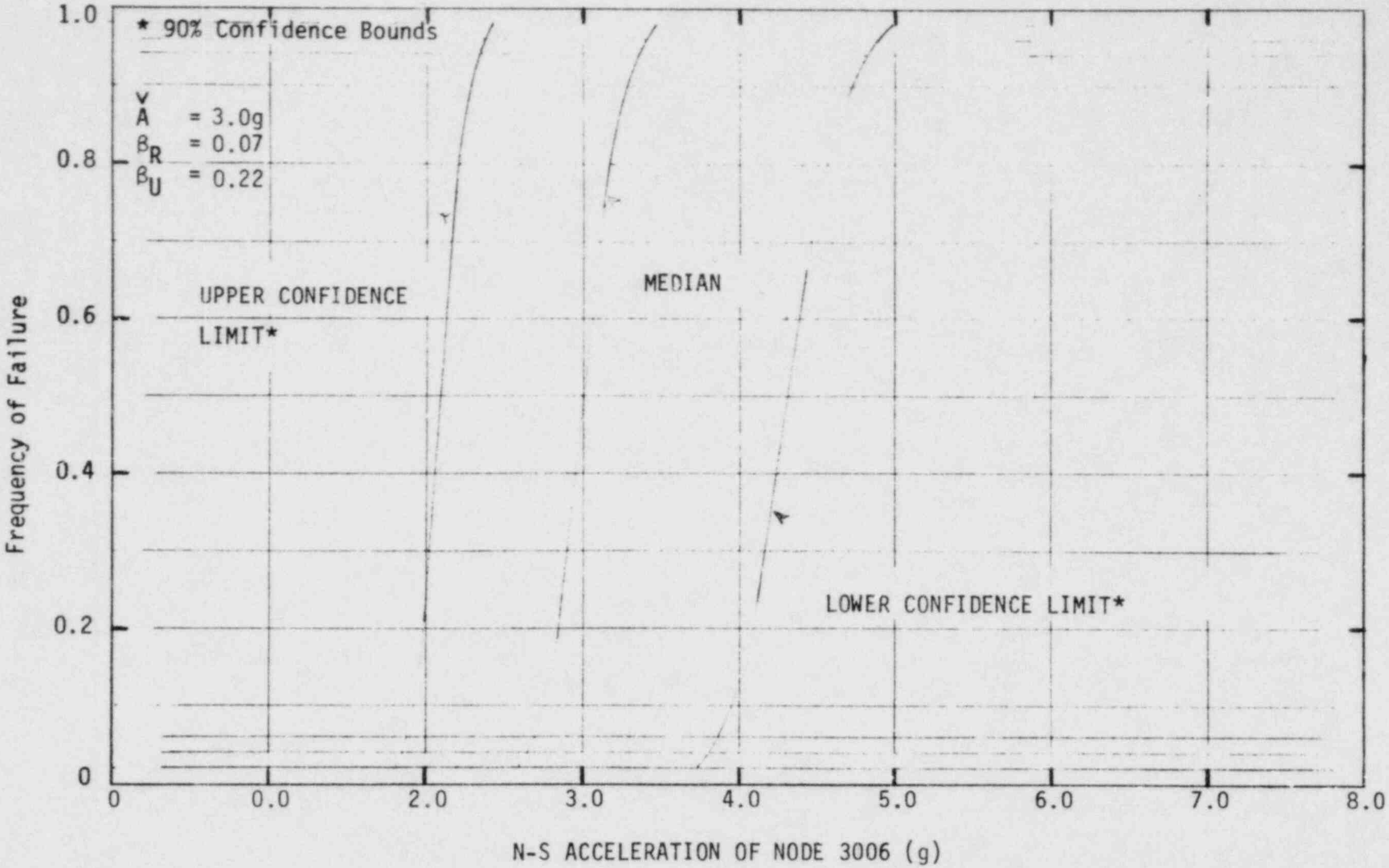

FIGURE 5-25. FAILURE OF AUXILIARY BUILDING ROOF DIAPHRAGM

6. CRIB HOUSE (INTAKE STRUCTURE)

6.1 CRIB HOUSE DESCRIPTION

The crib house of the Zion Nuclear Power Plant is a partially open, box-like reinforced concrete structure which acts as a reservoir for the circulating water pumps and also houses the circulating water pumps, the service water pumps, and the fire pumps. The structure is founded on a rectangular reinforced concrete slab 6 ft thick, 170 ft long in the E-W direction, and 179 ft wide in the N-S direction. The foundation slab is horizontal at elevation 545 ft on the intake end of the structure and slopes gently downward to another horizontal slab at elevation 537 ft under the pump suction area. Grade elevation is 591 ft. Figure 6-1 shows a vertical section through the structure.

The circulating water supply flows into the crib house through three 16 ft diameter circular intake pipes which extend approximately 2600 ft out into Lake Michigan. At the intake end of the crib house, reinforced concrete box structures anchor the intake pipe and channel the water flow into the structure (Figure 6-2). Above these box structures, two vertical walls (3 ft and 4 ft thick), spaced 14 ft apart, extend across the crib house. Between these two walls, a warming pipe runs from the side of the crib house to the center intake pipe.

At the back or west end of the crib house, longitudinal walls (Figure 6-3) form six cells which channel the flow of water into the pump suction areas. The longitudinal walls span from the foundation slab to the operating floor at elevation 594 ft. Except for one 7 ft. thick wall at the center of the crib house, all the longitudinal walls are 3 ft. thick. The lateral support of these walls is provided mainly by the operating floor and two deep beams (Figure 6-1). At the intake end of the six cells, stop log guides are provided. Water flowing into the cells passes through moving screens whose driving mechanisms are supported on the operating floor.

The operating floor is a 2 ft. thick reinforced concrete slab which covers the total width and approximately one-half the length of the crib house. The foundation walls at the open area are supported by two vertical walls and concrete beams which run approximately parallel to the foundation slab at about one-third the way down from the top of the foundation wall (Figure 6-5). A section view of a foundation wall in the open area is shown in Figure 6-6. The operating floor supports six vertical service water pumps spaced equally across its width, the two fire pumps, and the reinforced concrete pump enclosure. Figure 6-7 indicates the location of the service pumps and fire pumps inside the enclosure. The enclosure was constructed of 18-inch thick reinforced concrete roof slab and walls. The roof plan of the pump enclosure at elevation 613'-6" is shown in Figure 6-8. Several large openings in the roof slab are shown in the figure.

The circulating water pump room, located under the operating floor and behind the service water pumps, houses six vertical circulating water pumps. The room is enclosed by three foundation walls (4 ft. thick), one 4-ft. thick vertical wall, the operating floor, and the floor slab at elevation 552 ft. 3 in. The pump floor slab (2 ft. 9 in. thick) is supported by short vertical walls below which is located the pump suction area (Figure 6-9). The circulating water pump drives are located on the operating floor directly over the circulating water pumps.

The elevations of the crib house aboveground structure are shown in Figures 6-10 and 6-11. It encloses the entire area from the center line of the stop log guides (see Figure 6-7) to the west end of the crib house. The exterior walls are 12-inch thick, horizontally reinforced, concrete block walls. Figure 6-7 indicates the location of the missile walls which also have vertical reinforcing. The roof plan of the above ground structure is shown in Figure 6-12. The roof slabs at elevation 613'-0" and 624'-0" are 3-1/2-inch thick precast concrete channel slabs supported by steel braced roof framing. The 12-inch concrete block walls are attached to the steel columns and roof beams as shown in Figure 6-13.

The structural steel framing at elevation 649'-0" supports the 15 ton trolley which runs in the north-south direction along the entire length of the service pump enclosure. The frame has diagonal bracing along the N-S direction only (Figure 6-10). In the E-W direction, the steel columns adjacent to the high roof (elevation 624 ft.) are connected to the high roof braced steel framing (Figure 6-11) and are not diagonally braced.

6.2 CRIB HOUSE FAILURE

The primary safety related function of the crib house is to provide a reservoir and to house the service water pumps. Thus, only failures which would interrupt intake and flow of water or cause failure of the service water pumps are considered in this investigation. Thus, failure modes of the crib house which result only in damage to the circulating water pumps are not treated.

The box-like crib house is symmetric about its E-W direction axis but is not symmetric in the N-S direction due to lack of north-south direction shear walls near the center of the crib house. The major vertical shear resisting structural elements for N-S ground motions are the west side foundation wall, circulating water pump east wall, and the short walls below the pump room. For the E-W ground motions, the vertical shear resisting elements are the north and south foundation walls and the E-W direction longitudinal guide walls (Figure 6-3). The structure is deeply embedded on all sides. In essence, only the part of the structure above the operating floor is above grade.

No reanalysis of the crib house was conducted as part of Phase I of the SSMRP. The evaluation of the structure fragility levels was based on seismic loads developed by Sargent & Lundy as part of the original design analyses (Ref. 25). In addition to a consideration of the strength and ductility capacities for the structure, the design loads were modified as discussed in Section 3.3 to account for expected structure response. The design calculations were not checked as part of this investigation.

However, the model was reviewed and is expected to provide representative loads. Consequently, the assumption was made that the loads developed from the model were median centered based on the assumed input.

The service water pumps are located in the reinforced concrete pump enclosure room which is in turn enclosed by the concrete block walls. The portion of the operating floor not enclosed by the pump enclosure room is covered by precast concrete channel section roof slabs supported by a braced steel roof frame. On top of the service water pump enclosure, a steel braced frame supports the trolley. The steel braced frame is laterally supported by the high roof as discussed previously. The masonry block walls are expected to crack at the base from out-of-plane response at relatively low ground acceleration due to lack of vertical wall reinforcing. This will be locally modified in the areas designated as missile walls by the presence of vertical reinforcing steel. For the unreinforced masonry walls, the failure will be essentially vertical, in-place collapse once the p-Δ effects become critical. However, failure of either rooftop steel frame or enclosing masonry block walls is not expected to cause sufficient flow blockage to be a critical item. Likewise, the service water pumps and the buried service water pipes are not expected to be damaged by collapse of the block walls and concrete roof slabs. Therefore, no fragility curves are provided for this mode of failure.

6.2.1 Failure of the Pump Enclosure Room Roof

The pump enclosure at the operating floor is a 165 ft long by 28 ft wide reinforced concrete box-type structure (Figure 6-7). The enclosure structure is essentially symmetric about the two orthogonal directions. Thus, no torsion occurs except that resulting from the response of the remaining part of the structure which supports the pump enclosure room. Because of the unusually high aspect ratio of the roof slab, some horizontal response amplification of the roof slab results.

The lowest capacity failure mode results from loss of the roof diaphragm due to E-W response. The roof is somewhat lower in capacity than the north and south shear walls of the pump enclosure room due to the large hatches provided (Figure 6-8). Although hatch covers are provided, the shear capacity is reduced. Once the diaphragm capacity is lost, loads are transferred to the north and south walls which must resist the E-W roof inertia loads by out-of-plane bending. The out-of-plane capacity of these walls is substantially less than the roof diaphragm capacity. Consequently, diaphragm failure is expected to be followed essentially at the same time by flexural failure of the north and south walls with rigid body rocking and vertical collapse of the roof structure. Collapse of the roof is expected to result in loss of the service water pumps.

The fragility curves for the crib house are developed for peak ground acceleration levels. Figure 6-14 shows the fragility curves for failure of the pump enclosure room roof. Two sets of curves are shown. The first set consisting of the solid lines includes the estimated effects of structure response. The second set shown in dashed lines is provided for comparison and includes only the capacity effects for strength and ductility. As is apparent in Figure 6-14, including the structure response effects (notably the estimated deamplification due to embedment) results in somewhat higher median ground acceleration level capacity. However, the uncertainty is also increased significantly.

6.2.2 Crib House Shear Wall Failure

At ground acceleration levels above that required for failure of the pump enclosure roof, failure of various shear walls within the crib house may be expected. Failure of these walls can result from N-S and E-W response depending on the specific shear walls under consideration. Under N-S response, the N-S intake guide walls (Figure 5-2) are expected to fail at a median ground acceleration capacity of approximately 2.5g. Inertia loads are then transferred to the 4 ft thick foundation walls and the E-W intake guide walls which must carry the N-S inertia loads in out-of-plane bending. The capacity of these walls in out-of-plane bending is significantly lower than the N-S intake guide walls in shear so that collapse of the intake end of the structure should be expected with failure of the intake guide walls. Failure of the E-W intake guide walls is expected at a median ground acceleration of approximately 5.4g. Failure of the intake end of the structure is expected to result in at least partial flow blockage. It is considered unlikely that the blockage would completely prevent flow to the service water pumps. However, the flow could be partially restricted.

Failure of the guide walls under the pump room (Figure 6-4) from N-S response is expected at a median ground acceleration level of approximately 3.9g. Failure of these walls may be expected to result in loss of the service water pumps and service water pipes located within the structure. The capacity of these walls to E-W response is considerably greater as is the capacity of a number of other possible crib house failure modes investigated. It should be noted, however, that the median ground acceleration levels discussed in this section for shear wall failure are considered inconceivable. The fragility curves for the shear wall failure modes discussed in this section are shown in Figures 6-15 through 6-17.

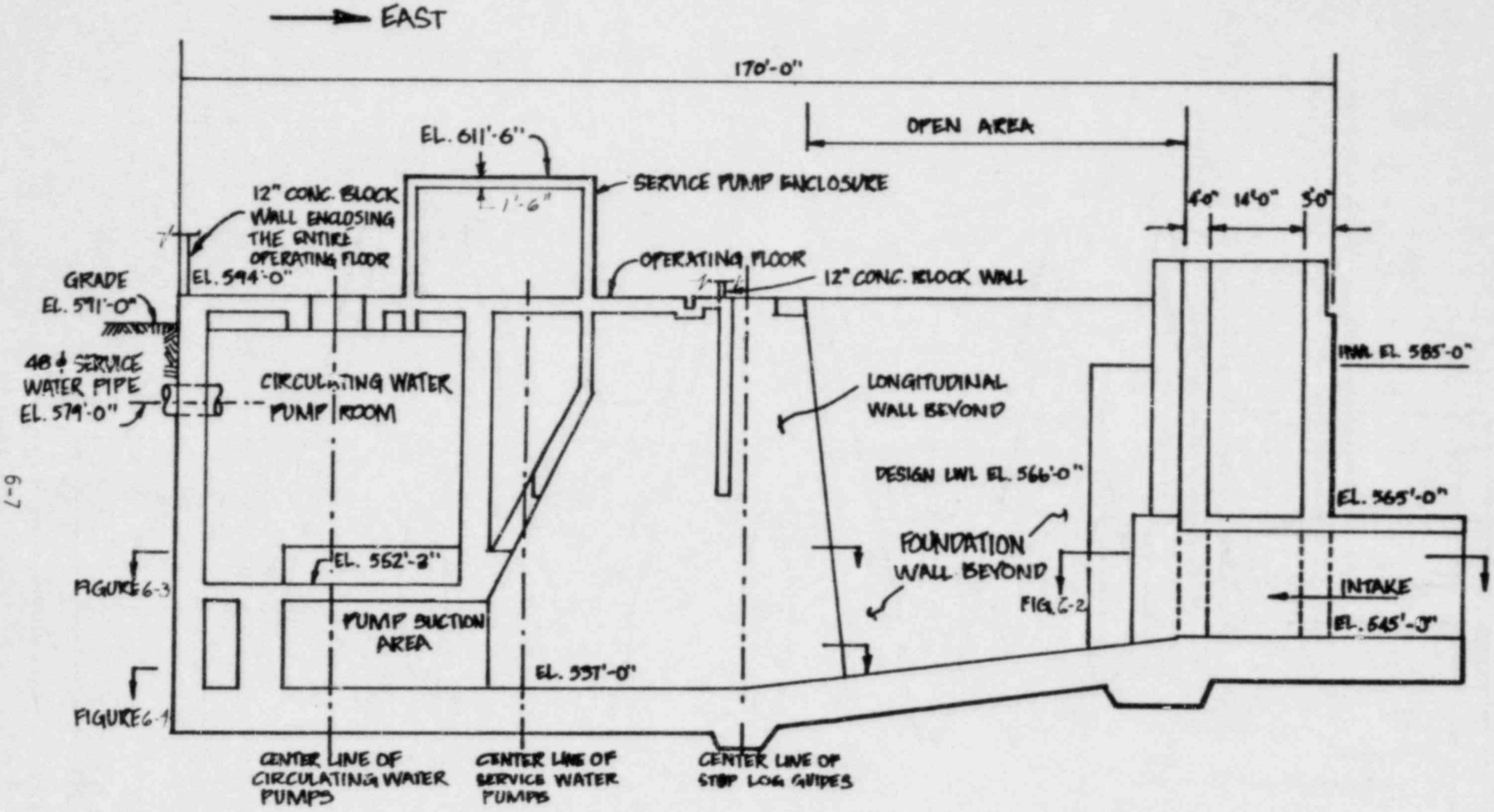

FIGURE 6-1. EAST-WEST SECTION OF THE CRIB HOUSE

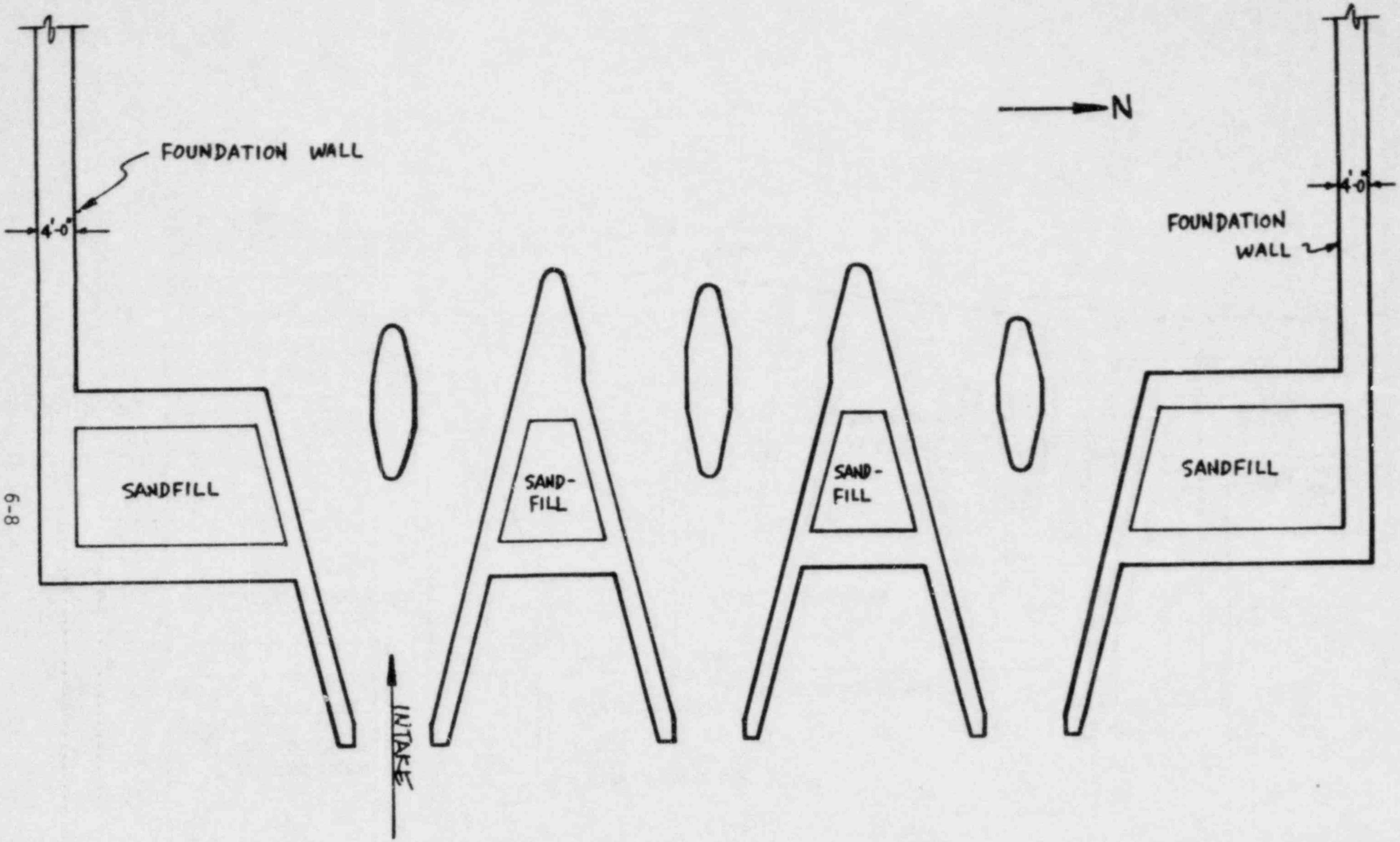

FIGURE 6-[illegible]. SECTION AT THE INTAKE END OF THE CRIB HOUSE

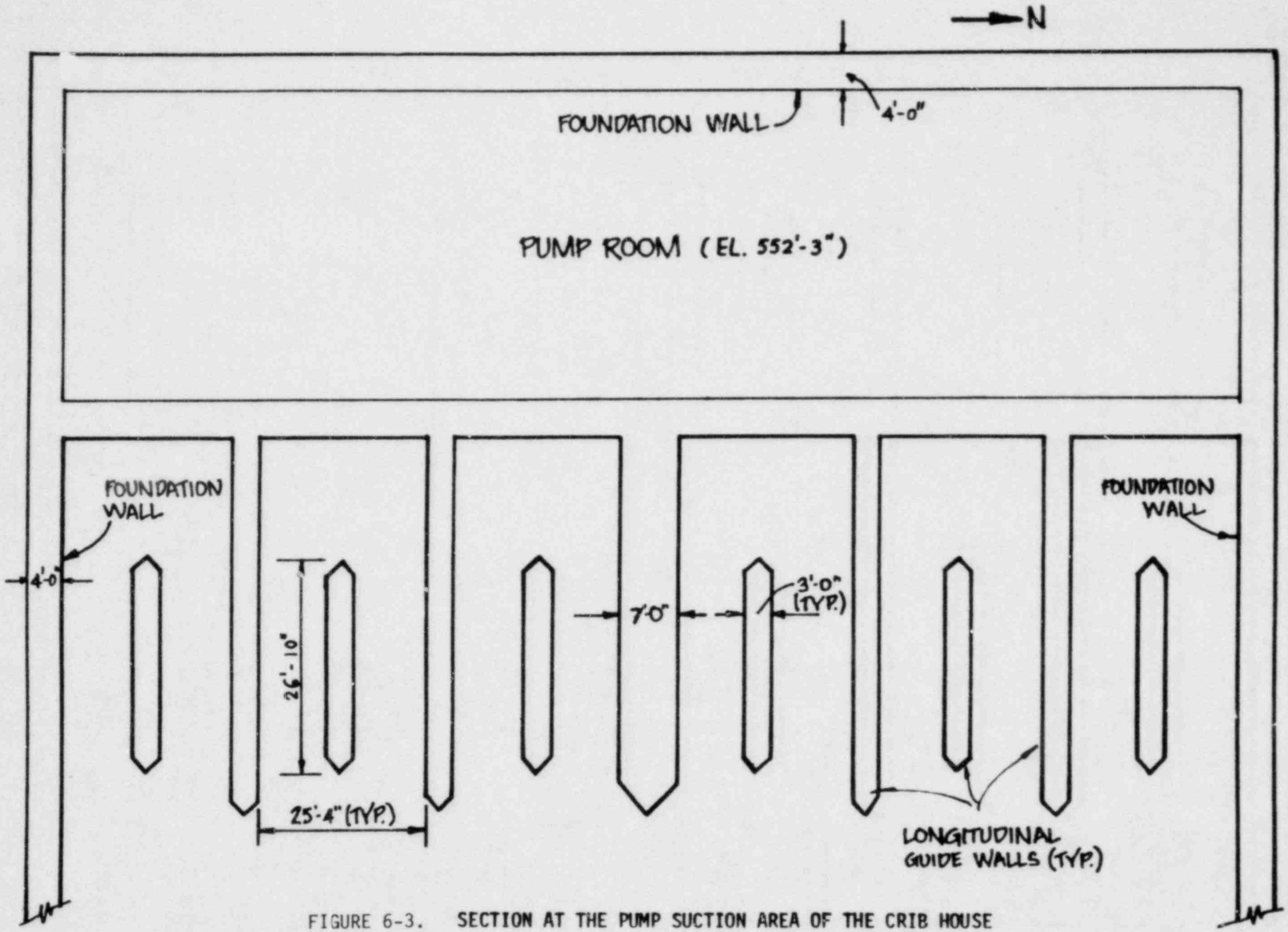

FIGURE 6-3. SECTION AT THE PUMP SUCTION AREA OF THE CRIB HOUSE

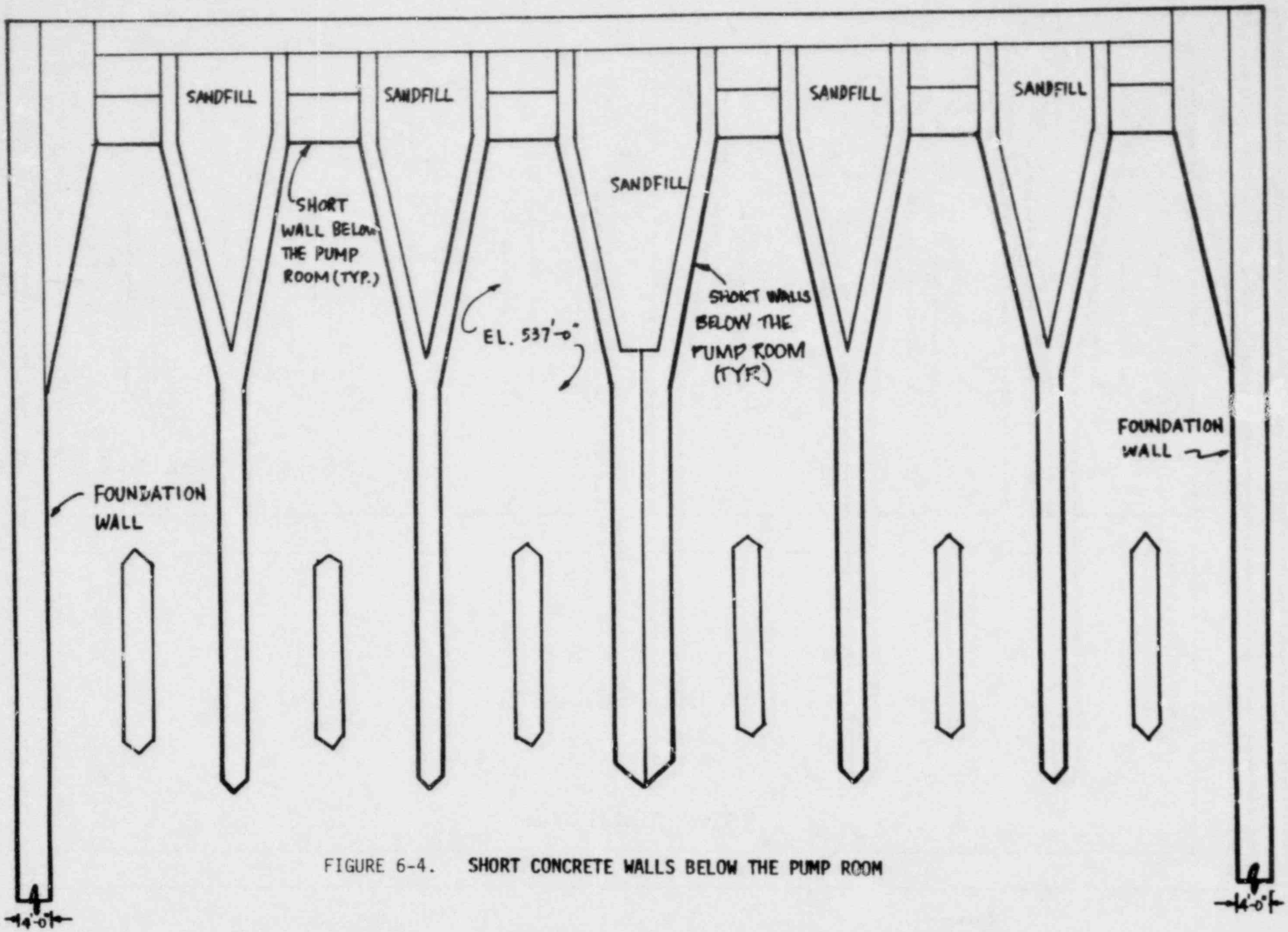

FIGURE 6-4. **SHORT CONCRETE WALLS BELOW THE PUMP ROOM**

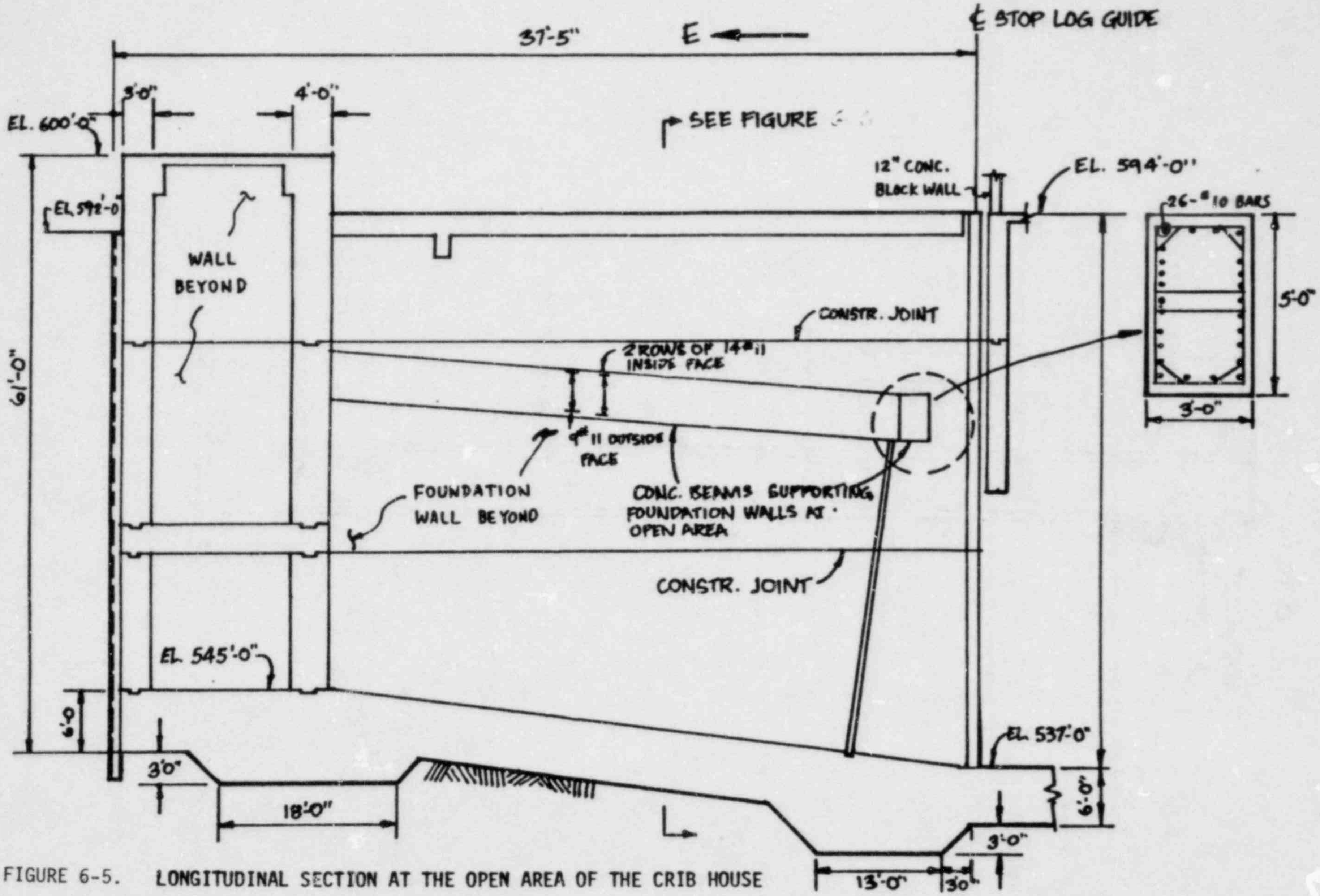

FIGURE 6-5. LONGITUDINAL SECTION AT THE OPEN AREA OF THE CRIB HOUSE

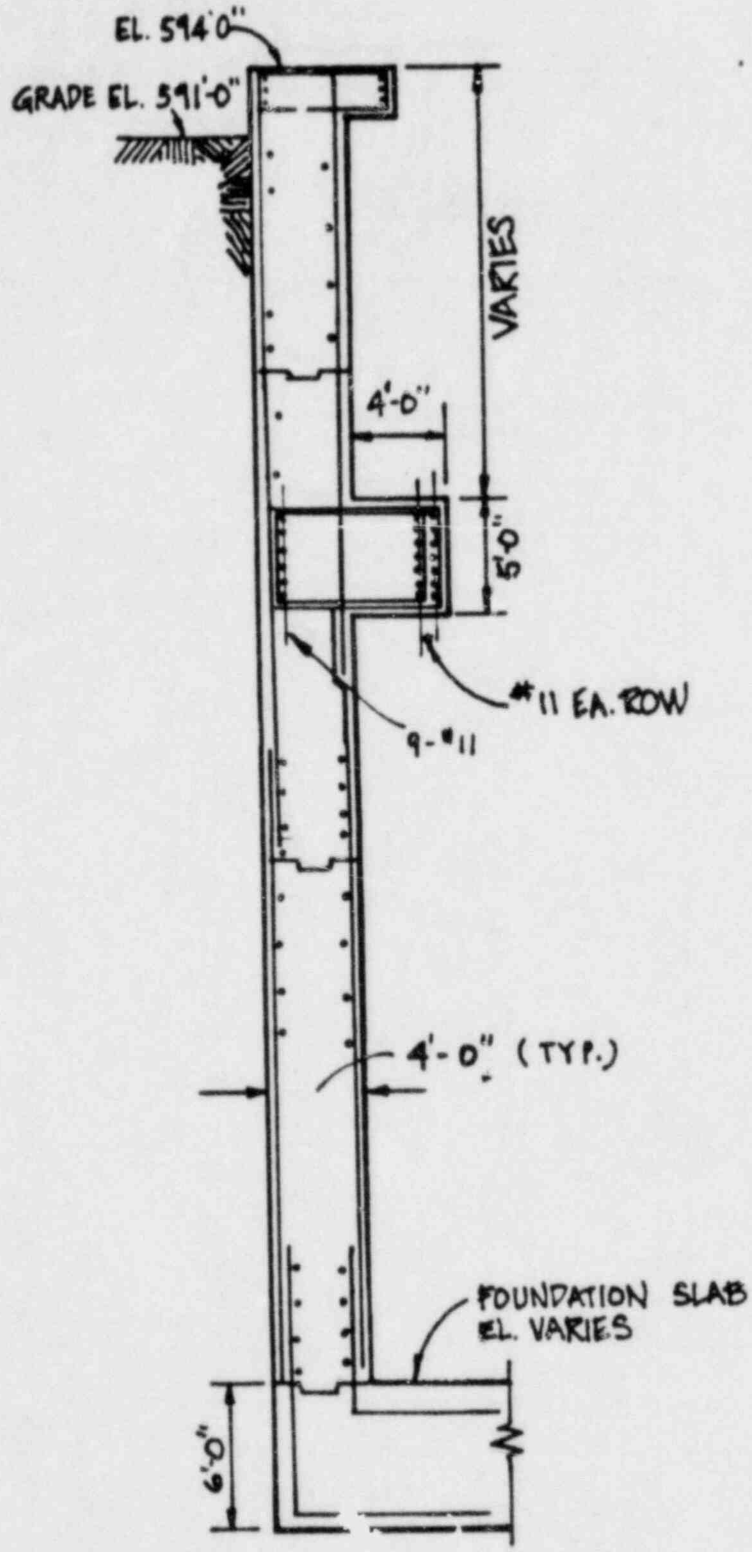

FIGURE 6-6. FOUNDATION WALL AT THE OPEN AREA

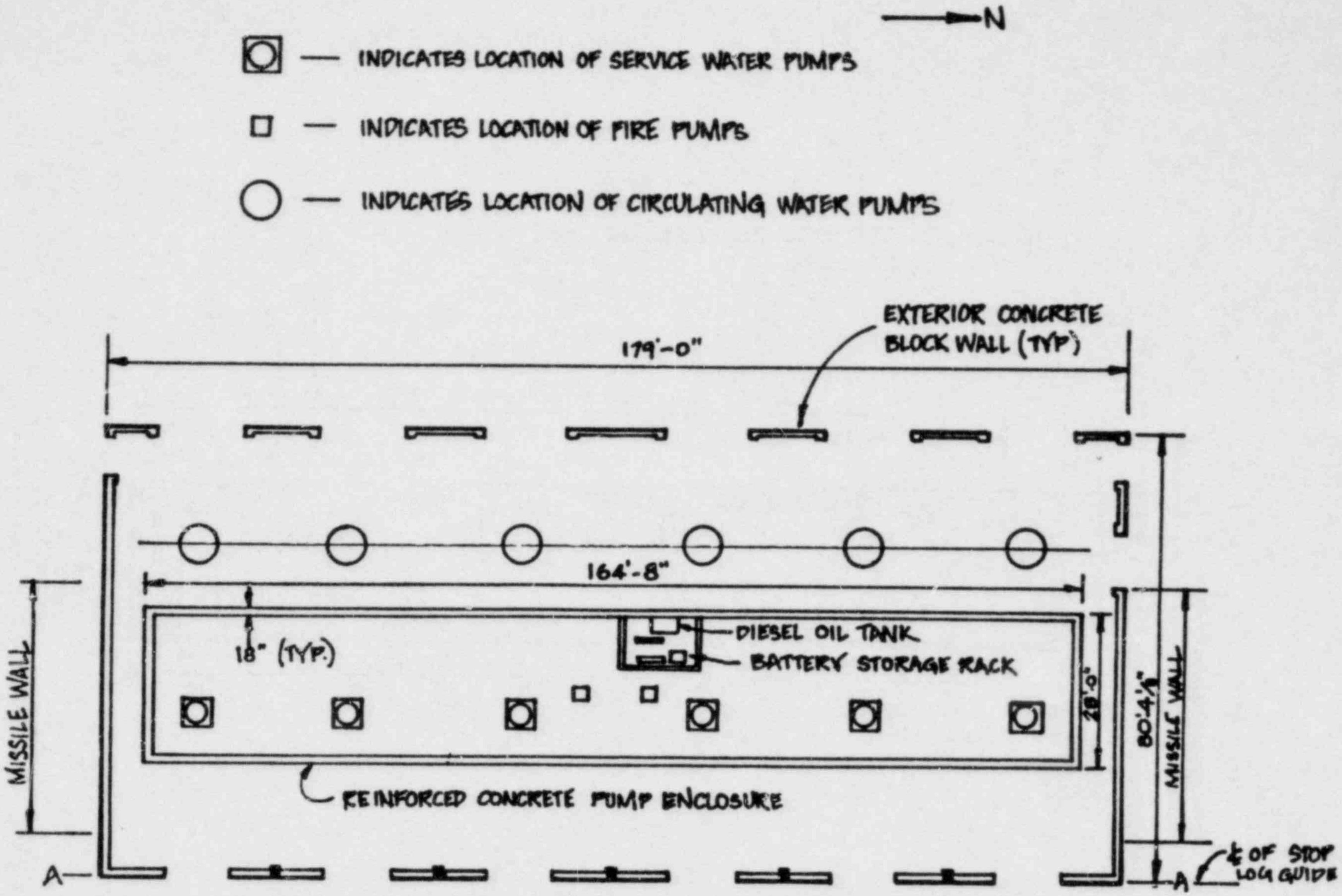

CRIB HOUSE GOUND FLOOR PLAN (EL. 594'-0")

NOTE: OPERATING FLOOR SLAB STOPS AT LINE A-A

FIGURE 6-7. OPERATING FLOOR PLAN

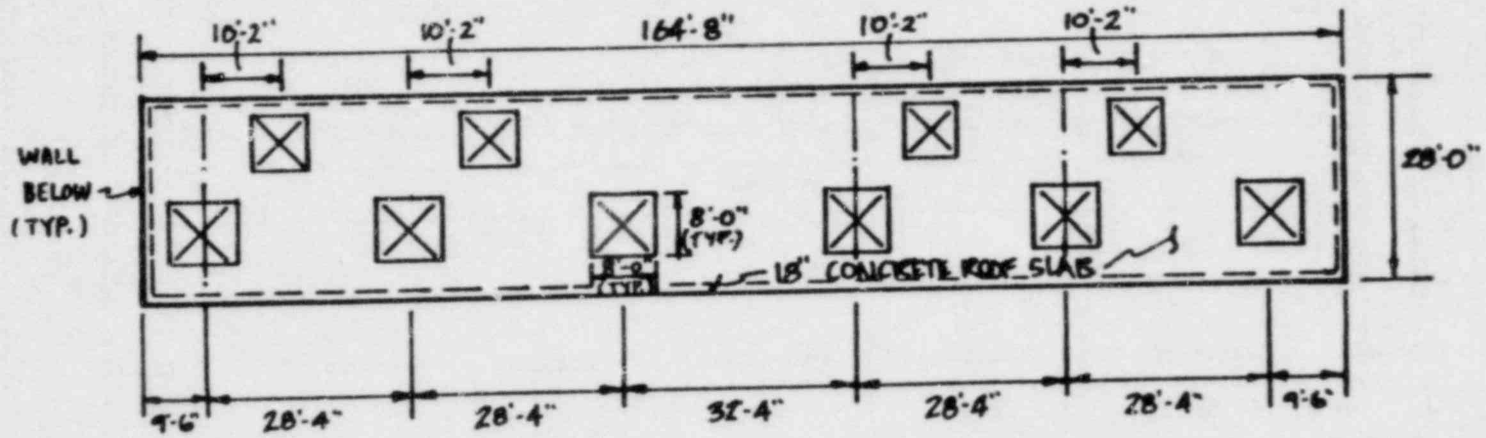

FIGURE 6-8. **PUMP ENCLOSURE ROOF PLAN (EL. 616'-6")**

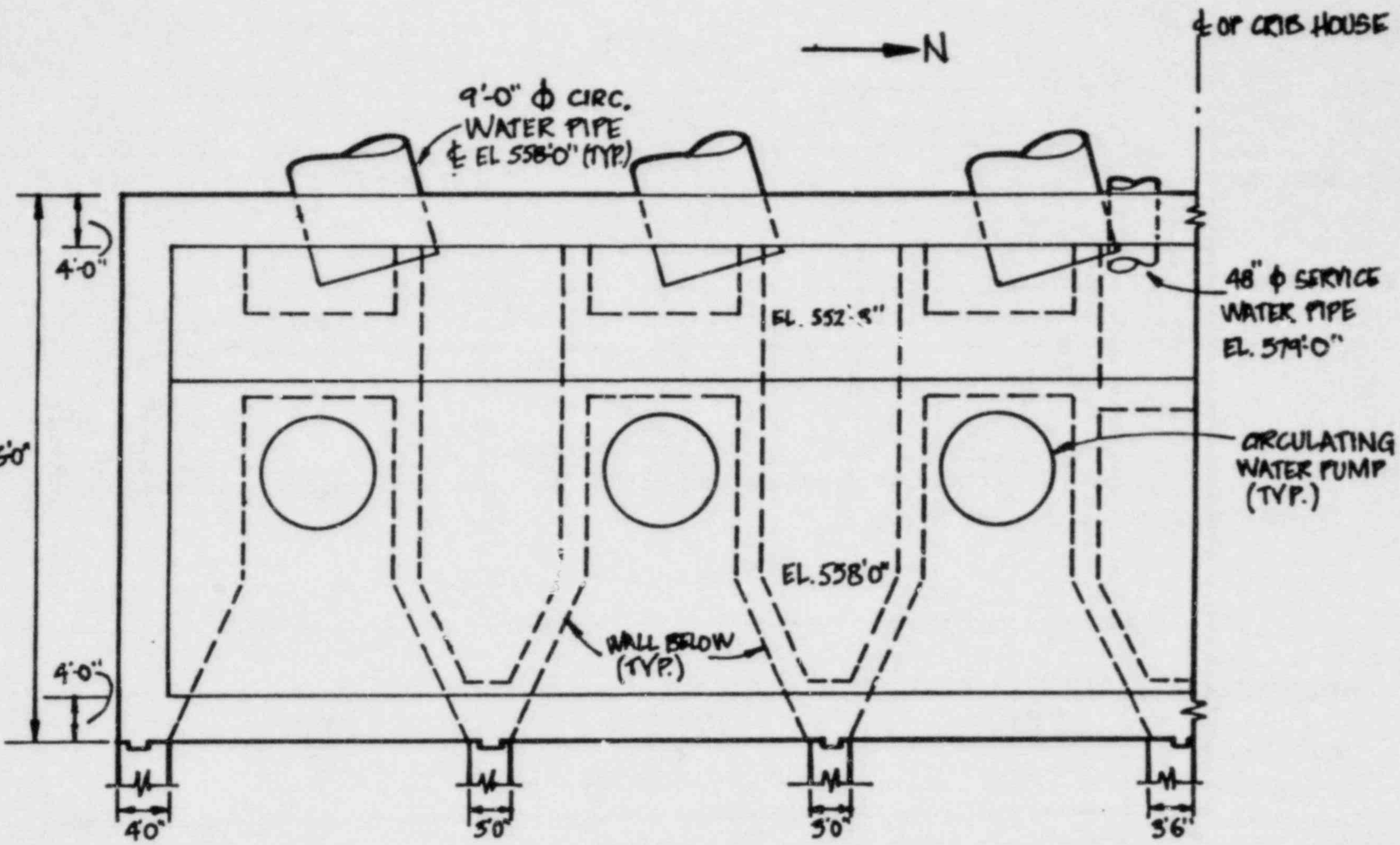

FIGURE 6-9. PUMP ROOM FLOOR SLAB

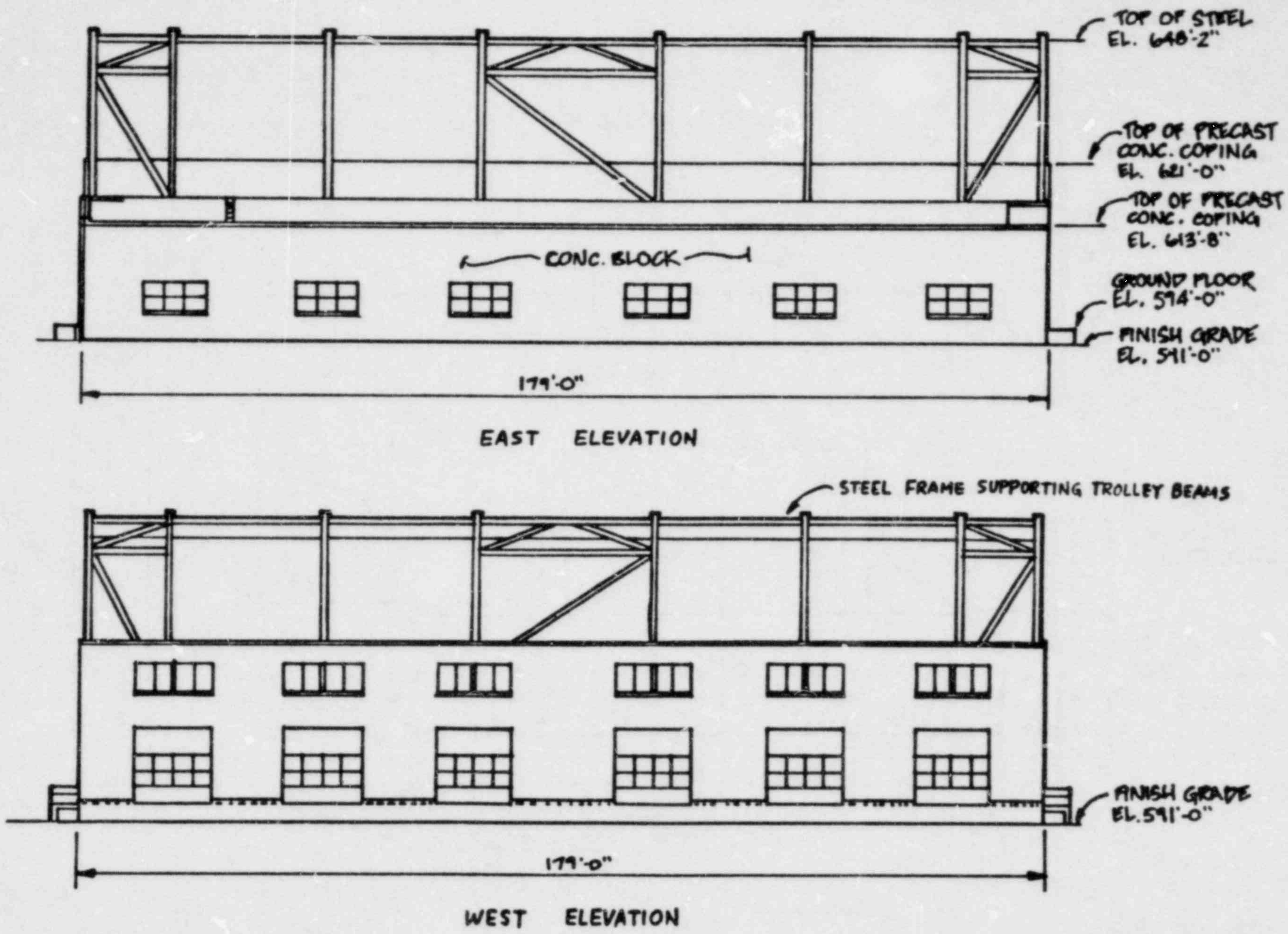

FIGURE 6-10. **ELEVATION OF CRIB HOUSE**

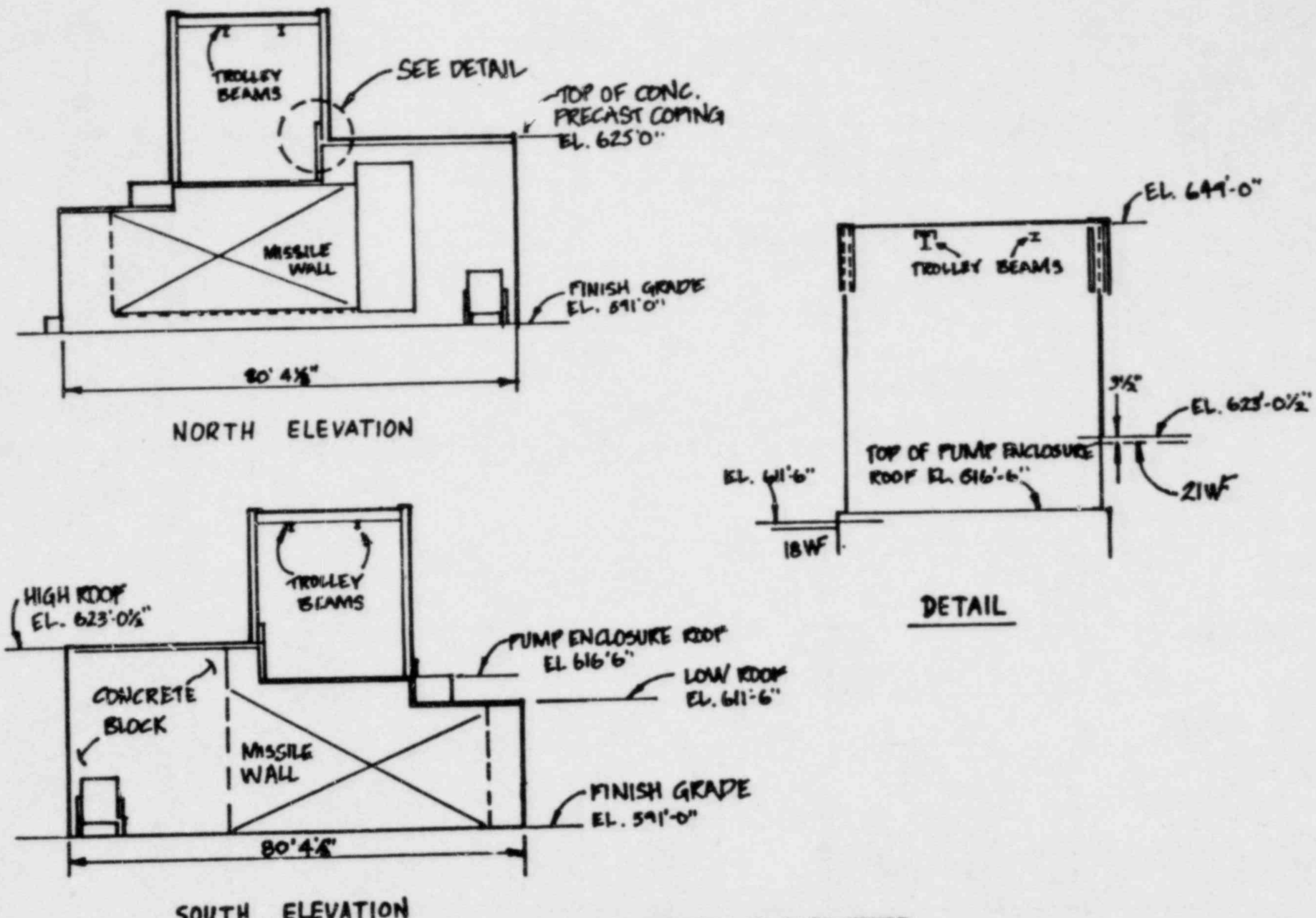

FIGURE 6-11. ELEVATION OF CRIB HOUSE

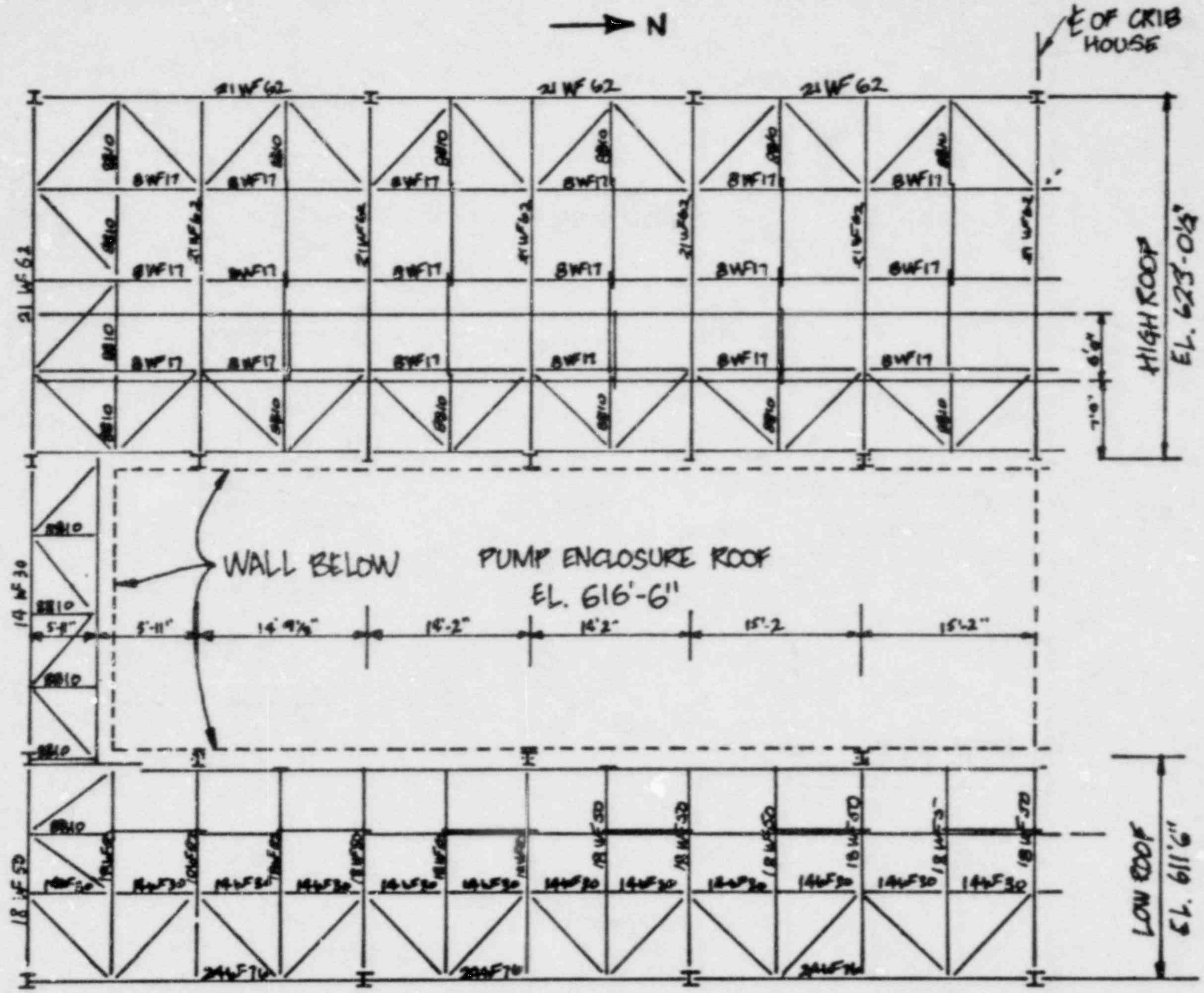

FIGURE 6-12. **CRIB HOUSE ROOF PLAN**

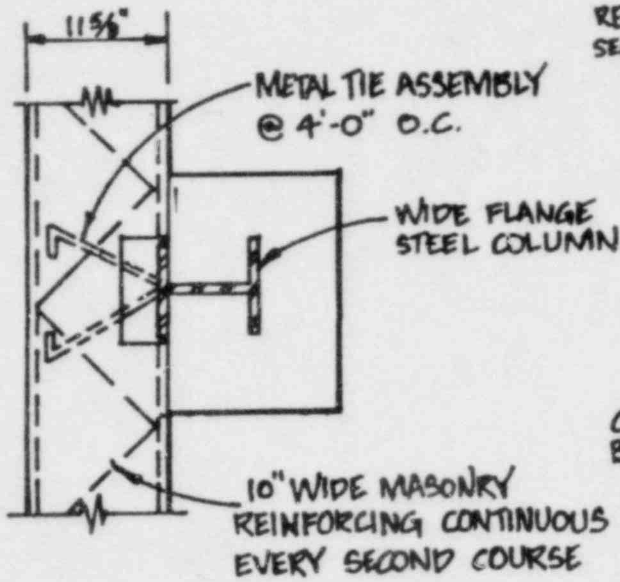

TIE BETWEEN BLOCK WALL AND STEEL COLUMN

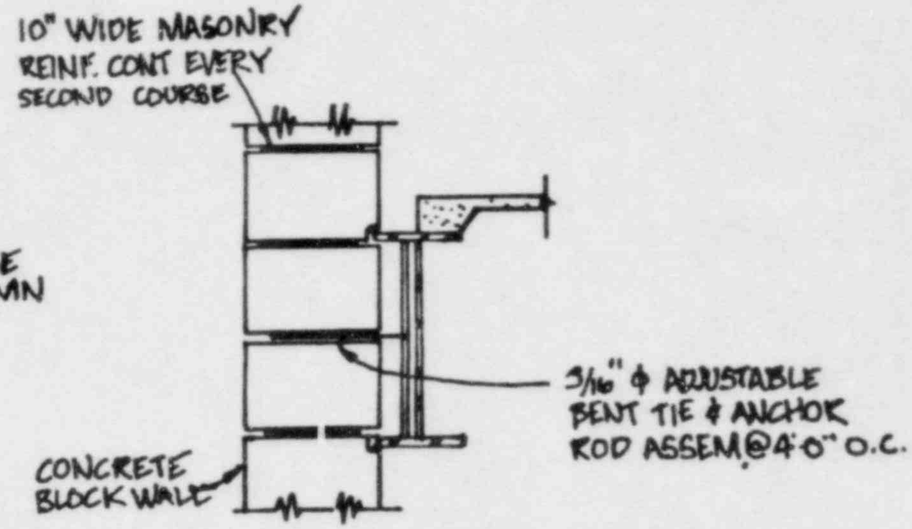

TIE BETWEEN BLOCK WALL AND STEEL BEAM

FIGURE 6-13. **CONSTRUCTION DETAIL OF MASONRY BLOCK WALL**

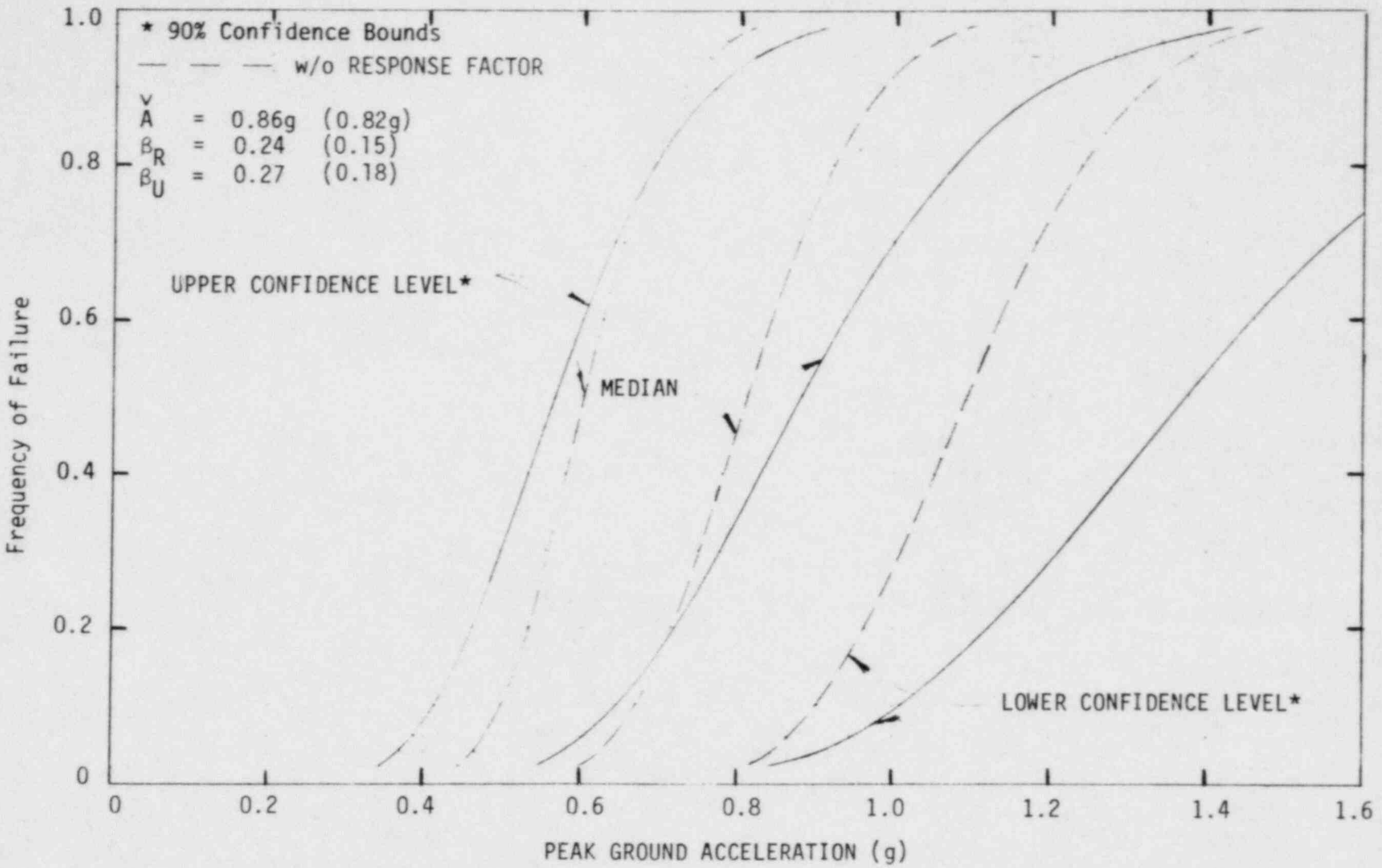

FIGURE 6-14. FAILURE OF CRIB HOUSE PUMP ENCLOSURE ROOF

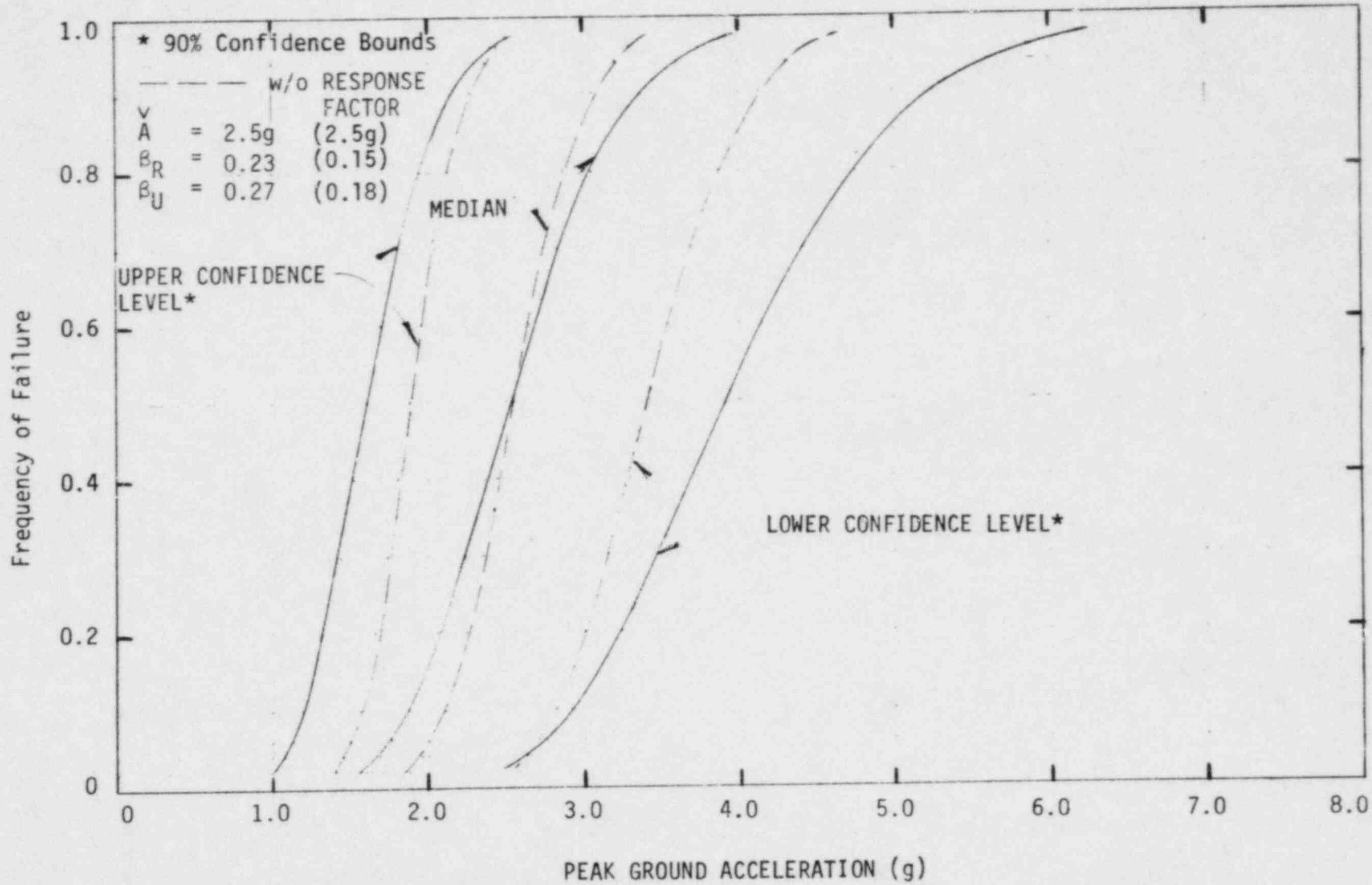

FIGURE 6-15. FAILURE OF N-S CRIB HOUSE INTAKE WALLS

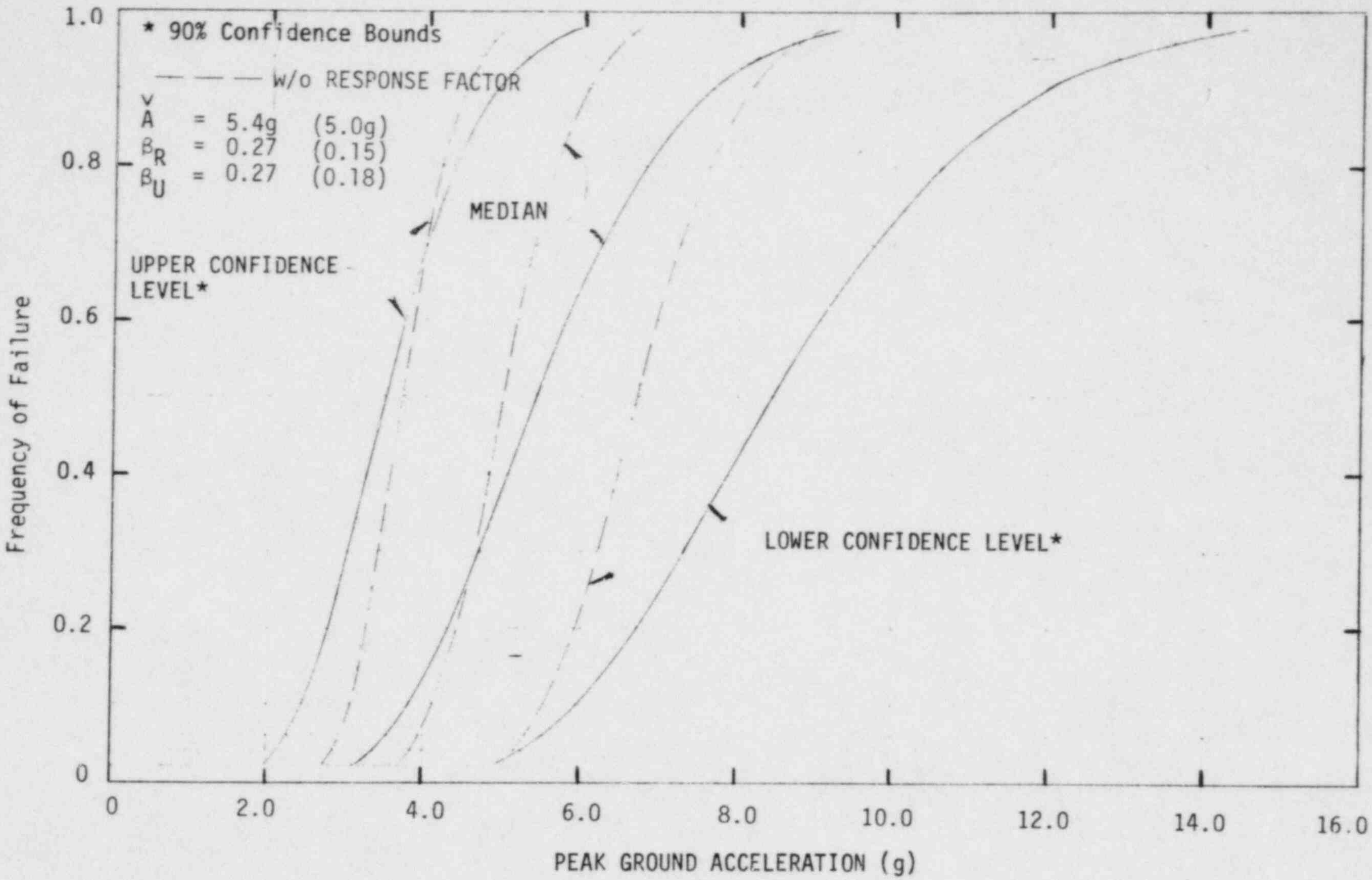

FIGURE 6-16. FAILURE OF E-W CRIB HOUSE INTAKE WALLS

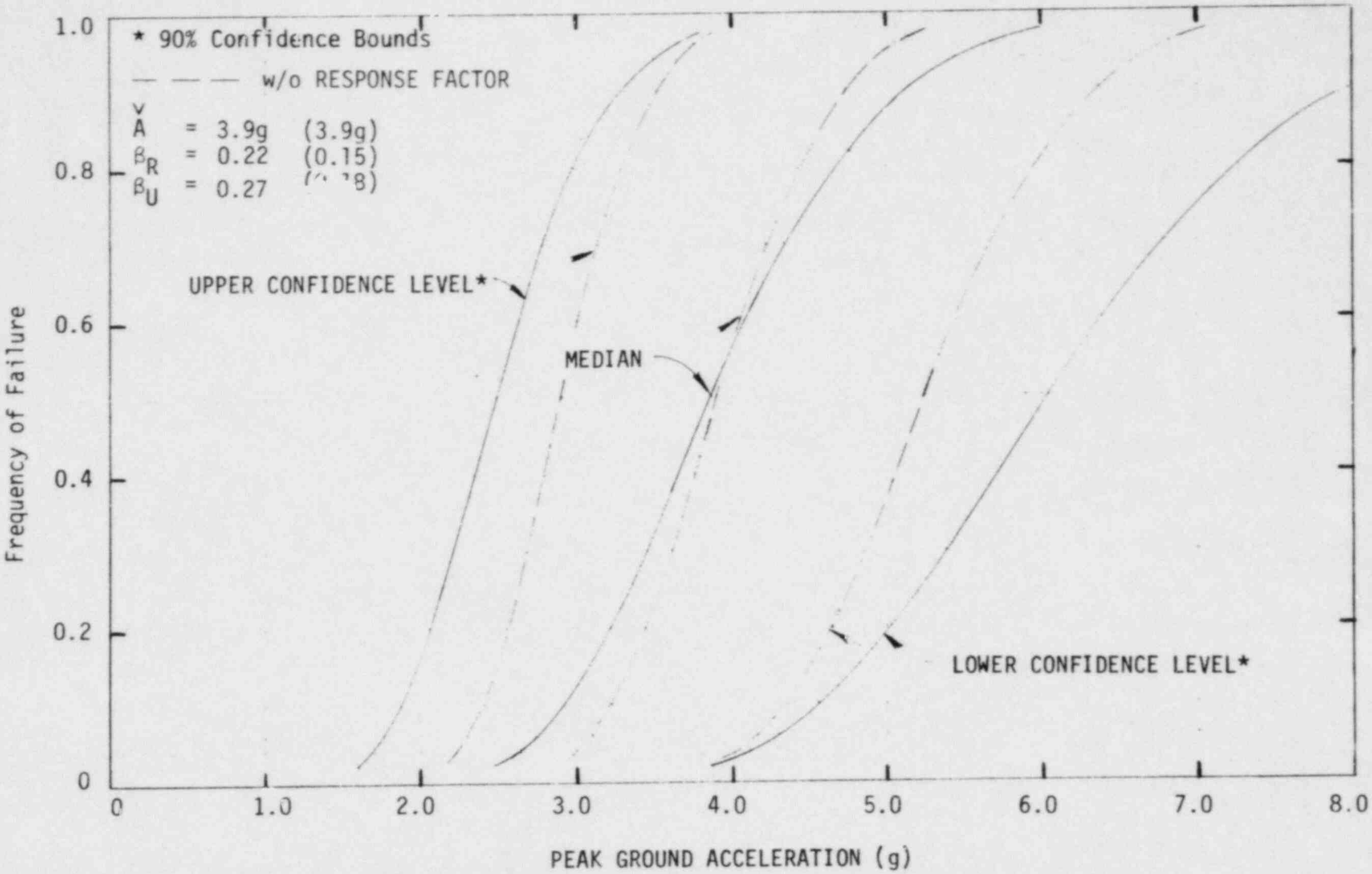

FIGURE 6-17. FAILURE OF N-S CRIB HOUSE GUIDE WALLS

7. MISCELLANEOUS STRUCTURES

As part of the Phase I SSMRP structures fragility program, preliminary failure investigations were conducted on two additional structures. These structures were the condensate storage tanks and a typical buried pipe. The buried pipe chosen was the 48-inch diameter service water pipes from the crib house to the auxiliary building. Other buried pipes are expected to have somewhat higher seismic capacities.

7.1 CONDENSATE STORAGE TANK

The condensate storage tank is a field erected water tank with approximately 500,000 gallon capacity. The tank is approximately 21 ft high with a 32'-6" radius. The tank is fabricated from 5454-H 112 aluminum plate of various thicknesses. The 60 hold-down straps are 6061-T6 aluminum. Each strap is 4" x 1/4" and is embedded 1'-4" in the concrete base. Failure of the tank results from strap pullout from the concrete which allows uplift of the tank base plate and compressive buckling of the side wall. Failure of the wall plate weld with subsequent loss of the tank contents is assumed to occur upon buckling. The median ground acceleration capacity for this mode of failure is expected to be approximately 0.81g. The seismic fragility curves associated with failure of the condensate storage tanks are shown in Figure 7-1.

7.2 UNDERGROUND PIPING

Several underground pipelines are considered essential to safety. Among these are the lines from the condensate storage tank and the service water lines. Because of the relatively large D/t ratio the service water pipe was selected for evaluation. Smaller diameter pipes may be expected to have somewhat greater capacity.

The service water pipes are 48-inch diameter with 1/2-inch wall thickness fabricated from ASTM A515 Grade 60 steel. There is one line for each unit. The lines exit the crib house at centerline elevation 579 ft and are embedded in the turbine building foundation slab at centerline elevation 550 ft - 4 inches before entering the auxiliary building. Grade elevation is 591 ft. The expected failure mode is local circumferential buckling near an elbow due to compressive stress resulting from crib house and turbine building relative displacements. Weld failure and pipe leakage may be expected following buckling. Although fracture of the pipe may be expected, this mode of failure is displacement limited so that total flow blockage is not expected. The median ground acceleration capacity for the service water pipes is approximately 1.7g. Figure 7-2 shows the fragility curves with underground piping. These curves are based on the assumption that the turbine building and crib house will remain essentially intact during the seismic event and the pipe penetrations will not be damaged. Damage to the penetrations is assumed to be governed by the supporting structure or details of the penetrations themselves.

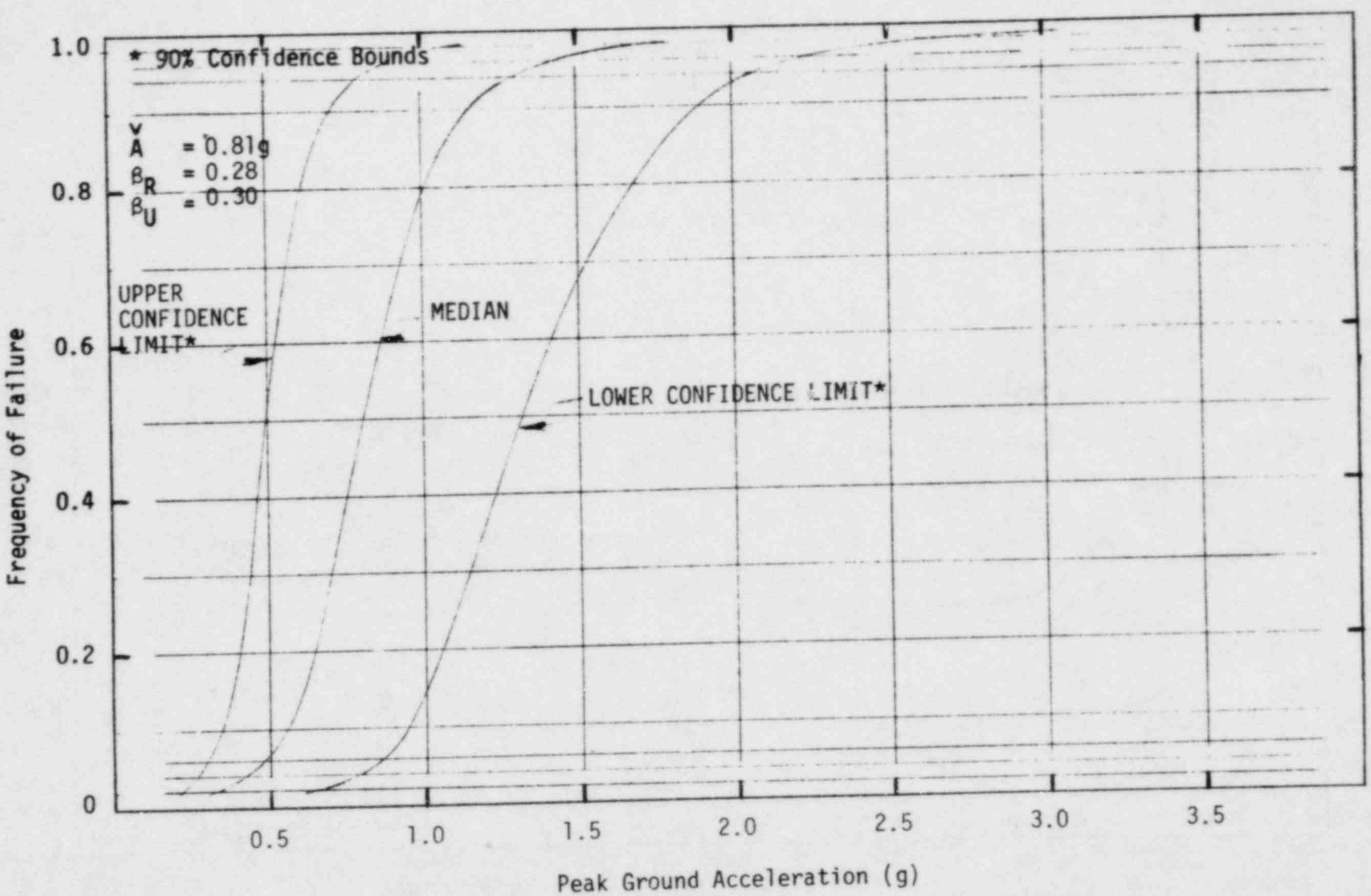

FIGURE 7-1. CONDENSATE STORAGE TANK FAILURE

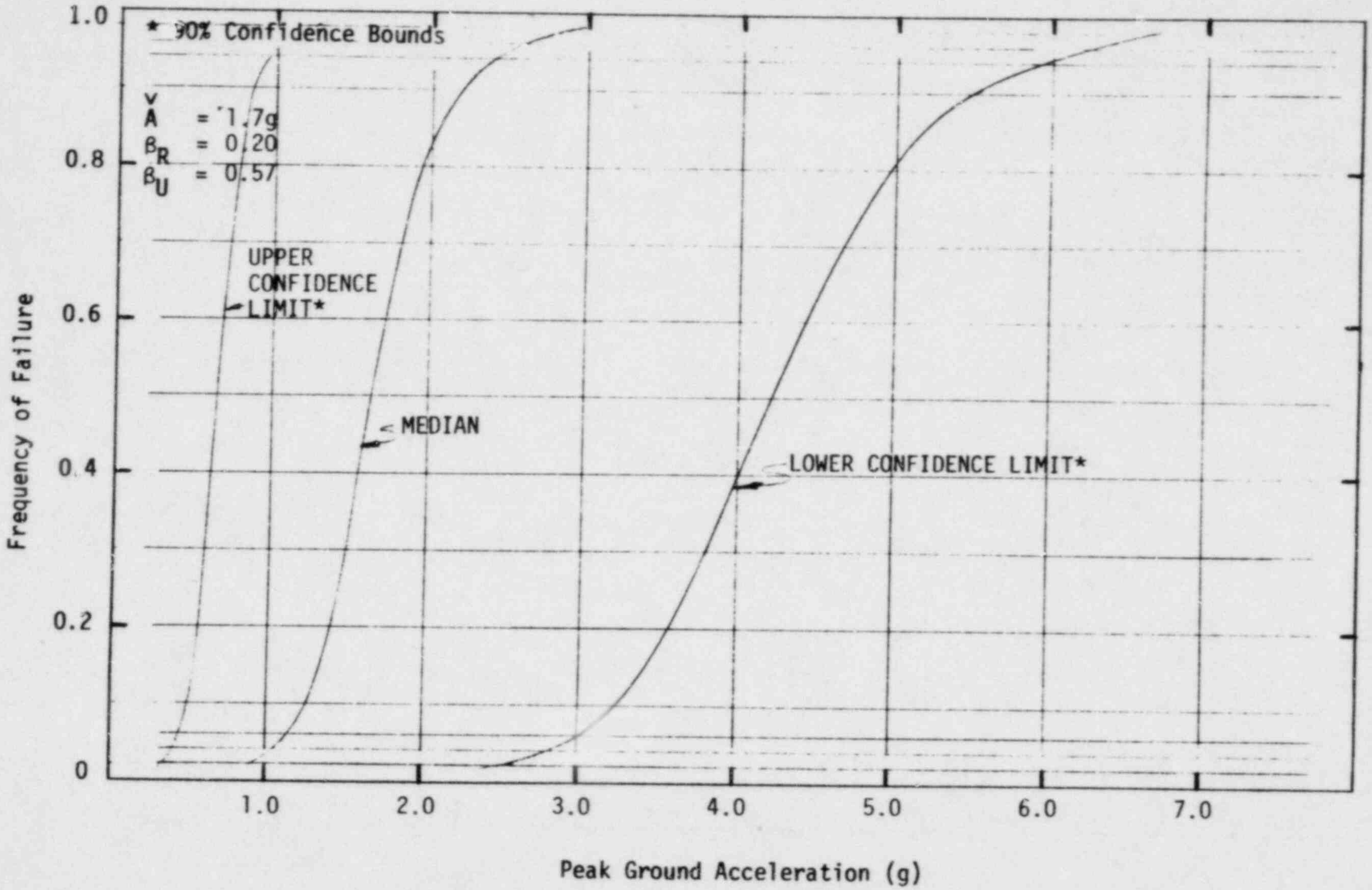

FIGURE 7-2. SERVICE WATER PIPE FAILURE

REFERENCES

1. Smith, P. D., et al, "Seismic Safety Margins Research Program - Program Plan", UCID-17824, Lawrence Livermore Laboratory, Livermore, California, August, 1978.

2. Freudenthal, A. M., J. M. Garrelts, and M. Shinozuka, "The Analysis of Structural Safety", Journal of the Structural Division, ASCE, ST1, February, 1966, pp. 267-325.

3. Kennedy, R. P., "A Statistical Analysis of the Shear Strength of Reinforced Concrete Beams", Technical Report No. 78, Department of Civil Engineering, Stanford University, Stanford, California, April, 1967.

4. Final Safety Analysis Report (FSAR), Zion Station, Commonwealth Edison Company.

5. ACI-318-63, "Building Code Requirements for Reinforced Concrete", American Concrete Institute, 1963.

6. USNRC Regulatory Guide 1.61, "Damping Values for Seismic Design of Nuclear Power Plants", ^ tober, 1973.

7. Newmark, N. M. and W. J. Hall, "Development of Criteria for Seismic Review of Selected Nuclear Power Plants", report prepared for the U.S. Nuclear Regulatory Commission, 30 September 1977.

8. Newmark, N. M., "Inelastic Design of Nuclear Reactor Structures and Its Implications on Design of Critical Equipment", SMiRT Paper K 4/1, 1977 SMiRT Conference, San Francisco, California.

9. NUREG-75-087, "Standard Review Plan for the Review of Safety Analysis Reports for Nuclear Power Plants", USNRC, 1975. (now published as NUREG-0800)

10. USNRC Regulatory Guide 1.92, "Combining Modal Responses and Spatial Components in Seismic Response Analysis", Rev. 1, February, 1976.

.. USNRC Regulatory Guide 1.60, "Design Response Spectra for Seismic Design of Nuclear Power Plants", Rev. 1, December, 1973.

12. "A Study of Vertical and Horizontal Earthquake Spectra", WASH 1255, Nathan M. Newmark Consulting Engineering Services, prepared for USAEC, April, 1973.

13. Benjamin, J. R., and C. A. Cornell, Probabi'ity Statistics, and [illegible]cision for Civil Engineers, McGraw-Hill B[illegible]ok Company, New York, 1970.

14. Kennedy, R. P. and C. V. Chelapati, "Conditional Probability of a Local Flexural Wall Failure for a Reactor Building as a Result of Aircraft Impact", Holmes and Narver, Inc., prepared for General Electric Company, San Jose, California, June, 1970.

15. Walser, A. to D. A. Wesley, Personal Communication, April, 1980.

16. Troxell, G. E., H. E. Davis and J. W. Kelly, Composition and Properties of Concrete, McGraw-Hill, 1968.

17. Mirza, S. A., M. Hatzinikolas, and J. G. MacGregor, "Variability of Mechanical Properties of Reinforcing Bars". J. Structural Division, ASCE, May, 1979.

18. ACI-318-77 "Building Code Requi[illegible] Reinforced Concrete", American Concrete Institute, 19[illegible]

19. Barda, F., J. M. Hanson, and W. G. Co[illegible]ley, "Shear Strength of Low-rise Walls with Boundary Elements', ACI Symposium, "Reinforced Concrete Structures in Seismic Zones", ACI, Detroit, Michigan, 1976.

20. Shiga, T., A. Shibata, and J. Tabahashi, "Experimental Study on Dynamic Properties of Reinforced Concrete Shear Walls", 5th World Conference on Earthquake Engineering, Rome, Italy, 1973.

21. Cardenas, A. E., et al, "Design Provisions for Shear Walls", ACI Journal, Vol. 70, No. 3, March, 1973.

22. Oesterle, R. G., et al, "Earthquake esistant Structural Walls - Tests of Isolated Walls - Phase II", Construction Technology Laboratories (Division of PCA), Skokie, Illinois, October, 1979.

23. Riddell, R. and N. M. Newmark, "Statistical Analysis of the Response of Nonlinear Systems Subjected to Earthquakes", Department of Civil Engineering Report UILU 79-2016, Urbana, Illinois, August, 1979.

24. Merchant, H. C. and T. C. Golden, "Investigations of Bounds for the Maximum Response of Earthquake Excited Systems, Bulletin of the Seismicological Society of America, Vol. 64, No. 4, pp. 1239-1244, August, 1974.

25. "Seismic Analysis of the Zion Crib House", Sargent and Lundy Engineers, Chicago, Illinois, April, 1968.

26. Kennedy, R. P., S. A. Short, D. A. Wesley, and T. H. Lee, "Effect of Nonlinear Soil-Structure Interaction Due to Base Slab Uplift on the Seismic Response of a High Temperature Gas Cooled Reactor Plant", Transactions of the 3rd International Conference on Structural Mechanics in Reactor Technology, London, U.K., Paper K3/5, 1975.

27. Blodgett, O., Design of Welded Structures, Lincoln Arc Welding Foundation, 1966.

28. Manual of Steel Construction, American Institute of Steel Construction, 1974.

29. Kennedy, R. P., "A Review of Procedures for the Analysis and Design of Concrete Structures to Resist Missile Impact Effects", Nuclear Engineering and Design, March, 1976.

APPENDIX

A sample calculation showing the determination of the factors of safety and logarithmic standard deviations for a typical failure mode for one of the Zion structures is presented in this appendix. The mode of failure selected is the failure of a shear wall in the diesel generator room of the auxiliary building. The location and extent of this potential mode of failure together with some of the consequences are discussed in Section 5.4.2 of the report.

The loads for the auxiliary building were obtained from the results of LLL time history analyses selected by LLL personnel as providing typical results. The most highly stressed wall for this failure mode was modelled as a single element in the finite element model of the combined turbine/auxiliary building. The strength of these walls is determined using the methods described in Section 3.1.3 together with the median experimentally determined strengths of the reinforcing steel and concrete. The additional capacity expected for this mode of failure resulting from inelastic energy dissipation is included as are the determinations for the variabilities for random effects and uncertainty. The final acceleration response capacity at node 3006 and the logarithmic standard deviations were used to generate the fragility curves shown in Figure 5-22 which correspond to the generator building shear wall failure.

East-West Diesel Generator Building Shear Wall

Possible failure of the shear wall on Line 35 between Elevations 592' to 617' of the Diesel Generator Building is anticipated. This wall is modelled by Element 519 of LLL's model.

Strength Factor

h = wall thickness

= 2'-0

h_w = wall height

= 25'-0

l_w = wall length

= 42'-0

reinforcement = #6 @ 12" each face, each way

$\check{f}'_c$ = median concrete compressive strength

= 6600 psi

$\check{f}_y$ = median reinforcement yield strength

= 66,000 psi

$\check{v}_{CU}$ = ultimate concrete shear strength

$$= 10\sqrt{\check{f}'_c} - 3.4\sqrt{\check{f}'_c}\,(h_w/l_w)$$

$$= 10\,\sqrt{6600} - 3.4\,\sqrt{6600}\left(\frac{25}{42}\right)$$

= 648 psi

ρ = reinforcement ratio

$$= \frac{2(0.44)}{12(24)}$$

= 0.00306

$\check{v}_{SU}$ = ultimate steel shear strength

$= \rho\check{f}_y$

= 0.00306 (66,000)

= 202 psi

$\check{v}_U$ = median shear strength

$= \check{v}_{CU} + \check{v}_{SU}$

$= 648 + 202$

$= 850$ psi

$V_U = \varepsilon[V_U h\ (0.8\ l_w)]$

ε = uncertainty variable with median of 1, logarithmic standard deviation associated with uncertainty of 0.15 (based on comparison of predicted strength versus test strength)

$\check{V}_U$ = median shear strength

$= 0.850\ (2)\ (0.8)\ (42)\ (144)$

$= 8230$ k

Median wall shear stress for 10 time histories = 19,400 psf

Wall thickness as modelled = 1.75'

Wall length as modelled = 42'

$\check{V} = 19.4\ (1.75)\ (42)$

$= 1430$ k

$$F_S = \frac{\dfrac{V_{CU}}{V_D} - \dfrac{V_N}{V_D}}{\dfrac{V_\ell}{V_D} - \dfrac{V_N}{V_D}}$$

$$\approx \frac{V_{EU}}{V_\ell}$$

V_{EU} = effective shear capacity

V_D = design shear capacity

V_ℓ = shear load

V_N = non-seismic portion of shear load

≈ 0

$$\check{F}_S = \frac{8230}{1430}$$

$= 5.8$

Randomness

$$\beta_{vu} \approx \sqrt{\frac{\left(\beta_{v_{CU}} \check{v}_{CU}\right)^2 + \left(\beta_{v_{SU}} \check{v}_{SU}\right)^2}{\check{v}_U^{\ 2}}}$$

$$\beta_{v_{cu}} = \frac{1}{2} \beta_{f'_c}$$

$$= \frac{1}{2} (0.13)$$

$$= 0.065$$

$$\beta_{v_{su}} = \beta_{f_y}$$

$$= 0.09$$

$$\beta_R = \sqrt{\frac{[0.065\ (648)]^2 + [0.09\ (202)]^2}{850^2}}$$

$$= 0.05$$

Uncertainty

$$\beta_u \approx \beta_\varepsilon$$

$$= 0.15$$

$$\check{F}_S = 5.8$$

$$\beta_R = 0.05$$

$$\beta_U = 0.15$$

<u>Inelastic Energy Absorption Factor</u>

The system ductility ratio for shear wall failure is normally estimated to be about 2. However, failure of this shear wall is primarily localized because of load redistribution and nonlinear response of this wall will not significantly deamplify response of the structure as a whole. Accordingly, a reduced system ductility ratio of 1.2 is estimated. Logarithmic standard deviations associated with randomness and uncertainty of the ductility ratio are estimated to be 0.06 and 0.03.

ϕ_u = Newmark's response deamplification factor

$= (p\mu - q)^{-r}$

$\left.\begin{array}{l} p = 2.50 \\ q = 1.50 \\ r = 0.399 \end{array}\right\}$ Amplified acceleration region of response spectrum

ε = uncertainty variable associated with accuracy of ϕ_u, median of 1, β_U of 0.10.

$$F_\mu = \varepsilon \frac{1}{\phi}$$

$$= \varepsilon(p\mu - q)^r$$

$$\check{F}_\mu = \check{\varepsilon}(p\check{\mu} - q)^r$$

$$= 1[2.50\ (1.2) - 1.50]^{0.399}$$

$$= 1.18$$

Randomness

$$\beta = \sqrt{\beta_\varepsilon^{\ 2} + \left(\frac{rp\beta_\mu \check{\mu}}{p\check{\mu} - q}\right)^2}$$

$$\beta_U = \frac{0.399\ (2.50)\ (0.06)\ (1.2)}{2.50\ (1.2) - 1.50}$$

$$= 0.05$$

Uncertainty

$$\beta_U = \sqrt{0.10^2 + \left[0.05\ \left(\frac{0.03}{0.06}\right)\right]^2}$$

$$= 0.10$$

$$\check{F}_\mu = 1.2$$

$$\beta_R = 0.05$$

$$\beta_U = 0.10$$

Median Acceleration Capacity and Its Variability

$$\check{F} = \check{F}_s \check{F}_\mu$$
$$= 5.8 (1.2)$$
$$= 7.0$$

Median E-W acceleration at Node 3006 = 0.15g

$\check{A}$ = median acceleration capacity at Node 3006

$$= \check{F} A$$
$$= 7.0 (0.15g)$$
$$= 1.1g$$

$$\beta = \sqrt{\beta_{F_s}^2 + \beta_{F_\mu}^2}$$

$$\beta_R = \sqrt{0.05^2 + 0.05^2}$$
$$= 0.07$$

$$\beta_U = \sqrt{0.15^2 + 0.10^2}$$
$$= 0.18$$

*U.S. GOVERNMENT PRINTING OFFICE: 1981 361-297/1419 1-3

U.S. NUCLEAR REGULA...

BIBLIOGRAPHIC DATA SHEET

NUREG/CR-2320
UCRL-15380

4. TITLE AND SUBTITLE (Add Volume No., if appropriate)

Seismic Structural Fragility Investigation for the Zion Nuclear Power Plant

Seismic Safety Margins Research Program (Phase I)

2. (Leave blank)

D. A. Wesley, P. S. Hashimoto - Structural Mechanics Associates

5. DATE REPORT COMPLETED

MONTH	YEAR
March	1981

9. PERFORMING ORGANIZATION NAME AND MAILING ADDRESS (Include Zip Code)

Lawrence Livermore National Laboratory
P. O. Box 808
Livermore, CA 94550

DATE REPORT ISSUED

MONTH	YEAR
October	1981

6. (Leave blank)

8. (Leave blank)

12. SPONSORING ORGANIZATION NAME AND MAILING ADDRESS (Include Zip Code)

Office of Nuclear Regulatory Research
U.S. Nuclear Regulatory Commission
Washington, DC 20555

10. PROJECT/TASK/WORK UNIT NO.

11. CONTRACT NO.

FIN A0126

13. TYPE OF REPORT

Technical

PERIOD COVERED (Inclusive dates)

15. SUPPLEMENTARY NOTES

14. (Leave blank)

16. ABSTRACT (200 words or less)

An evaluation of the seismic capacity of the essential structures for the Zion Nuclear Power plant in Zion, Illinois, was conducted as part of the Seismic Safety Margins Research Program (SSMRP). The structures included the reactor containment building, the turbine/auxiliary building, and the crib house (intake structure). The evaluation was devoted to seismically induced failures rather than those resulting from combined Loss of Coolant Accident (LOCA) or other extreme load combinations. The seismic loads used in the investigation were based on elastic analyses. The loads for the reactor containment and turbine/auxiliary buildings were developed by Lawrence Livermore National Laboratory using time history analyses. The loads used for the crib house were the original seismic design loads developed by Sargent & Lundy. No nonlinear seismic analyses were conducted. The seismic capacity of the structures account for the actual concrete and steel material properties including the aging of the concrete. Median centered properties were used throughout the evaluation including levels of damping considered appropriate for structures close to collapse as compared to the more conservative values used for design. The inelastic effects were accounted for using ductility modified response spectrum techniques based on system ductility ratios expected for structures near collapse. Sources of both inherent randomness and uncertainties resulting from lack of knowledge or approximations in analytical modeling were considered in developing the dispersion of the structural dynamic characteristics. Coefficients of variation were developed assuming lognormal distributions for all variables.

17. KEY WORDS AND DOCUMENT ANALYSIS

17a. DESCRIPTORS

17b. IDENTIFIERS/OPEN-ENDED TERMS

18. AVAILABILITY STATEMENT

UNLIMITED

19. SECURITY CLASS (This report)
UNCLASSIFIED

21. NO. OF PAGES

20. SECURITY CLASS (This page)
UNCLASSIFIED

22. PRICE
$

UNITED STATES
NUCLEAR REGULATORY COMMISSION
WASHINGTON, D. C. 20555

OFFICIAL BUSINESS
PENALTY FOR PRIVATE USE, $300

POSTAGE AND FEES PAID
U.S. NUCLEAR REGULATORY
COMMISSION

U.S. MAIL

120555064215 2 ANRDRM
US NRC
ADM DOCUMENT CONTROL DESK
PDR
016
WASHINGTON DC 20555